DESIGN OF THROUGH-GRADE CULVERTS TO MITIGATE ROAD ROUGHNESS (CASE STUDY: PTH-68)

by

Ahmed S. A. S. Moussa

A Thesis
Submitted to the Faculty of Graduate Studies in Partial Fulfillment of the
Requirements for the Degree of

Master of Science

Department of Civil Engineering
University of Manitoba
Winnipeg, Manitoba

Abstract

Roadways over culverts experience severe roughness due to the differential frost heave and thaw settlement in cold regions. Five instrumented culvert sites with different designs to mitigate road roughness were constructed and monitored for two years in Manitoba, Canada. The sites were different in the culvert diameter, type of backfill material, depth of cover, geosynthetics, and thermal insulation. The objectives of the study was to provide design of culverts in cold regions to mitigate road roughness, and develop a numerical model for geotechnical engineering applications in cold regions. A 2-D thermal numerical model was established, validated, and applied on geotechnical engineering applications in cold regions. The study concluded that thermal insulation and geosynthetics had noticeable effect on mitigating road roughness over culverts, and different placements of thermal insulation at the vicinity of culverts could be used to reduce the severity of several geotechnical problems in cold regions.

Acknowledgements

I would like to recognize the assist of many individuals without which this research would not have been possible. First, I would like to show my gratitude to my advisor, Dr. Ahmed Shalaby, P.Eng. for his professional guidance, advice, and encouragement throughout this research. Sincere thanks to the members of my examination committee, Dr. Pooneh Maghoul, P.Eng. and Dr. David Kuhn, P.Eng..

I would like to thank the members of the Pavement Research Group. Special thanks to Dr. Leonnie Kavanagh, P.Eng. for her generous advice. I was fortunate to work side by side with her in several academic papers. I would also like to thank Mr. Scott Sparrow, the Pavement Laboratory Technician at the University of Manitoba. His technical and practical expertise contributed greatly to the field instrumentations and testing.

This research would not have been possible without the financial support of the University of Manitoba via Dr. Ahmed Shalaby. Also, I would like to thank Manitoba Department of Infrastructure (MI) for funding the experimental culverts project.

Last but not least, words would not describe my gratitude towards my father, my mother, and my brothers for their unconditional love and support despite the long distance.

Contributions to literature

Part of this manuscript can be found in conference proceedings and scientific journals:

- **Moussa, A.**, Kavanagh, L., Shalaby, A., (2018). "Boundary conditions for modeling the ground thermal profile near shallow culverts". Submitted to the **Transportation geotechnics** for publication as an article.

- **Moussa, A.**, Shalaby, A., Kavanagh, L., Maghoul, P. (2018). "'Use of rigid geofoam insulation to mitigate frost heave at shallow culvert installations". Submitted to the **ASCE cold regions engineering** for publication as an article.

- **Moussa, A.**, Kavanagh, L., Shalaby, A., (2018). "Evaluating pavement surface temperature prediction models in determining soil thermal profile below pavement surface in cold regions". **Transportation Research Board 97th Annual meeting**, Washington D.C. (No. 18-05078).

- **Moussa, A.**, Shalaby, A., Kavanagh, L., Maghoul, P. (2018). "Ground thermal profile and frost depth in the vicinity of through-grade culverts". **Geohazards 7** Conference, Canmore, AB.

- Kavanagh, L., Shalaby, A., **Moussa, A**., & Sparrow, S. (2017). "Analysis of measured strains in geotextile-reinforced clay backfill over through-grade culverts in cold climates". **Transportation Research Board 96th Annual meeting**, Washington D.C. (No. 17-06559).

- Kavanagh, L., **Moussa, A.**, Shalaby, A. (2018). *Recommendations for Innovative Options for Culvert Installation to Mitigate Bumps and Depressions at Through-Grade Culverts in Manitoba: Demonstration Project PTH 68. Submitted to Manitoba Department of Infrastructure.* Technical Report.

Dedication

To the memory of my beloved grandmother

Afaf Nasr

1942-2017

Table of Contents

List of Tables

List of Figures

Acronym

1-D	One Dimensional
2-D	Two Dimensional
AASHTO	American Association of State Highway and Transportation Officials
BWP	Between the Wheel Path
C-SHRP	Canadian Strategic Highway Research Program
EICM	Enhanced Integrated Climatic Model
FHWA	Federal Highway Administration
GPR	Ground Penetrating Radar
LTPP	Long-Term Pavement Performance
MHIS	Ministry of Highways and Infrastructure in Saskatchewan
MI	Manitoba Department of Infrastructure
MnDOT	Minnesota Department of Transportation
NYSDOT	New York State Department of Transportation
ODOT	Ohio Department of Transportation
OWP	On the Wheel Path
PCC	Portland Cement Concrete

PTH-68	Provincial Trunk Highway
RMSE	Root Mean Square Error
SHRP	Strategic Highway Research Program

Chapter 1: Introduction

1.1. General overview

The road roughness of through-grade culverts is a result of the nonuniform freezing and thawing cycles. The nonuniform freezing and thawing cycles are resulting from the thermal disturbance of the ground resulting from the culvert barrels, which act as heat source in the summer, and as a cooling source in the winter. Innovative solutions are considered in this study through an experimental program involving five instrumented culvert sites, to evaluate the effect of the type of backfill, the depth of cover, the use of geosynthetics, the use of thermal insulation on reducing the thermal disruption resulting from the culvert barrels and the corresponding deformation in the road (road roughness).

Through-grade culverts are structures built below the road level to convey water and fish without interrupting the integrity of the traffic on highway or railway (NYSDOT, 2006). The Ohio Department of Transportation (ODOT) (2017) added that the culverts are conduits with inlet open to air not to be confused with the storm sewer. In cold regions, culverts are important during the spring to discharge the large amount of melting snow without washing away the road embankment. This explains the large number of culverts in the cold regions. For instance, the Manitoba department of Infrastructure (MI) is responsible for more than 50,000 culverts across the Province of Manitoba (MI, 2017), and the Ministry of Highways and Infrastructure of Saskatchewan (MHIS) is responsible for more than 62,000 culverts across the province (MHIS, 2016).

The roadways over culverts in cold regions experience severe pavement distresses. The soil thermal disturbance from the shallow culverts severely impacts the pavement surface roughness

(Kavanagh et. al., 2018). Since the subgrade materials are exposed to negative temperatures during winter through the culverts' walls, the ground thermal regime is disturbed underneath the pavement surface. This increases the non-uniform frost heave during winter as well as thaw settlement in spring (Nixon, 1978). The thermal disturbance caused by the culvert openings creates noticeable irregularity in the roadway surface over culverts affecting the ride comfort and the safety of road users at high speeds (Kavanagh et. al., 2017). Therefore, to mitigate road roughness, the heat exchange between the culvert openings and subgrade (or backfill) materials must be reduced. The application of thermal insulation in the soil affects the depth of the freezing isotherm (Andersland and Ladanyi, 2004; and Farouki, 1992), and reduce the non-uniform frost actions near culverts.

1.2. Objectives

The objectives of this thesis are to

- Evaluate the effect of using clay and granular backfill materials, depth of culvert, and the use of geosynthetics (e.g. rigid insulation, geotextile, and geogrids) on the road roughness over through-grade culverts in cold regions through a field experiment.
- Evaluate the accuracy of the pavement temperature prediction methods when used as the pavement surface boundary conditions in a 2-D thermal numerical model.
- Calibrate and validate a 2-D thermal numerical model using the field data collected from the instrumented culvert sites (The field experiment).
- Determine the ground thermal profile and the frost depth at the vicinity of through-grade culverts.
- Determine the effective use of rigid thermal insulation near culverts to reduce the road roughness over through-grade culverts.

1.3. Methodology

The approach in achieving the objectives of the study is to construct culvert sites with different designs to reduce the road roughness over through-grade culverts. The sites are instrumented with thermistors and strain gauges to monitor the thermal changes in soil near the culvert barrels and strains in the geosynthetics (Chapter 3). Ground Penetrating Radar (GPR) scans are performed over the culverts to determine the deformations under the road surface. The temperature data collected from the sites are used to calibrate and validate 2-D thermal numerical model (Chapter 4). The 2-D thermal numerical model is used to predict the thermal changes, and the frost depth in the soil surrounding the culvert barrels along with a parametric study on the effective use of thermal insulation near culverts (Chapter 5).

1.4. Organization of the thesis

This thesis covers the research done over two years and has been organized (Figure *1.1*) as follows:

Chapter 2: Literature review

This chapter summarizes the basic information, the fundamentals, and the related works covered to develop better understanding to the culvert design problems and paves the way to find the appropriate approach to the solution.

Chapter 3: Design of the field experiment, monitoring and testing programs

The test sites, design, location, soil properties, the distribution of the instrumentation in the sites, and the field testing is presented in Chapter 3.

Chapter 4: Numerical Modeling, boundary conditions, and validation

The reason behind developing a numerical model, the input parameters, challenges in building the model, and validating the predictions with the field data are discussed in this chapter.

Chapter 5: Application of the numerical model

This chapter focuses on describing the numerical model, boundary conditions, and governing equations used in modeling culvert-related engineering applications, such as predicting the ground thermal profile and frost depth at the vicinity of culverts, and the effective placement of geofoam thermal insulation and recommended applications.

Chapter 6: Summary, conclusions, and recommendations

Chapter 6 is the summary of the work done in this research, the conclusions, and the recommendations based on the findings from the culvert test sites and the numerical models. Also, this chapter suggests extended works and future researches to be covered.

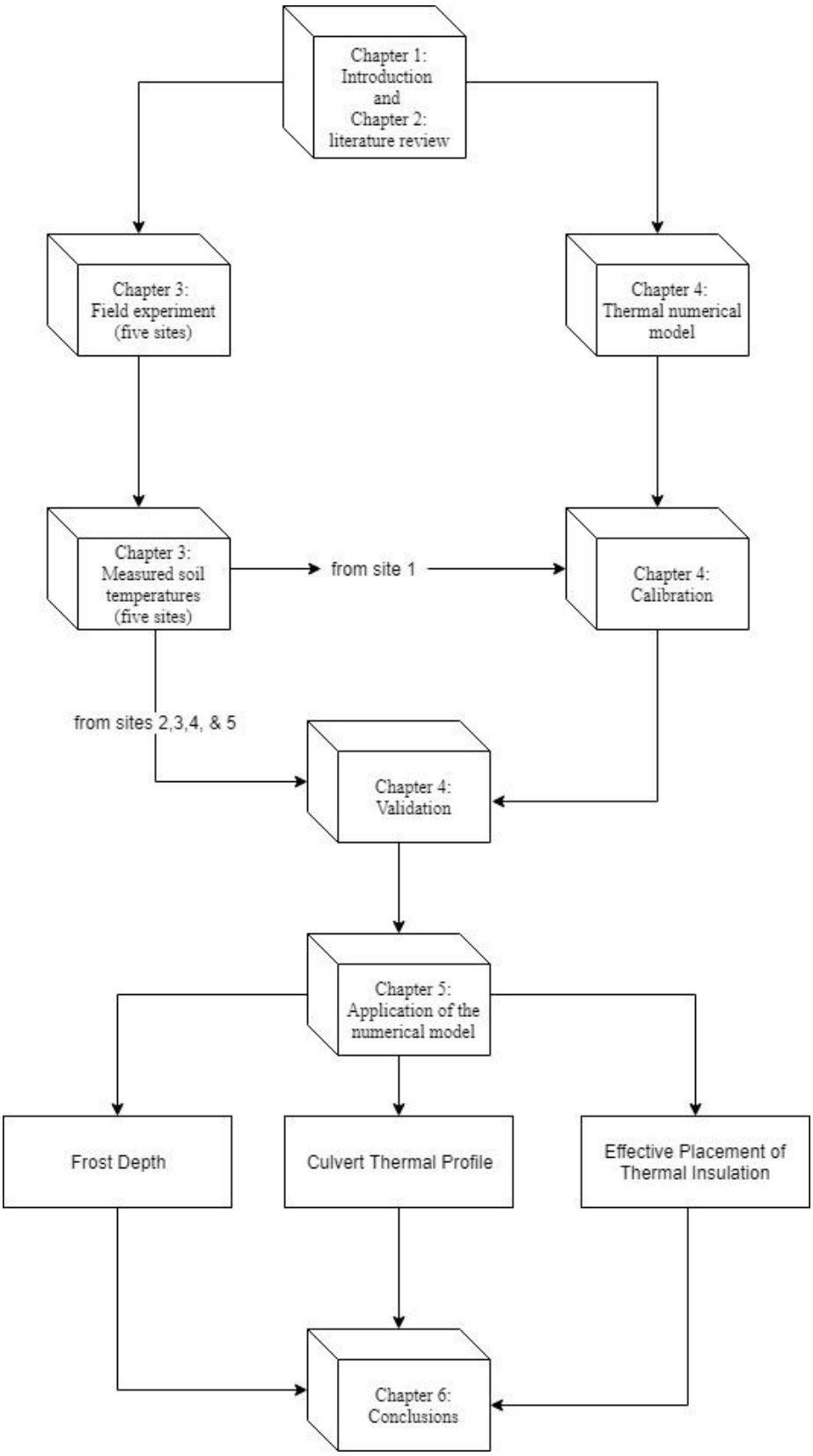

Figure 1.1:Breakdown of the thesis organization

Chapter 2: Literature review

2.1. Frozen ground and the active layer

The behavior of the ground changes at different temperatures and moisture contents. Frozen ground is defined as any soil with temperature lower than the freezing point of the water regardless of any other mechanical or thermal properties of the soil (e.g. density, porosity, latent heat, water content) (Andersland and Ladanyi, 2004). Frozen water within the soil body acts as a bonding agent or cementitious material between soil particles increasing the overall soil strength (Nishimura et. al., 2009; Zhang and Michalowski, 2015). Conversely, the thawing water within the soil body reduces the short-term strength of the soil due to the excessive increase in the soil pore-water pressure (Hinkel et. al., 2003; Shoop et. al., 2008). The ground in cold regions is divided to the active layer zone, also known as the seasonally frozen ground, and the permafrost zone. The active layer is the layer in the soil that experiences variation in the soil temperature between the freezing and the thawing temperatures depending on the season, while the permafrost are regions within the ground that have temperature lower than the freezing temperature ($0^{o}C$) continuously for a period of two or more successive years (Andersland and Ladanyi, 2004). Most of the geotechnical problems in cold regions occur in the active layer (Konrad and Lemieux, 2005).

2.2. Frost Heave

Frost heave occurs mainly in silt and clay soil due to the migration of ground water to the freezing isotherm (Konrad and Shen, 1996). Frost heave occurs as a result of the ice lenses formed during the migration of water to the freezing front within the soil body (Black and Hardenberg, 1991; Michalowski and Zhu, 2007). The disturbance in the soil thermal profile caused by the

culvert openings creates differential frost heave (Kavanagh and Shalaby, 2017) due to the nonuniform frost action, which creates bumps and sags on the roadway over a culvert.

2.3. Heat transfer fundamentals and assumptions

Heat transfer is the transfer of thermal energy though a medium (solid, liquid or gas) or between two different mediums, either in contact or apart from each other, due to the existence of a temperature gradient (Bergman et. al., 2011). Heat is transferred in three modes, conduction, convection, and radiation. The heat transfer modes are governed by the molecular distance between the medium's particles, the interaction between two mediums in different physical states, and the radiative properties of a material.

2.3.1. Conduction

Conduction is the heat transferred between two solid bodies in contact in which heat flows from the body with the higher temperature to the body with the lower temperature (Bergman et. al., 2011). The amount of energy being transferred by conduction per unit area in three-dimensions is governed by the Fourier's law Eq.(2.1).

$$q''_{Conduction} = -k\nabla T = -k\left(i\frac{\partial T}{\partial x} + j\frac{\partial T}{\partial y} + \mathrm{k}\frac{\partial T}{\partial z}\right) \quad (2.1)$$

where ∇ is the thermal gradient; and $i, j,$ k are the unit vectors in x, y and z-direction respectively.

2.3.2. Convection

Convection is defined as the heat transfer mode during which the thermal gradient that occurs between a stationary body and a moving fluid (e.g. liquids and gases) (Bergman et. al., 2011). Convective heat transfer is concerned with the transport of the thermal energy resulting from the kinetic energy of the body of fluid as a bulk, while conductive heat transfer is concerned with the energy transport due to the kinetic energy of the molecules (Andersland and Ladanyi, 2004). Convective heat transfer is governed by the speed and the temperature of the fluid and the temperature of the stationary surface as shown in Eq.(2.2).

$$q''_{Convection} = h\left(T_{Surface} - T_{\infty}\right) \tag{2.2}$$

where;

$q''_{\_Convection}$ is the heat transfer rate (heat flux) due to convection in W/m^2;

h is convection coefficient in $W/m^2.K$, which has typical values range from 2 to 25 $W/m^2.K$ for gases and from 50 to 1000 $W/m^2.K$ for liquids (Bergman et. al., 2011); and

$T_{Surface}$ is surface temperature, and T_{∞} is the temperature of fluid in motion.

2.3.3. Radiation

Radiation is another heat transfer mode during which thermal energy is emitted between two bodies with different temperatures and with no direct contact in the form of electromagnetic energy waves and in the absence of cooperative medium (e.g. the sun) Eq.(2.3) (Bergman et. al., 2011).

$$q''_{Radiation} = \varepsilon\sigma\left(T^4_{Surafce} - T^4_{Surrounding}\right) \quad (2.3)$$

where,

$q''_{\_Radiation}$ is the heat transfer rate (heat flux) due to radiation in W/m^2;

ε is the radiative property of surface which is known as *emissivity* with typical values range of 0.0 to 1.0;

σ is the Stefan Boltzmann constant with typical value of $5.67 * 10^{-8}\, W/m^2.K^4$;

$T_{Surface}$ is surface temperature; and

$T_{Surrounding}$ is the surrounding temperature, and is equal to zero for objects not surrounded by radiative surface.

2.4. Heat transfer in soil and asphalt pavement

Heat is transferred at the ground surface in three modes, conduction, convection, and radiation. While heat is transferred only by conduction and conviction within the soil body. However, conduction is assumed to be the main mode of heat transfer within the soil body (Zhu & Michalowski, 2005). Kim et. al. (2008) explained that convection within the soil body can be neglected; because the rate at which water migrates through frozen and unfrozen soil is very slow to create convective heat transfer in the soil. However, such assumption is invalid at the ground and the pavement surfaces. The heat transfer at the pavement surface occurs in all the heat transfer modes (Figure *2.1*).

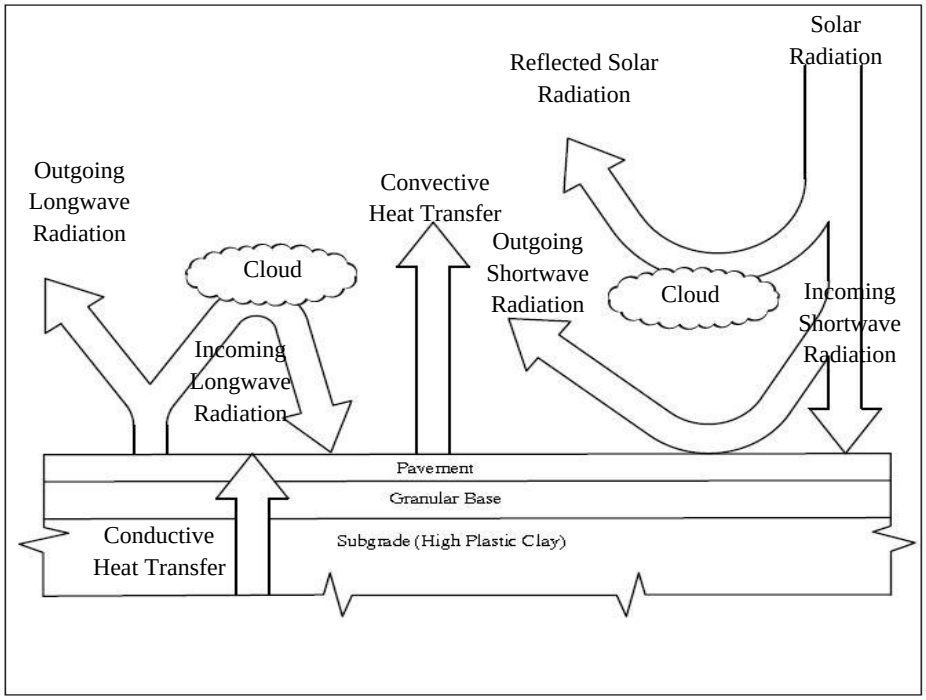

Figure 2.1: Heat transfer and energy balance at pavement surface

For the pavement structure (the asphalt concrete and the granular base), conductive heat transfer takes place within the pavement body and at the interface between the pavement layers and the subgrade. Convective heat transfer takes place at the pavement surface where fluids (e.g. air and water runoff) flow over the road surface. Radiation takes place also at the pavement surface in the form of incoming shortwave solar radiation, incoming long wave radiation (irradiation), outgoing shortwave reflected solar radiation, and outgoing long wave radiation (emission).

The energy balance at the pavement surface along its thickness for transient analysis is defined in Eq.(2.4) (Alavi et. al., 2014).

$$q''_{is} + q''_{il} - q''_{os} - q''_{ol} - q''_{conv} + q''_{cond} = H\left(\rho_{pavement}\, c_{pavement}\right)\frac{\partial T}{\partial t} \quad (2.4)$$

where,

q''_{is} is the heat flux due to outgoing shortwave radiation in $Watt/m^2$;

q''_{il} is the heat flux due to incoming longwave radiation in $Watt/m^2$;

q''_{os} is the heat flux due to outgoing shortwave radiation in $Watt/m^2$;

q''_{ol} is the heat flux due to outgoing longwave radiation in $Watt/m^2$;

q''_{conv} is the heat flux due to convection in $Watt/m^2$;

q''_{cond} is heat flux due to conduction in $Watt/m^2$;

H is the pavement thickness in meters;

$\rho_{pavement}$ is the dry density of asphalt concrete in kg/m^3; and

$c_{pavement}$ is the specific heat of asphalt concrete in $J/kg.^o\,C$.

In order to study the thermal profile in the soil subject to seasonal temperature variations at the ground surface as well as a thermal source due to the culverts openings in the ground, a transient conductive heat transfer analysis by considering the effect of pore-water phase change is carried out:

$$c_{app}\frac{\partial T}{\partial t} - \nabla . q''_{Conduction} = 0 \quad (2.5)$$

$$c_{app} = \rho c_p + \rho_w L_f \frac{\partial w_u}{\partial T} \quad (2.6)$$

$$\rho = \rho_s(1-n) + \rho_u\, w_u + \rho_f w_f \quad (2.7)$$

where c_{app} is the apparent volumetric heat capacity of soil in which ρ is the bulk density in kg/m^3;

c_p is the specific heat capacity of soil at constant pressure in $J/(kg.K)$;

ρ_w is the density of water in kg/m^3;

$L_f = 333kJ/kg$ is the latent heat of fusion for water; and

w_u is the unfrozen volumetric water content (decimals);

T is temperature of the soil in Kelvin.

n is the porosity;

w_u, w_f are the volumetric contents of unfrozen water, and ice, respectively; and

ρ_u, ρ_f are the unfrozen and the frozen water contents, respectively, and are considered equal to 1000 kg/m^3

Since the problem is considered as fully saturated, meaning that all voids are filled with water, the ice content may be expressed as the difference between the porosity and the unfrozen water content, i.e. $w_f = n - w_u$. The unfrozen water content in the frozen soil is defined as follows (Tice et. al., 1976)

$$w_u = \alpha T^{\beta} \tag{2.8}$$

where, T is the soil temperature in ^{o}C; and α, β are soil constants equals to 21.1, and -0.238, respectively.

2.5. Thermal properties of soil and asphalt pavement

The material properties required for the thermal numerical model are the soil density, the thermal conductivity, specific heat, and the latent heat. Several studies were done over various types of soil with various moisture contents at different temperatures to develop empirical equations that help in determining the thermal properties of the soil such as the work of Kersten (1949); McGaw (1969); and Johansen (1975). For this study, the methods considered in determining the thermal properties of soil are based on the recommendations of Farouki (1982).

2.5.1. Thermal conductivity in soil

Thermal conductivity of soils is the ability of the heat flux to transport through the soil body by conduction under the influence of thermal gradient (Farouki, 1982) as expressed in Eq.(2.8),

$$k = \frac{q''_{cond} \cdot \ell}{T_2 - T_1} \tag{2.9}$$

where,

k is the thermal conductivity within soil body in $W/m.K$;

q''_{cond} is conductive heat flux and can be determined by $q''_{cond} = \frac{Q}{A}$ where Q is the heat flow in watt and A is cross-sectional area normal to the direction of heat flow in square meters; and

$(T_2 - T_1)$ is the thermal gradient in kelvin between two points at distance ℓ in meters.

The accurate determination of the thermal conductivity of soil has been the concern of many researchers; because it is the main thermal property of the soil that have major effect on the conductive heat transfer within the soil body; therefore, different equations were developed to determine the effective thermal conductivity of the soil. Most of these methods can be divided into analytical and empirical methods. However, empirical methods are widely used (Johansen, 1975).

The thermal conductivity of a porous medium, such as soil, is dependent on the soil density, moisture content, and soil temperature; therefore, changes in soil temperature are accompanied by changes in soil moisture content, which influence the thermal conductivity of soil (Harlan and Nixon, 1978; Johansen, 1975; and Côté and Konrad, 2005).

The thermal conductivity of soil cannot be determined using Eq.(2.9), because soils are composed of several components and materials varying in their chemical and physical properties; therefore, several models were developed to determine the effective thermal conductivity (k_{eff}) as a representation of the overall thermal conductivities of the soil components combined.

The empirical equations for granular soils Eq. (2.11 & 2.13) and fine soils Eq. (2.10 & 2.12) in frozen and unfrozen states were developed by Kersten (1949) are used to determine the thermal properties of the soil for this study.

Unfrozen:

$$k_{u_{clay}} = 0.1442(0.9\log(w) - 0.2)10^{0.6243\rho_d} \qquad for \qquad w \geq 7\% \qquad (2.10)$$

$$k_{u_{granular}} = 0.1442(0.7\log(w) + 0.4)10^{0.6243\rho_d} \qquad (2.11)$$

Frozen:

$$k_{f_{clay}} = 0.001442(10)^{0.373\gamma_d} + 0.01226w(10)^{0.4994\rho_d} \qquad for \qquad w \geq 7\% \qquad (2.12)$$

$$k_{f_{granular}} = 0.01096(10)^{0.8116\gamma_d} + 0.00461w(10)^{0.9115\rho_d} \qquad (2.13)$$

where,

k is the thermal conductivity in $Watt/m.^o\,C$; the subscripts u and f are corresponding to unfrozen and frozen state of soil respectively;
w is the moisture content, and
ρ_d is the dry density of soil in g/cm^3.

Kersten's method accounts for the effect of moisture content and dry soil density on the thermal conductivity of soil. According to the formulation from Eq.(2.10) throughout Eq.(2.13), the soil dry density and the water content are the only soil parameters required to calculate the soil thermal conductivity; therefore, Kersten's equations are widely used in civil engineering appliactions (Andersland and Ladanyi, 2004; Doré and Zubeck, 2009). Farouki (1982) stated that Kersten's equations have variations up to $\pm 25\%$ from the measured thermal conductivities; however, they are still valid for engineering applications.

2.5.2. Heat capacity and specific heat

The specific heat (c_m) is defined as the amount of thermal energy per unit mass required to change the temperature of a matter by one degree (Andersland and Ladanyi, 2004). The heat capacity and the specific heat of frozen and unfrozen soil can be calculated using Eq.(2.14) to Eq.(2.16) (Ladanyi, 1996).

$$c_{vu} = \frac{\rho_d}{\rho_w}(0.17 + w)c_{vw} \tag{2.14}$$

$$c_{vf} = \frac{\rho_d}{\rho_w}\left(0.17 + w_u + 0.5w_f\right)c_{vw} \tag{2.15}$$

$$c_m = \frac{c_{vf}}{\rho_d\ (1 + w)} \tag{2.16}$$

where,

c_{vu}, c_{vf} are the volumetric heat capacity for unfrozen and frozen soil respectively in $MJ/(m^3.^o\ C)$;

ρ_d, ρ_w are the densities of dry soil and water respectively in kg/m^3; and

c_{vw} is the volumetric heat capacity of water typically 4.187 $MJ/(m^3.^o\ C)$; c_m is the specific heat in $MJ/(kg.^o\ C)$;

2.5.3. Latent heat of fusion

The latent heat of fusion Eq.(2.17) is defined as the amount of energy required to change the physical state of water (Andersland and Ladanyi, 2004). The latent heat is not a soil property; however, it affects the heat transfer of materials experiencing phase change (e.g. water). Since the study of the thermal behavior of soil during freezing and thawing is a major part of the analysis, latent heat of fusion is considered.

$$L = \rho_d L'(w - w_u) \quad (2.17)$$

where,

L is the volumetric latent heat of fusion in kJ/m^3;

L' is the mass latent heat for water at 0^oC which equals to 333.7 kJ/kg;

ρ_d is the dry density of soil in kg/m^3; and

w is the total frozen and unfrozen moisture contents in the soil; and w_u is the unfrozen moisture content in the frozen soil.

2.5.4. Thermal diffusivity

The thermal behavior of soil in the steady state condition is governed by the thermal conductivity, while in the transient condition the thermal behavior is governed by the rate of the change between the thermal conductivity and the heat capacity per unit volume, which is known as thermal diffusivity (α). The thermal diffusivity is the ratio of thermal conductivity and heat capacity per unit volume Eq.(2.18) (Andersland and Ladanyi, 2004). Materials with high thermal diffusivity tend to have high rate of change of temperature with time.

$$\alpha_u = \frac{k}{c_v} \quad (2.18)$$

where,

α_u is the thermal diffusivity in m^2/s;

k is the thermal conductivity in $J/s.m.^o C$; and

c_v is the volumetric heat capacity in $J/m^3.^o C$.

Chapter 3: Design of field experiment, monitoring, and testing program

3.1. Sites location and overview

The study consists of five culvert sites (Figure *3.1*). Each site consists of two circular concrete culverts buried under granular or clay backfill. The sites have road structure of 100 mm asphalt layer and 525 mm thick of granular base rest over the culvert backfill. The sites vary in the diameter of the culvert barrels, type of the backfill material, the rigid insulation, the geosynthetics, and the depth of cover, which is measured from road surface to the top of the culvert barrels (Figure *3.2* and Table *3-1*). Detailed cross section for each site can be found in Appendix A. All the sites are located within a 10-kilometer long section on the Provincial Trunk Highway – 68 (PTH68), Manitoba, Canada. The foundation soil (subgrade) is a high plastic clay classified as (A-7-6) according to AASHTO soil classification, with liquid limit of 50%, plastic limit of 30%, moisture content of 25%, and dry density of 1657 kg/m^3. The sites are at latitude 51^{o}N in the cold-dry freeze climate zone. A summary of the sites is presented in Table 4.1.

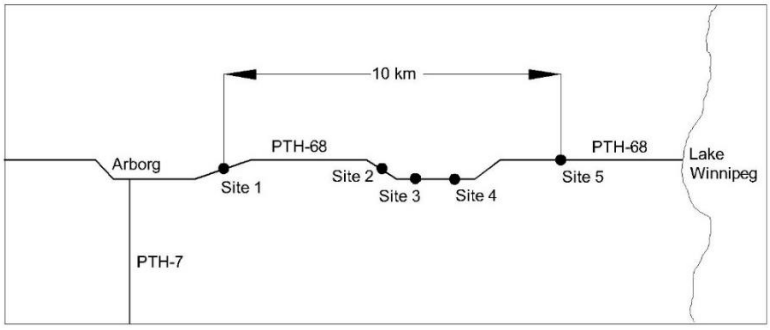

Figure 3.1: Location of the sites in the Province of Manitoba along the Provincial Truck Highway (PTH68)

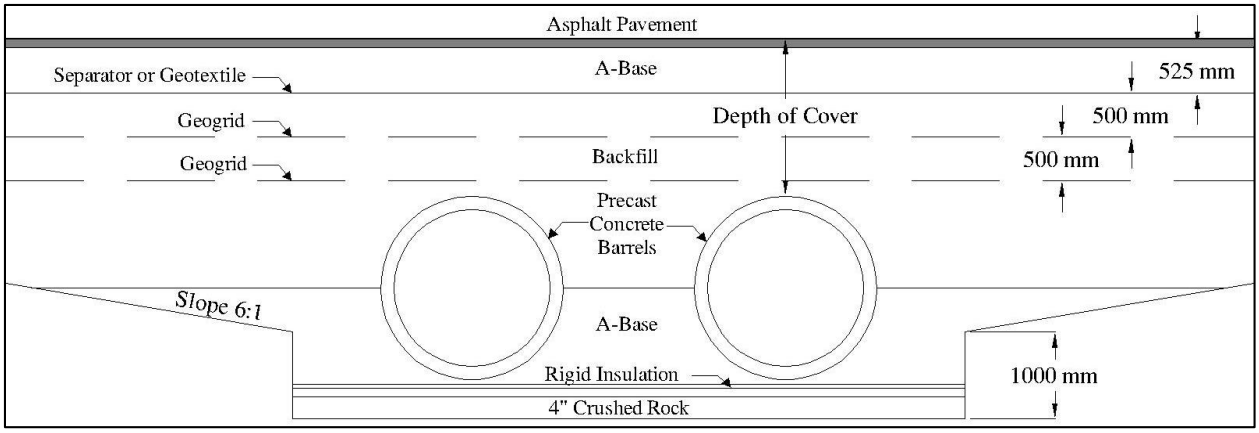

Figure 3.2: Typical Cross section of the sites

Table 3-1: Summary of culvert sites information

Site	Backfill	Culvert Outer Diameter (m)	Distance between barrels (m)	Depth[1] of Cover (m)	Rigid Insulation	Geosynthetics (Geogrid + Geotextile)
1	Clay	1.80	1.5	2.8	NO	NO
2	Granular	1.95	1.5	1.9	NO	NO
3	Granular	1.95	1.5	1.3	YES	NO
4	Clay	2.10	1.5	1.8	NO	YES
5	Clay	1.80	1.5	0.8	YES	NO

[1]Measured from the top of the road surface to the top of the culvert.

3.2. Design of field experiment

Five culvert test sites with different design approaches are considered to reduce the road roughness over culverts. The sites are constructed using the open-cut method with transition slopes 6:1. Non-woven geotextile is placed on the natural soil for separation. A 250mm thick layer of crushed rock is placed on top of the non-woven geotextile. Granular materials are placed on top of the crushed rock layer up to the center line of the culvert barrels to prevent heave right below the culvert. The

backfill on top of the culverts varies between clay and granular materials. Another separator is placed the between the culvert's backfill and the granular road base. Two layers of geogrids are installed at the top of the culvert barrels with 500mm spacing, and a layer of woven geotextile is placed on top of the backfill at site 4 to increase the soil stiffness and to distribute the deformations in the soil over a larger area. Thermal rigid insulation is placed 100mm below the culvert barrels at sites 3 and 5 to prevent frost actions in the natural subgrade below the culverts. Detailed cross section for each site can be found in Appendix A.

3.3. Layout of field instrumentation

Two sets of thermistors U-shaped (*Figure 3.4-a*), and L-shaped (*Figure 3.4-b*) strings are installed at each site around one of the concrete culvert barrels (*Figure 3.3-a*) to monitor the changes in the ground thermal regime in the vicinity of the culvert openings. Additional thermistors are installed in the natural soil away from the culvert barrels to monitor the natural changes in the soil thermal regime away from the culvert effect (*Figure 3.3-b*). A 50 mm rigid thermal insulation is installed below the culverts at sites 3 and 5 (Figure *3.5*) with thermal resistivity of 0.88 K.m²/W (5 ft^2.h.^oF/Btu). The performance of the thermal insulation in reducing the frost penetration below the culverts is evaluated. The depth of the thermistors is illustrated in Figure *3.3-a),* and the depths of rigid insulation measured from the road surface are presented in Table *3-2*). The thermal data is collected on hourly basis using a Campbell Scientific data logger installed at each site, and the data is downloaded periodically (Figure *3.6*) throughout the 2-year study period. Weather station is installed in each of the five sites to measure the air temperature.

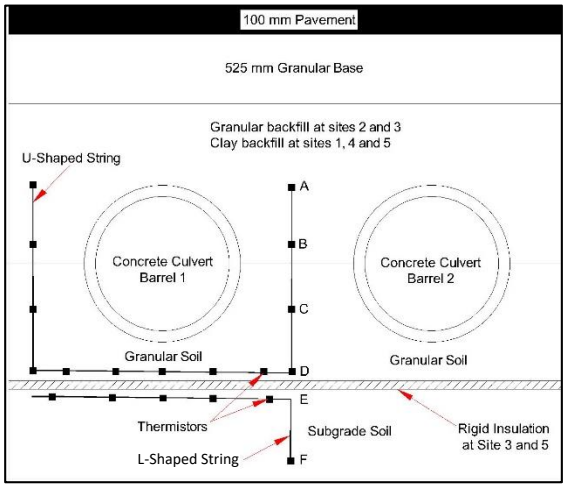

(a) Around Culvert opening

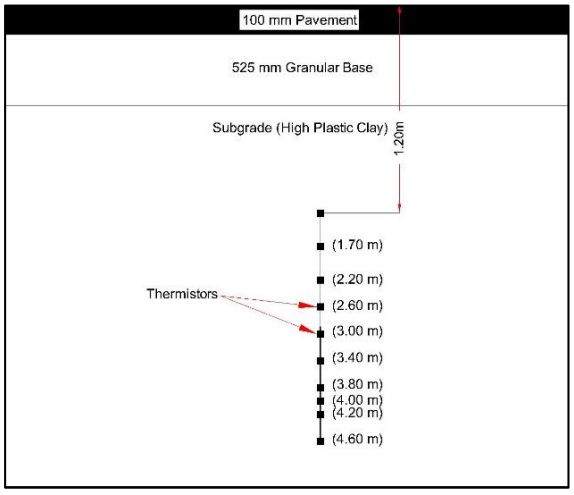

(b) Undisturbed Soil (Away from Culvert openings)

Figure 3.3: General layout of the thermistor strings at the sites

a) U-shaped Thermistor String.

b) L-shaped Thermistor String.

Figure 3.4: Placement of field thermistor instrumentation in site 3.

Table 3-2: Depth of thermistors in each site in meters

	Thermistor No.	Thermistor locations[1] (m)				
		Site 1	Site 2	Site 3	Site 4	Site 5
Thermistor Sensors	A	2.8	2.0	1.4	1.8	0.8
	B	3.4	2.6	2.0	2.4	1.4
	C	4.0	3.2	2.6	3.0	2.0
	D	4.6	3.8	3.3	3.6	2.6
	E	4.7	4.0	3.4	4.0	2.8
	F	5.4	4.6	4.0	4.7	3.4
Depth of Rigid Insulation (m)		-[2]	-	3.35	-	2.7

[1] Measured from the top of the road surface
[2] No Rigid Insulation installed at this site

Figure 3.5: Rigid insulation placement under the culverts at site 3

Figure 3.6: On site data download from the Campbell scientific data-logger

At site 4, strain gauges are attached to the geosynthetics to measure the strains in the geotextile and the geogrid resulting from the deformation of the soil around the culverts. A detailed discussion on the attachment technique of the strain gauges to the geosynthetics can be found in Kavanagh et. al. (2017). Three sets of strain gauges, designated as Cable 1, Cable 2, and Cable 3, are attached to the first two layers of the three geosynthetics layers installed in site 4 (*Figure 3.7-a*). Each cable measures the strains in the longitudinal and the transverse direction. The Cable 1 measures the longitudinal and the transvers strains in the geosynthetics on the Outer Wheel Path (OWP) between the culvert barrels. The Cable 2 measures the strains of the geosynthetics between

the Wheel Path (BWP) at the top of one of the culvert barrels. While Cable 3 measures the strains between the Wheel Path (BWP) at the edge of one of the culvert barrels (*Figure 3.7-a*) and (*Figure 3.7-b*). In addition to the three strain gauge cables, two dummy strain gauge cables, attached to the geosynthetics are protected by a wooden box (*Figure 3.8*), and installed in the site to measure the changes in the strains of the geosynthetics due to temperature effect only (*Figure 3.9*). The strain data are also collected on hourly basis using a scientific Campbell data logger in the site 4.

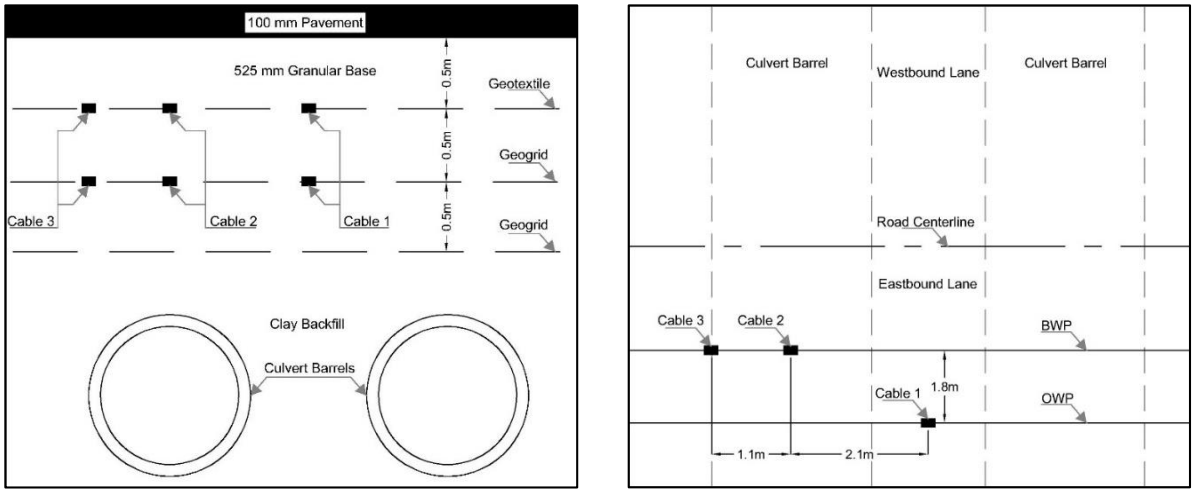

a) Cables location in the profile view b) Cables location in the plan view

Figure 3.7: Cables (Strain gauges) distribution at site 4

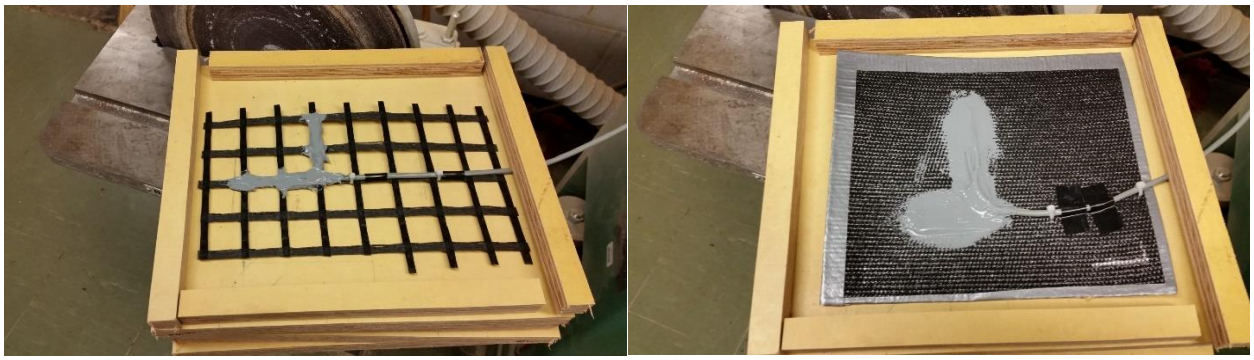

(a) Geogrid (b) Geotextile

Figure 3.8: Dummy strain gauges protected by wooden boxes to measure the strains in the geosynthetics due to the temperature only.

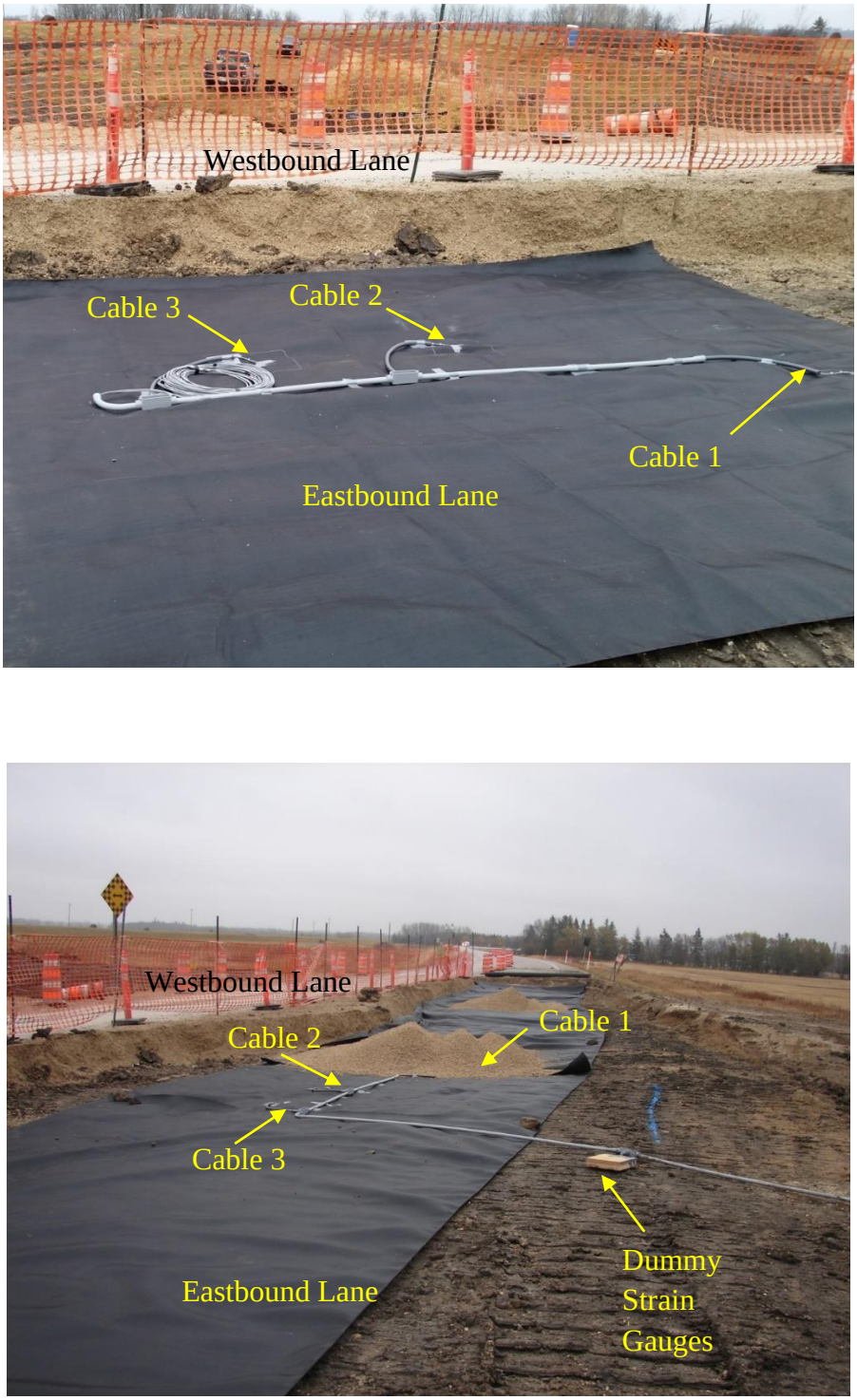

Figure 3.9: Strain gauges distribution in the site

3.4. Ground penetrating Radar (GPR)

Ground Penetrating Radar (GPR) scan are performed in October 2017 over the sites with 2 GHz and 400 MHz antennas (Figure *3.10*) to provide more information on the soil deformations under the road. The 400 MHz antenna penetrate the ground to the depth of 5 m below road surface providing clear information on the soil deformation at the sites with granular backfill (Figure *3.11-a*). However, the 400 MHz antenna could not provide clear information for the sites with the clay backfill (*Figure 3.11-b*). The 2GHz antenna could penetrate the soil to 0.5 m below road surface providing clear information about the asphalt layer thickness for each site (Figure *3.12*).

Figure 3.10: Performing 400MHz GPR scan over Site 4

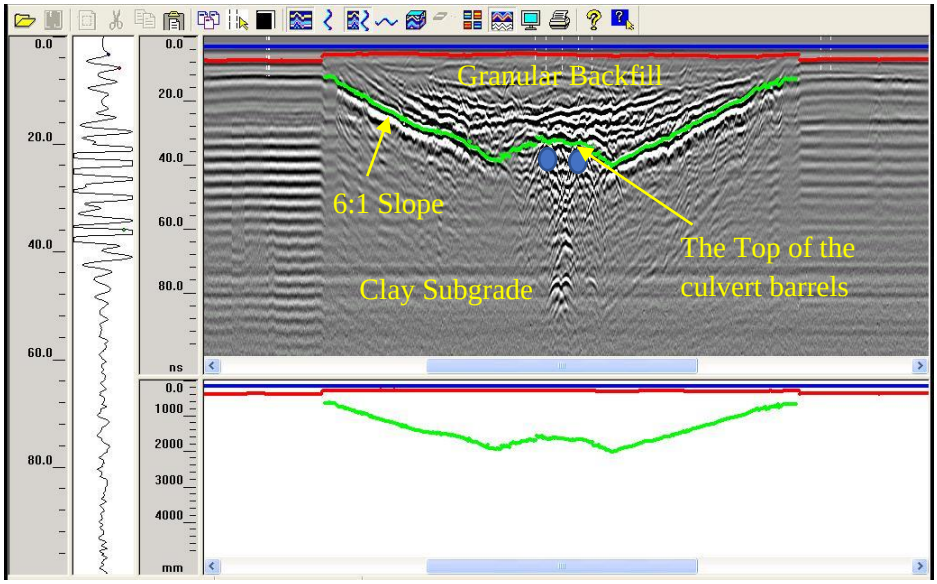

a) Granular backfill (Site 4)

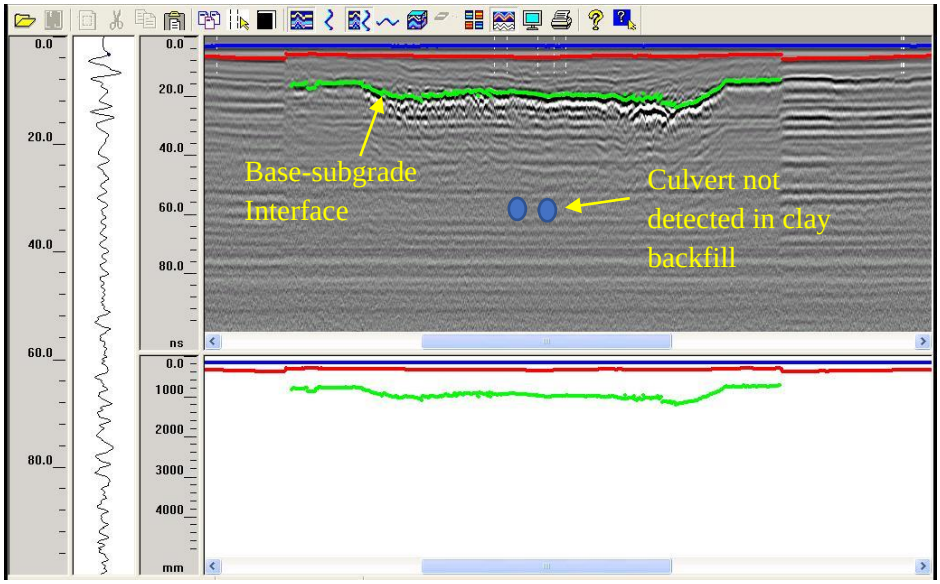

b) Clay Backfill (Site 2)

Figure 3.11: GPR scan with 400 MHz antenna

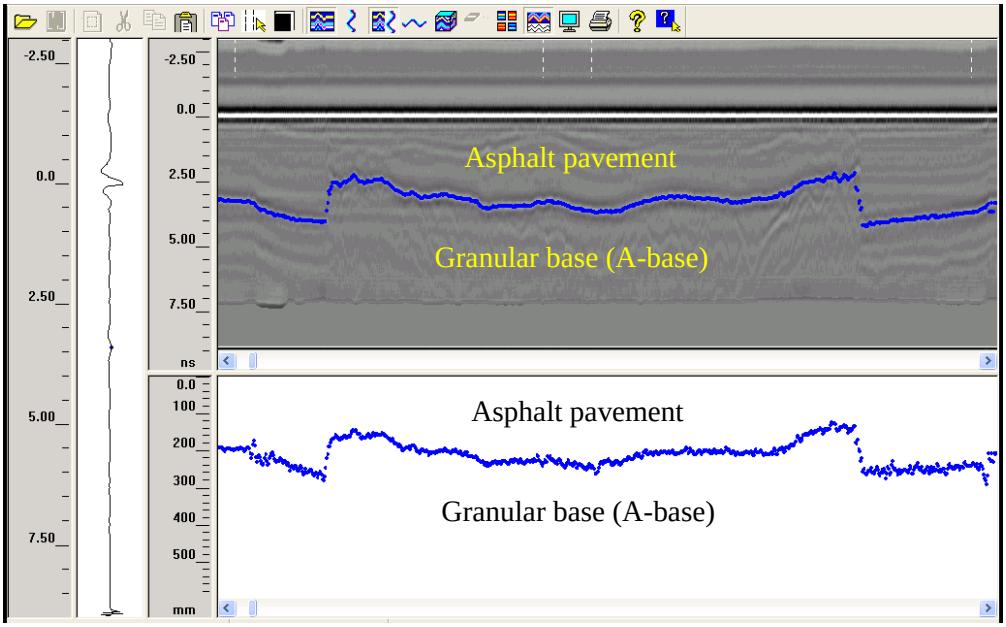

Figure 3.12: GPR scan of site 2 using the 2 MHz antenna

3.5. Findings from the field data

3.5.1. Temperature data

The findings from the field data are based on the analysis of the measured temperatures with time and depth. The measured thermal data of the soil and the air are used to calculate the freezing index of air, the time lag between the freezing in the air and the ground, and the frost depth.

The freezing and thawing indices are the algebraic difference between the consecutive minimum and maximum cumulative air temperature (Andersland and Ladanyi, 2004) (Figure *3.13*) or the summation of the negative daily air temperatures (Doré and Zubeck, 2009) Eq.(4.1). The freezing and thawing indices of air in 2016 and 2017 are calculated (Table *3-3*). The freezing index of air is an important input parameter in the frost depth prediction models in the soil, such as the frost prediction model developed by Argue and Denyes (1974); Selezneva et. al. (2008); and Haitham et. al. (2008).

$$FI = \sum_{0}^{t} -MDAT \tag{4.1}$$

where FI = Freezing Index (ºC.days); MDAT = Mean Daily Air Temperature (ºC)

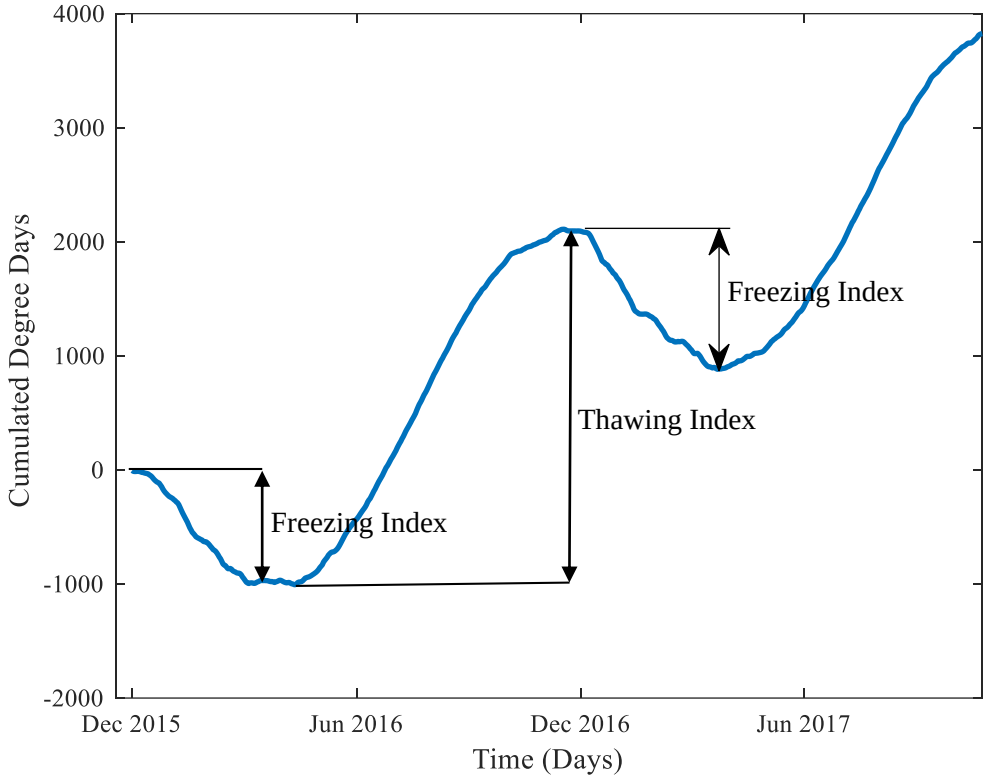

Figure 3.13: Cumulated degree days air temperatures used in determining freezing index for each site

Table 3-3: Calculated Freezing and Thawing Indices

Site	Freezing Index (Air) (ºC.Days)	Thawing Index (Air) (ºC.Days)
Year 1	1010	2950
Year 2	1100	2800

The time lag between the ground at different depths and the air temperatures provides an understanding of the rate at which the frost penetrates the ground. The time lag between ground surface and air temperatures is defined as the difference between the time require for the air and the ground surface to be equal to the mean annual air temperature (Andersland and Ladanyi, 2004). The time lag in this analysis is calculated based on the difference between the time required for the air temperature to reach its lowest temperature and the time required for the ground temperature to reach its lowest temperature at any depth (Figure *3.14*). The time when the lowest air temperature is reached, is determined using the best fit sinusoidal wave (Figure *3.15*).

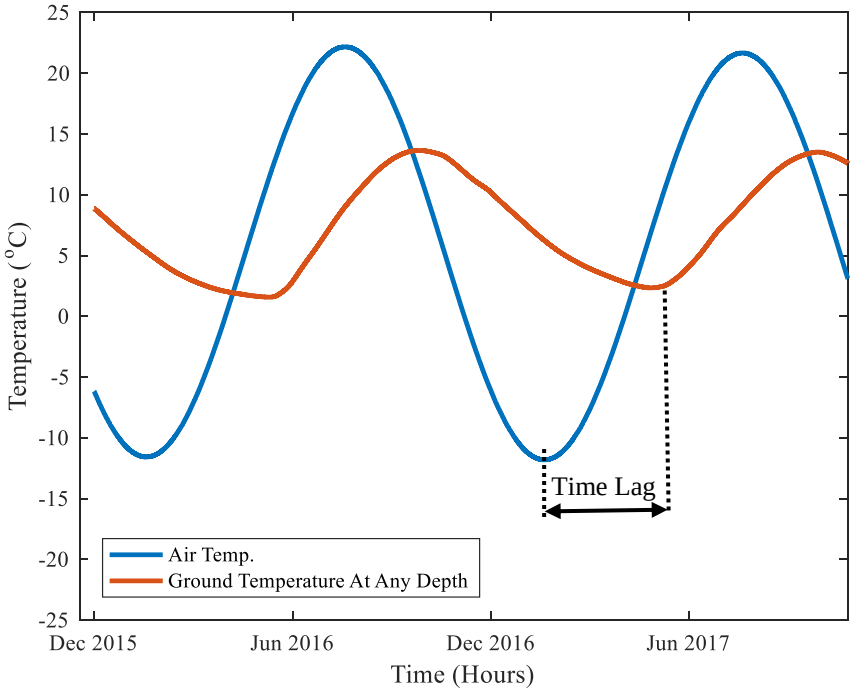

Figure 3.14: Definition of time lag between ground and air temperature

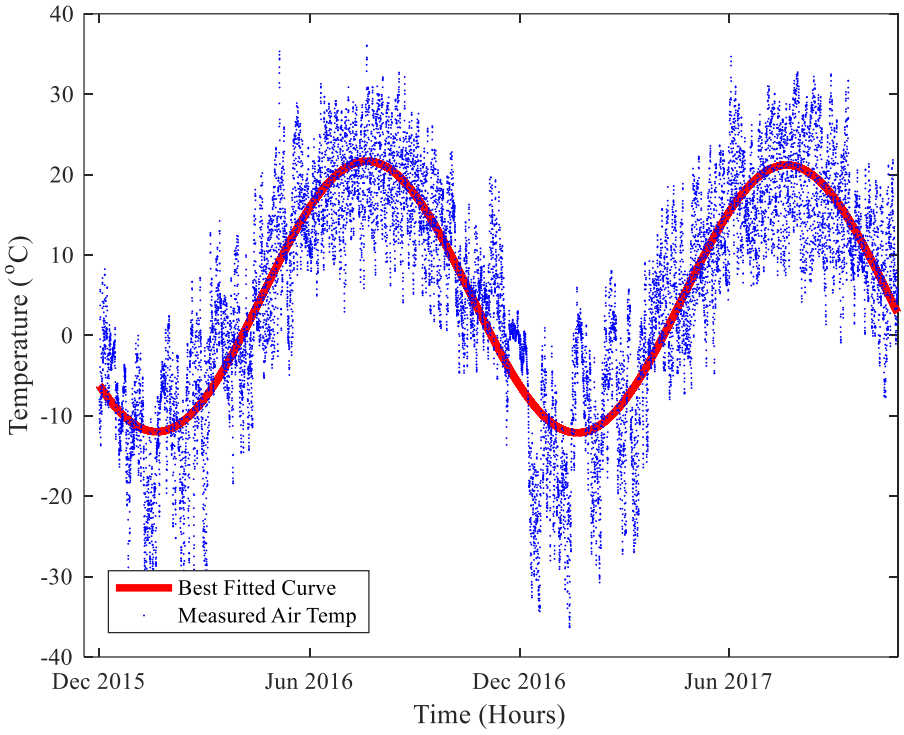

Figure 3.15: Measured hourly air temperature from the on-site weather station

The lag between ground and air temperature is affected by the air freezing index, type of soil, water content, and the thermal disturbance of the ground due to man-made factors such as thermal insulations or culverts or both. The lag between undisturbed clay subgrade at various depths and air measured at culvert site 2 (Figure *3.16*), and between culvert barrels and air temperature (Figure *3.17*) increased with depth. The average lag between air temperature and ground in the 2-year study at 1.2 m below pavement surface is 38 days. The average lag increases up to 105 days at 4.6m below the road surface. This means that when the air temperature dropped below the freezing point with freezing index of 1100 ^{o}C.days the frost depth will reach the depth of 1.2m after 38 days in undisturbed clay subgrade (Table *3-4*). The culvert openings disturbed the

ground thermal regime resulting in changes in the lag between ground and air temperature, and the frost depth at the culvert sections (Table *3-4*).

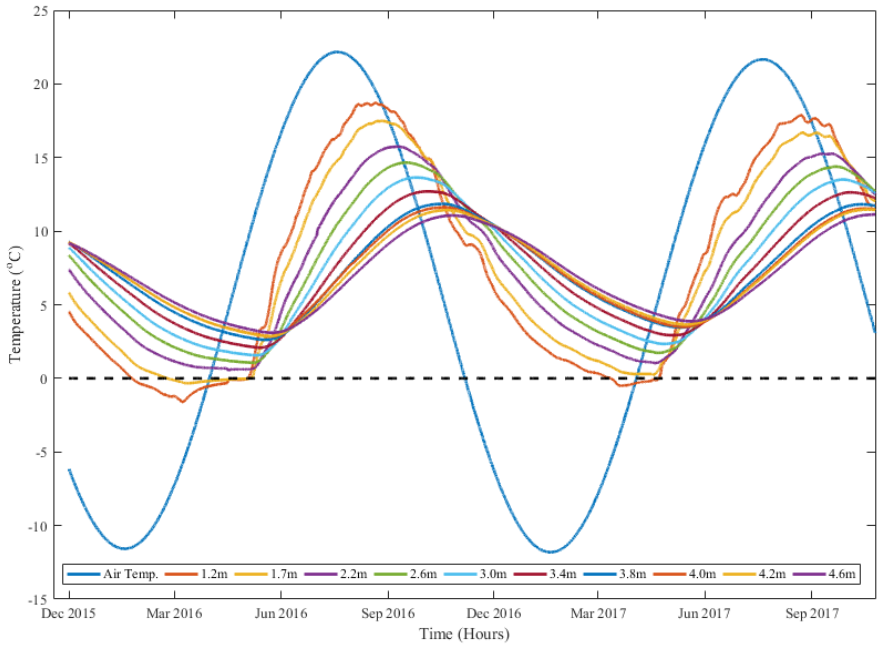

Figure 3.16: The lag between ground and air temperature at various depths in undisturbed clay subgrade away from the culvert barrels.

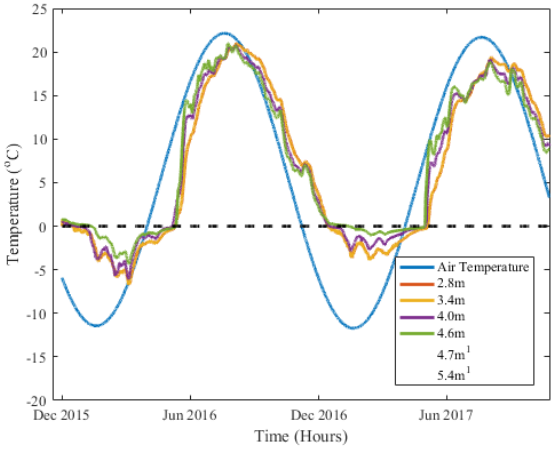

a) Site 1

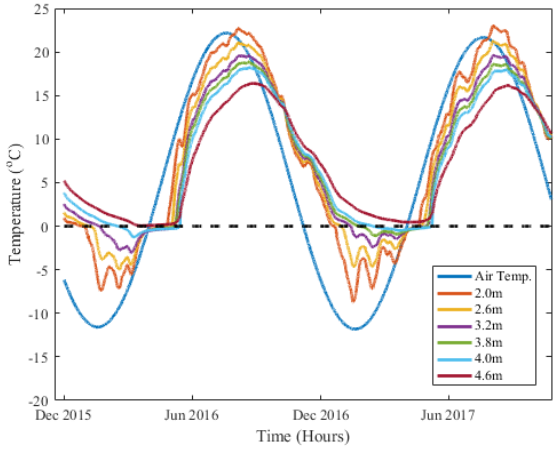

b) Site 2

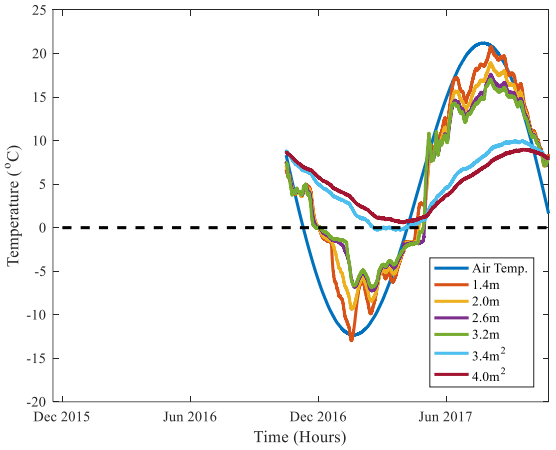

c) Site 3

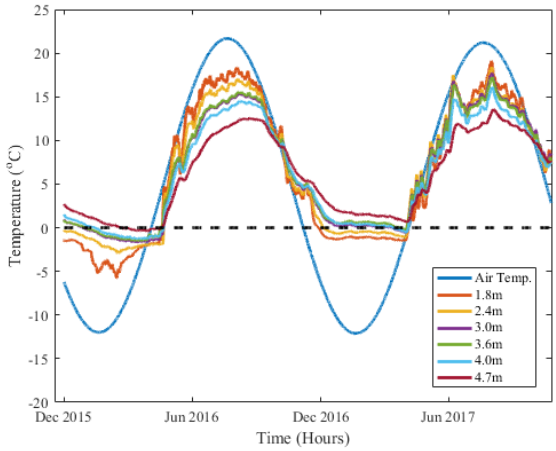

d) Site 4

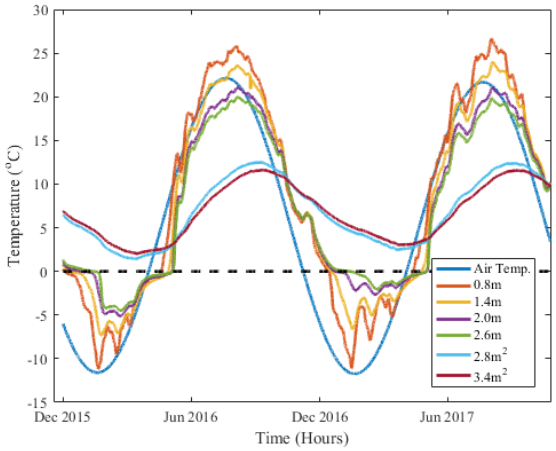

e) Site 5

Figure 3.17: The lag between ground and air temperature at various depths between culvert barrels

Table 3-4: The time lag between soil and air temperature at the sites

Culvert	Backfill	Depth of Thermistor (m)	Lag in year 1 (Days)	Lag in year 2 (Days)	Average Lag (Days)
Undisturbed Natural Soil (Away from Culvert barrels)	Clay[1]	1.2	38	38	38
		1.7	46	45	46
		2.2	57	58	58
		2.6	67	68	68
		3	76	77	77
		3.4	84	86	85
		3.8	94	96	95
		4.0	96	98	97
		4.2	99	101	100
		4.6	104	106	105
Culvert 1	Clay	2.8	24	19	22
		3.4	25	22	24
		4.0	30	28	29
		4.6	38	36	37
		4.7	N/A[2]	N/A	N/A
		5.4	N/A	N/A	N/A
Culvert 2	Granular	2.0	21	17	19
		2.6	23	19	21
		3.2	27	23	25
		3.8	31	28	30
		4.0	37	34	35
		4.6	44	42	43
Culvert 3	Granular	1.4	-	14	14
		2.0	-	17	17
		2.6	-	21	21
		3.2	-	25	25
		3.4	-	51[3]	51
		4.0	-	62[3]	62
Culvert 4	Clay	1.8	7	7	7
		2.4	9	12	11
		3.0	9	9	9
		3.6	15	8	12
		4.0	23	12	18
		4.7	29	20	25
Culvert 5	Clay	0.8	16	12	15
		1.4	21	17	19
		2.0	23	20	22
		2.6	24	21	23
		2.8	48[3]	47[3]	48
		3.4	54[3]	54[3]	54

[1]The clay was undisturbed subgrade; [2]Malfunction sensors at site 2; [3]Lag under the effect of thermal insulation

The data in *Table 3-4)* is plotted in Figure *3.18*) where time lag in days is plotted against depth for all the sites including the undisturbed subgrade. The soil near culverts freezes earlier than the soil away from the culvert openings (the natural undisturbed soil) (Figure *3.18*) due to the cooling coming from the culvert barrels. This means that the frost depth is expected to be greater between culvert barrels than the frost depth at the undisturbed natural subgrade. The time lag the soil at the top and at the bottom of thermal insulation is 30 days.

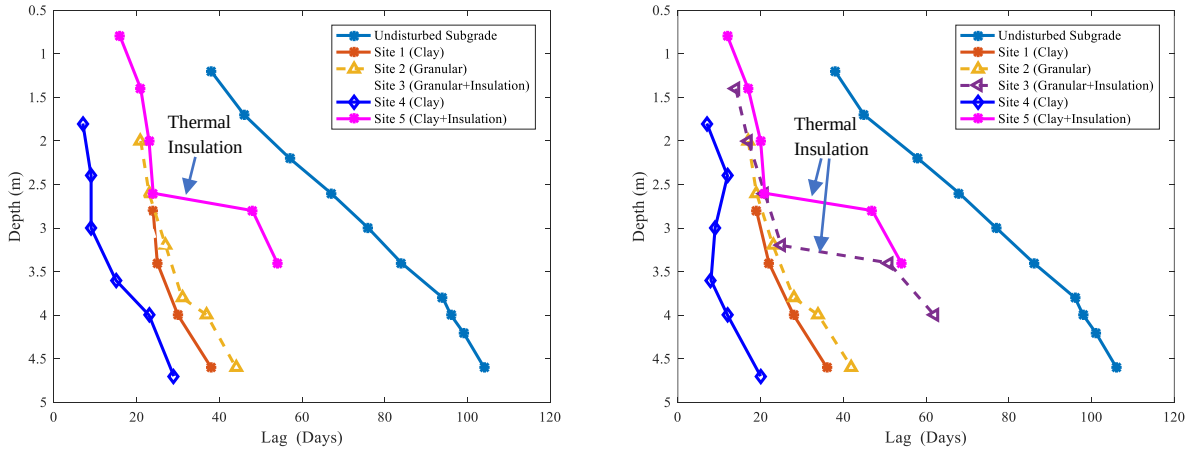

a) 2016 b) 2017

Figure 3.18: Lag time in days between soil and air temperature in 2016 and 2017.

The frost depth at the culvert is greater than the frost depth in the undisturbed natural soil. Frost depth can be estimated by determining the temperature of the freezing isotherm. Andersland and Ladanyi (2004) defines the freezing isotherm as "the interface location between frozen and unfrozen soil". The temperature of the freezing isotherm is -1 ^{o}C (Adamson et. al., 1973; and Trogersen, 1976). While according to Andersland and Ladanyi (2004) the temperature of the freezing isotherm ranges between -1 ^{o}C to 0 ^{o}C. For highway applications, the Long Term Pavement Performance (LTPP) and the Enhanced Integrated Climatic Models (EICM) used by departments of transportation in North America assumes a 0 ^{o}C for freezing isotherm for

determining the frost depth below pavement surface (Selezneva et. al., 2008). This assumption increases the factor of safety in determining the frost penetration depth (Andersland and Ladanyi, 2004). For this study, a freezing isotherm with a 0 ^{o}C is assumed to determine the frost penetration depth (Figure *3.19*). A summary of the measured frost depths was presented in (Table 3.5).

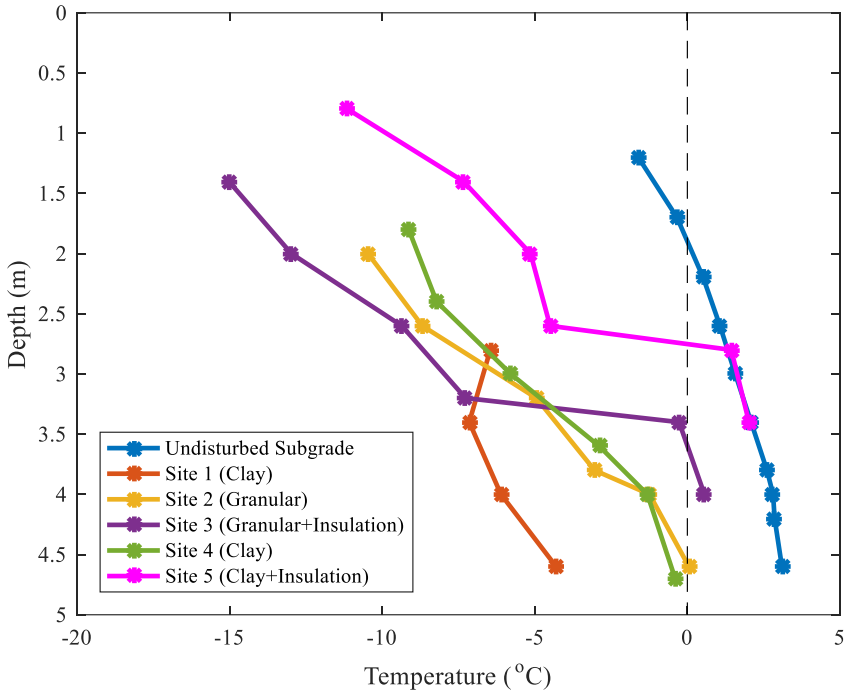

Figure 3.19: Maximum frost penetration depth in each of the site

Table 3-5: Maximum measured frost depths in each site

Site	Depth of Cover (m)	Depth to the bottom of the Culver Barrels (m)	Maximum Frost Depth (m)
Undisturbed Subgrade	-	-	1.9
Site 1	2.8	4.6	N/A[1]
Site 2	1.8	3.9	4.5
Site 3 (Insulated)	1.3	3.3	3.6
Site 4	1.8	3.9	4.8
Site 5 (Insulated)	0.8	2.6	2.8

[1] Sensors Malfunction

3.5.2. Strain data

The strains are divided into thermal strains and load strains. The thermal strains are the strains resulting from the elongation and the shortening of the geosynthetics under the influence of the temperature only, and measured from the Dummy Cables. While, the load strains are measured from in the longitudinal and the transverse directions from Cables 1, 2, and 3 by deducting the thermal strains measured from the Dummy Cables. The strains in the transverse and the longitudinal direction of the geogrid and the geotextile are plotted against time (Figure *3.20*). The transverse strains of the geotextile in Cable 2 and Cable 3 (*Figure 3.20-f*) and (*Figure 3.20-h*) are not considered in the analysis due to strain gauges malfunction.

A dramatic increase in the strains by 0.1% to 0.2% in December of each year, and steep reduction in the strains in April of each year are observed (Figure *3.20*). The permanent strains at the end of the 2-year study are summarized in Table *3-6*). The Table *3-6*) shows that the maximum strains in the geosynthetics occur at the top of the culvert barrels indicating that the deformations due to freezing and thawing cycles at the top of the culvert barrels are greater than other location near the culvert. Also, the data presented in (Table *3-6*) show the geogrid transverse strains are relatively higher than the strains in the longitudinal direction indicating large deformation in the transverse direction of the road (the longitudinal direction of the culvert barrels).

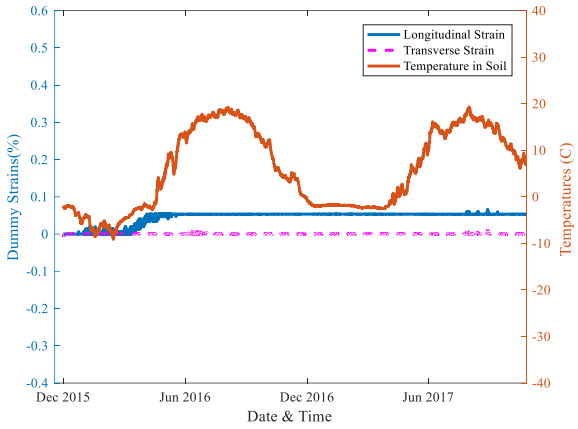

a) Geogrid strains due to temperature

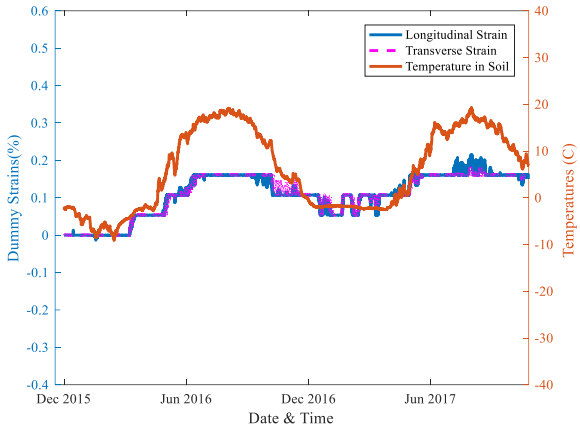

b) Geotextile strains due to temperature

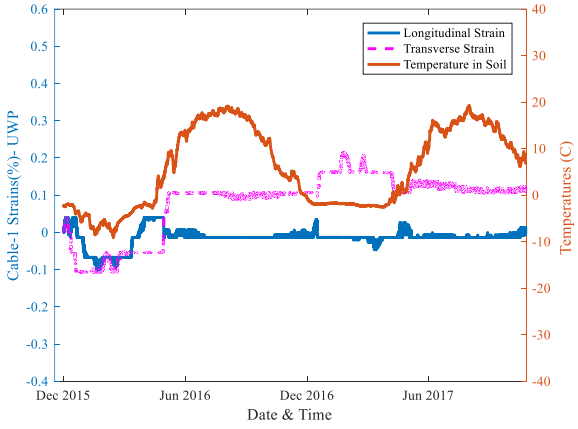

c) Geogrid strains between culvert barrels

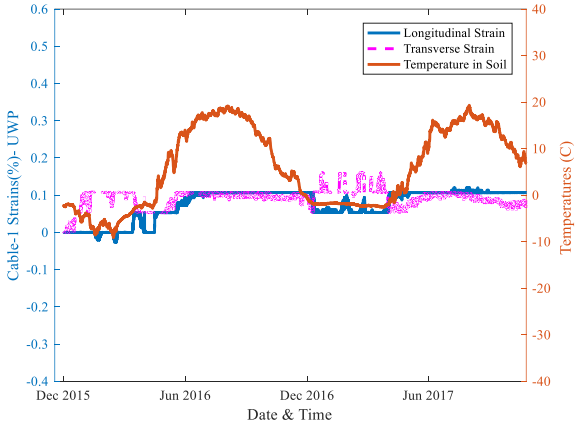

d) Geotextile strains between culvert barrels

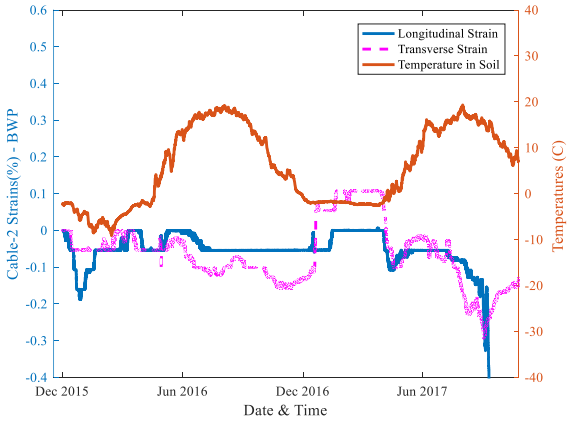

e) Geogrid strains at the top of the culvert barrels

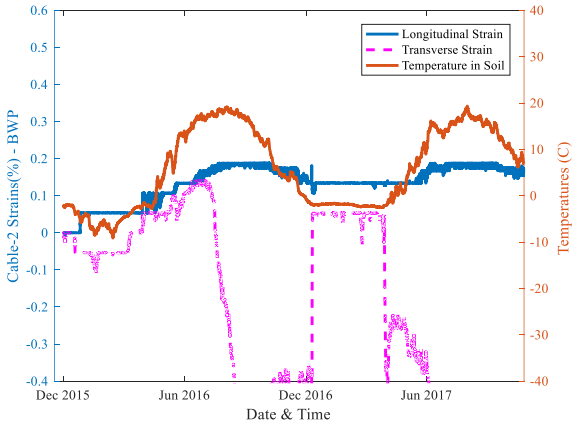

f) Geotextile strains at the top of the culvert barrels (Malfunction in transvers strain gauge)

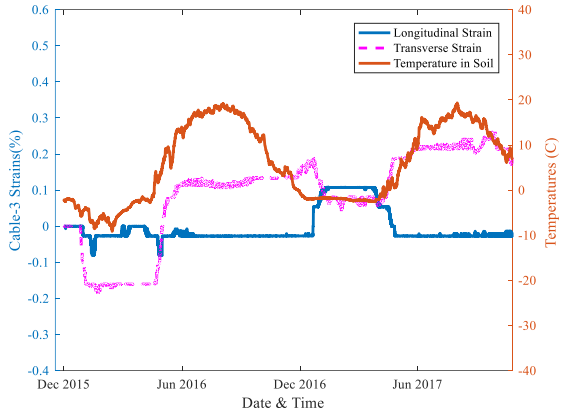

g) Geogrid strains at the edge of the culvert barrels

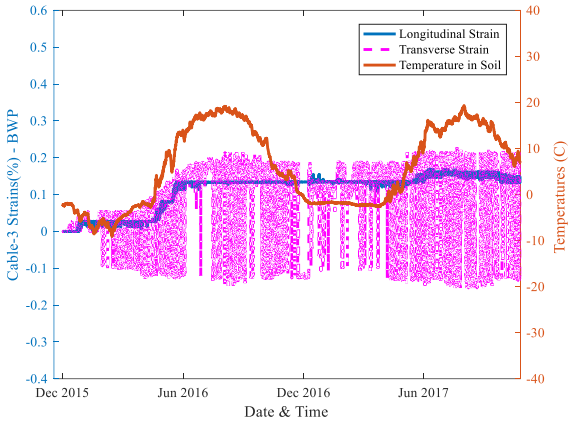

h) Geotextile strains at the edge of the culvert barrels (Malfunction in transvers strain gauge)

Figure 3.20: Cumulative strains in geogrid (Left) and geotextile (Right)

Table 3-6: The permanent recorded strains in the geogrid and the geotextile in 26-Oct-2017

Strain Cable		Location relative to culvert Barrels	Direction of Strain	Strain (%)
Geogrid	Cable 1	Between Culvert Barrels	Longitudinal	0.01
			Transverse	0.1
	Cable 2	At the top of the Culvert Barrel	Longitudinal	0.2
			Transverse	0.2
	Cable 3	At the Edge of the Culvert Barrel	Longitudinal	0.05
			Transverse	0.25
Geotextile	Cable 1	Between Culvert Barrels	Longitudinal	0.01
			Transverse	0.02
	Cable 2	At the top of the Culvert Barrel	Longitudinal	0.18
			Transverse	N/A[1]
	Cable 3	At the Edge of the Culvert Barrel	Longitudinal	0.15
			Transverse	N/A[1]

[1]Strain gauge malfunction

The 2 GHz GPR scans show that the maximum settlement of pavement layer is at the centerlines of the culvert barrels (the top of the culvert barrels) for all the sites (Figure *3.21*) except for site 5 which shows settlement at the left barrel only (*Figure 3.21-e*). The deformations of the pavement over the culverts with the clay backfill is greater than the deformations over the culvert

with the granular backfill. The pavement on site 4 with the geosynthetics has the lowest settlements (*Figure 3.21-d*) relative to the pavement on site 1 with no geosynthetics (*Figure 3.21-a*), and both are backfilled with clay.

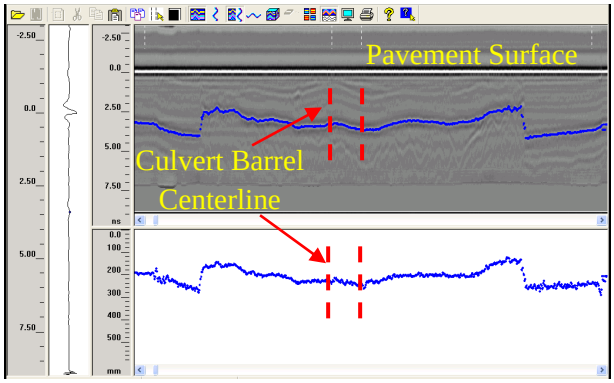

a) Site 1

b) Site 2

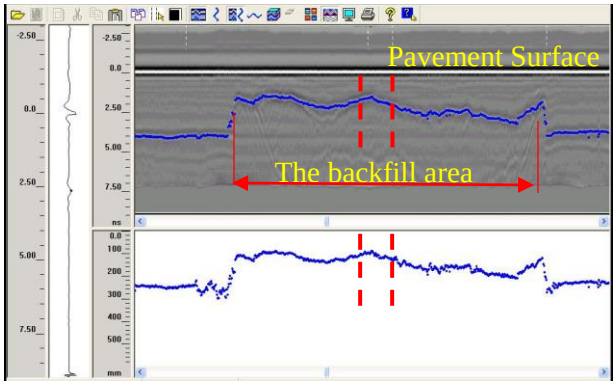

c) Site 3

d) Site 4

e) Site 5

Figure 3.21: GPR scans for the culvert sites showing the maximum settlement at the location of the culvert barrels, the red lines indicate the centerline of culvert barrels.

3.6. Conclusions from the field experiment

This chapter presented the 2-year monitoring and analysis of the ground thermal data, the strains data and the GPR scans collected from the five instrumented culvert sites located along the Provincial Trunk Highways PTH68. The five sites are designated as site 1, 2, 3, 4, and 5. The sites 1,4, and 5 are backfilled with clay, while sites 2, and 3 are backfilled with granular soil. Three layers of geosynthetics are installed at site 4, rigid insulation is installed at sites 3 and 5. The U-shaped and L-shaped string are installed around the left culvert barrel in all the sites with various number of thermistors to measure the ground temperature near the culvert barrels. The undisturbed ground temperatures are measured using 12 thermistors installed at virous depths. Strain gauges are attached to the geosynthetics at site 4 to determine the soil deformations due to temperature, and load.

The following are the finding from the analysis of the 2-year thermal and strains data

- Strains data showed that depression of soil at the top of the culvert barrels is greater than the other locations in most of the sites. That is due to the settlement of the soil at the top of the culvert barrels.
- The rigid insulation keeps the soil temperature underneath the culvert barrels greater than $0^{o}C$ which prevents potential formation of ice lenses and so frost heave below the insulation level.
- The geosynthetics reduces the road roughness on site 4 relative to sites 1 and 5 with similar backfill by redistributing the differential depression of soil over larger area.

Chapter 4: Numerical Modeling, boundary conditions, and validation[1]

4.1. Introduction

The numerical model is established to simulate the thermal performance of the culverts, provide better understanding of the changes in the ground thermal profile, and predict the culvert performance for future scenarios. The model is validated with the thermal field data with a good agreement, increasing the reliability of the model in predicting future thermal events in the soil.

The thermal data collected from the culvert sites are used to calibrate and validate a 2-D numerical model by evaluating the predicted and measured soil temperatures near the culverts, and in the natural soil. The validated model is used to predict the temperatures and the disturbance in the soil thermal profile caused by the culvert barrels.

4.2. Numerical model geometry and material properties

A 2-D numerical model is implemented to study the thermal changes in the soil surrounding the culvert (*Figure 4.1-b*), and away from the culvert barrels (*Figure 4.1-a*). The phase change of the moisture within the soil is assumed to occur within soil temperatures range from -1 ^{o}C to 0 ^{o}C (Andersland and Ladanyi, 2004). Heat is assumed to be transferred within the soil body by conduction only (Zhu and Michalowski, 2005). The 0.1m four-node quadratic mesh elements applied to the thermal numerical model in this study were used by Zhu and Michalowski (2005);

[1] Part of the manuscript in this chapter can be found in the proceeding of the Transportation research Board 97th Annual meeting, and submitted to transportation geotechnics for publication as an article.

and Zhang and Michalowski (2015) in modeling the thermal disturbance in the soil. The size of the model is reduced to shorten the analysis time (Appendix B).

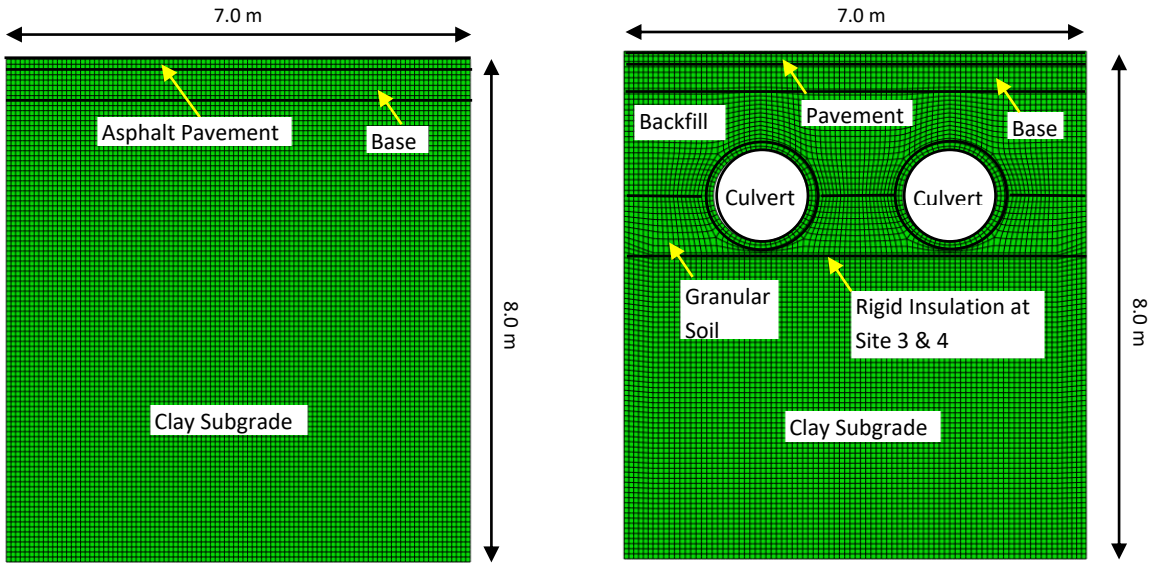

a) Undisturbed subgrade b) Subgrade with culvert barrels

Figure 4.1: the 2D Numerical model geometry, mesh, and soil types

Table *4-1*) is a summary of the material properties and their values required for the numerical thermal model. The thermal properties of the different soils are calculated using the equations (2.10) to (2.18). The thermal conductivity and the specific heat of the hot mix asphalt layer, presented in Table *4-1*), are assumed based on the work of Luca and Mrawira (2005).

Table 4-1: Finite element numerical model material input parameter

Material Properties	Specific Heat $(kJ/kg.^oC)$		Thermal Conductivity $(kJ/hr.m.^oC)$		Latent Heat (kJ/kg)	Solidus[3] Temp (^oC)	Liquidus[3] Temp (^oC)	Dry Density (kg/m^3)
	Frozen	Unfrozen	Frozen	Unfrozen				
Hot Mix Asphalt	0.674[1]	0.674[1]	5.4[1]	5.4[1]	N/A[2]	-	-	2371
Granular Base	0.909	1.174	2.041	0.650	1.229	-1	0	1834
Clay Subgrade	0.995	1.407	3.841	0.886	1.32	-1	0	1657
Precast Concrete Culvert	1.174	1.174	0.909	0.909	-	-	-	2200
Insulation	-	-	0.036	0.036	-	-	-	100

[1] based on the work of Luca and Mrawira (2005)
[2] not applicable because moisture content in asphalt layer is negligible
[3] Solidous and liquidus temperatures are the upper and lower temperature limits for the phase change.

4.3. Challenges in building the model

The thermal interaction between pavement structure (asphalt layer and base) and culverts is different than the pavement structure interaction with the undisturbed natural soil. The pavement surface temperature is expected to have thermal impact on the structures underneath (e.g. culverts). The literature review for a standard or consistent use of the pavement temperature as the boundary condition of thermal geotechnical problems below the pavement surface is found to be unclear. This explains why different approaches are often used for the boundary conditions of the pavement surface temperature in modeling thermal geotechnical problems. Some researchers assume constant pavement temperature with time when modeling culverts underneath pavement structure such as Ishikawa et. al. (2016). Others assume linear change between the warm and cold pavement surface temperatures such as Zhang and Michalowski (2015).

Several methods were developed to predict pavement surface temperature from air temperature and are used as the boundary condition for the pavement surface in thermal

geotechnical models. Five pavement temperature prediction methods are evaluated in this study. The first method is the air temperature method which, for the pavement surface, is assumed to be equal to the air temperatures. The second method is the n-factor, which is the ratio of the freezing or the thawing indices of any surface and the air. The thawing and the freezing indices consider the cumulative effect of the increase and the decrease in the temperature respectively. The third method is the Strategic Highway Research Program (SHRP) method which was developed using many test sites distributed across North America. The fourth method is the Canadian Strategic Highway Research Program (C-SHRP), which updated the SHRP low temperature method by including more test sites from Canada. The last method, the Long-Term Pavement Performance Program (LTPP) method, is developed by the Federal Highway Administration (FHWA) through the LTPP program. The n-factor, SHRP, CSHRP, and LTPP have two equations each to predict the pavement temperature in warm season (when the air temperature (Tair)>0) and cold season (when Tair≤0). The five methods are used as the pavement surface boundary condition in a numerical model. The objective is to find the pavement temperature methods that most accurately provide soil thermal predictions below the pavement surface when compared to the thermal data measured from the instrumented culvert sites.

4.4. Boundary conditions

The boundary conditions of the model (*Figure 4.2-a* and *Figure 4.2-b*) are the subsurface boundary condition, the upper half and the lower half of the culvert openings, the sides of the model, and the surface boundary condition. The subsurface boundary condition, which is the deepest part in the model represents the level where the soil temperature is constant along the year below the pavement surface. The sides of the model are assumed to be adiabatic. The boundary conditions

at the culvert openings are divided into the top half and the bottom half based on the water or the ice level in the culvert barrels. The pavement surface boundary conditions are assumed to be equal to the pavement temperature calculated from the n-factor, the LTPP, the SHRP, the C-SHRP, and the air temperature.

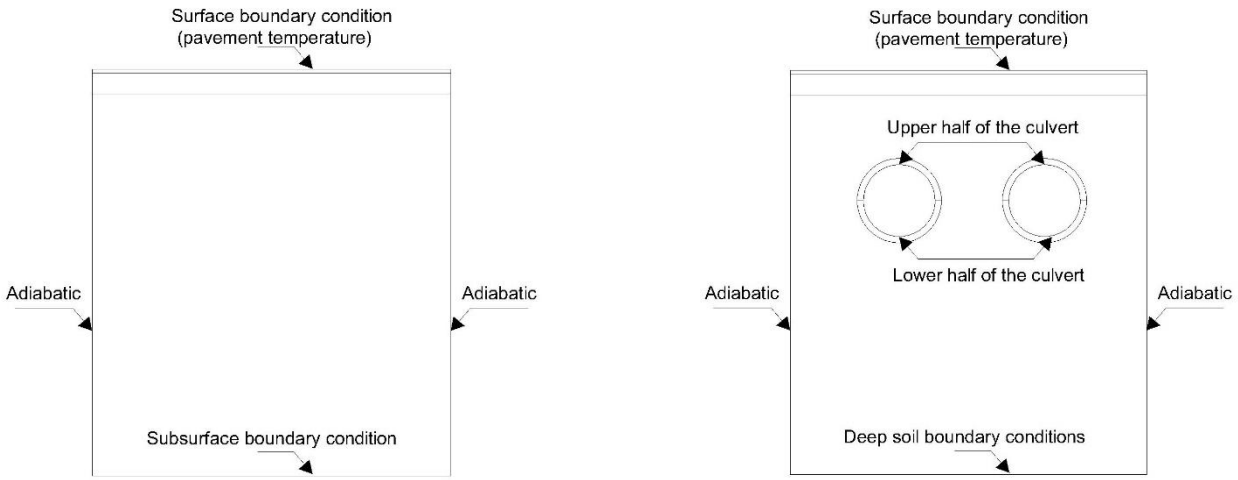

Figure 4.2: Model geometry and boundary conditions of: (a) away from culvert opening; (b) near culvert opening

4.4.1. Subsurface boundary conditions

The location of the subsurface boundary conditions is selected at the depth where soil temperature is constant all year long, and independent from seasonal climatic changes. Thermal data collected from the sites are extrapolated using soil temperature equations Eq.(5.1) throughout Eq.(5.4) (Andersland and Ladanyi, 2004) to create Figure *4.3*). A temperature of 9.5 ^{o}C with a variation less than 0.3 ^{o}C/year is assumed at depth of 8m below the road surface as concluded from Figure (5.4).

$$T_{S,t} = T_m + A_s \sin\left(\frac{2\pi t}{p}\right) \quad (5.1)$$

$$A_z = A_s \exp\left(-z\sqrt{\frac{\pi}{\alpha_u p}}\right) \quad (5.2)$$

$$T_{z,t} = T_m + A_z \sin\left(\frac{2\pi t}{p} - z\sqrt{\frac{\pi}{\alpha_u p}}\right) \quad (5.3)$$

$$T_{zmin} = T_m + A_z \; ; \qquad T_{zmax} = T_m - A_z \quad (5.4)$$

where,

$T_{S,t}$ is the ground surface temperature;

T_m is the mean annual temperature of soil at depth "z" which is calculated from data thermal data collected from field;

A_s is the amplitude of surface temperature;

t is time;

p is the period of time considered (365 days);

A_z is the ground temperature amplitude below ground surface;

$T_{z,t}$ is the ground temperature at depth "z" and time "t";

z is the depth measured from pavement surface;

α_u is the soil thermal diffusivity in (m^2/s) calculated from Eq.(2.18);

T_{zmin}, T_{zmax} is the minimum and maximum ground temperature at depth "z"

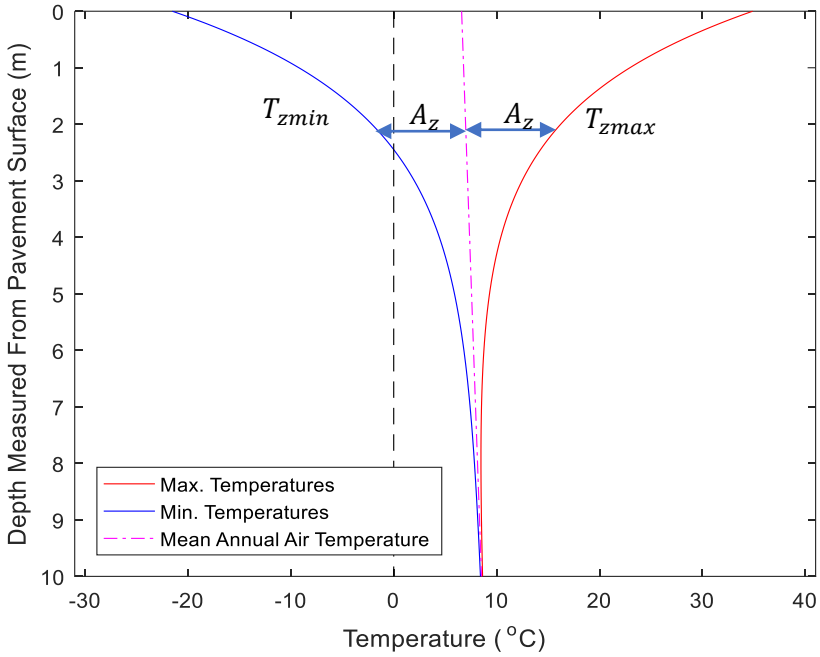

Figure 4.3: Change in the maximum and minimum annual ground temperature with depth

4.4.2. Culvert surface boundary conditions

The inner surface of the Portland Cement Concrete (PCC) culvert barrels are filled or partially filled with air, water, and snow. Therefore, the temperature of the PCC culvert barrels changes with time. The temperatures of the concrete culvert barrels are not measured throughout the study period due to difficulty in installing and maintaining the thermistors on the inner surface of the culvert barrels. Most of the empirical concrete surface temperature methods were developed to predict the temperature of straight concrete panels such as the work of Bentz (2000). According to the heat transfer principals, the geometry of a body affects the heat transfer mechanism (Bergman et. al., 2002). Therefore, Bentz model is not used to predict the temperature of the inner concrete culvert surface. In this study, the n-factor is used in determining the temperature of the inner surface of the PCC culvert barrels.

The freeze and the thaw n-factors for the upper half of the culverts are 0.6 and 1.2 respectively, while the values are 0.95 and 1.6 for the lower half of the pipe for freeze and thaw n-factors respectively. The upper half of the culvert is assumed to be warmer than the lower half in the summer but colder in the winter, because the inner surface of the concrete culvert is subjected to air temperature most of the year, while the lower half is cover either by water or ice throughout the year (Figure *4.4*).

(a) Fall (October – 2016)

(b) Winter (February – 2016)

(c) Spring (March – 2016)

Figure 4.4: Culvert barrels conditions in different season

4.4.3. Pavement surface boundary conditions

The boundary conditions at the road surface is selected based on the pavement temperature, which varies with time. Several methods were developed to predicted pavement temperature such as the work done by Wang (2015), Gedafa et. al. (2013), Alavi et. al. (2014). Some pavement temperature prediction methods are not considered in this study, because they require input parameters measured under very restricted conditions, such as BELLS equations, which requires infrared temperature measurement that can easily be affect by the shading effect which is the blockage of sun light during measuring pavement temperature (Lukanen et. al, 2000). Some other methods are not considered in the analysis, because they are site specific, such as the work of Ryynänen (2000). The Enhanced Integrated Climatic Model (EICM) is widely used in determining the changes in pavement temperature and moisture distribution. Nevertheless, the EICM model is not considered as the pavement boundary condition for the 2-D numerical thermal model, because the EICM model was built for one dimensional (1-D) analysis (Liu and Yu, 2011). Moreover, the EICM model does not provide pavement surface temperature as an output which would be a solution to overcome the 1-D analysis limitation. The pavement temperature prediction alternatives considered in this study are the n-factor, SHRP, C-SHRP, and LTPP models, because they are valid to be applied at any site in North America, and they are most often used by transportation agencies in determining pavement temperatures.

The n-factor, SHRP, C-SHRP, and LTPP models predict pavement temperature by applying adjustments to air temperature. For instance, the n-factor method predicts pavement temperature by multiplying the air temperature by a factor, while the SHRP method predicts pavement temperature by applying shifts to the sinusoidal trend of the air temperature. The C-SHRP, and the LTPP methods predict pavement temperature by both factorizing and applying

shifts to the air temperature. Researchers include a control method by assuming that pavement temperature is equal to the air temperature as an additional alternative to evaluate the changes on ground temperature. The predicted pavement temperatures from each alternative are used as the pavement surface boundary condition in the finite element model.

4.4.3.1. Alternative 1: Air Temperature approach

In this alternative, the pavement temperature is assumed to be equal to air temperature. This alternative is compared to the other alternatives in predicting the ground thermal profile below the road surface.

4.4.3.2. Alternative 2: n-factor method

The n-factor method is used to predict pavement surface temperature by applying factor to the air temperature that considers the effect of all heat transfer modes at the pavement surface. The n-factor is the ratio of the freezing and thawing indices of the pavement surface and the air. The equations (5.5) and (5.6) (Andersland and Ladanyi, 2004) are used to predict pavement temperature using the n-factor.

$$T_{high} = n_t T_{air} \qquad for \quad T_{air} > 0 \qquad (5.5)$$

$$T_{low} = n_f T_{air} \qquad for \quad T_{air} \leq 0 \qquad (5.6)$$

Where,

T_{high} = high asphalt pavement temperature at surface in ^{o}C.

T_{low} = low asphalt pavement temperature in ^{o}C.

T_{air} = Air temperature in ^{o}C.

n_t = The thaw factor which is the n-factor of asphalt concrete during thaw.

n_f = The Freeze factor which is the n-factor of asphalt concrete during freeze.

The recommended n-factors for asphalt pavements are 0.29 to 1.00 for freezing and 1.4 to 2.3 for thawing (Lunardini, 1978). However, the n-factor ranges for asphalt surface were updated to become 0.80 to 0.95 for freezing and 1.60 to 3.00 for thawing (Doré and Zubeck, 2009). For this study, the n-factors used for pavement surface boundary conditions are 0.95 for low temperatures (air temperatures below the freezing point) and an n-factor of 1.6 for warm temperatures (air temperatures greater than the freezing point).

4.4.3.3. Alternative 3: SHRP method

The Strategic Highway Research Program developed the SHRP method for predicting pavement temperature by correlating the measured air temperatures to the measured pavement temperatures collected from many test sites distributed across North America. The empirical models are shown in Eq.(5.7) and Eq.(5.8).

$$T_{high} = T_{air} - 0.00618Lat^2 + 0.2289Lat + 24.4 \qquad for\ T_{air} > 0 \qquad (5.7)$$

$$T_{low} = T_{air} + 0.051H - 0.000063H^2 \qquad for\ T_{air} \leq 0 \qquad (5.8)$$

T_{high} = high asphalt pavement temperature at surface in ^{o}C.
T_{low} = low asphalt pavement temperature in ^{o}C.
T_{air} = Air temperature in ^{o}C.
Lat = latitude of site in degrees.
H = depth from pavement surface in mm.

4.4.3.4. Alternative 4: C-SHRP method

The Canadian Strategic Highway Research Program (C-SHRP) modified the low pavement temperature method developed by SHRP, by including more data from many tests sites from

Canada, as shown in Eq.(5.7) and Eq. (5.9). No changes were applied to the SHRP high pavement temperatures method in Eq.(5.7).

$$T_{high} = T_{air} - 0.00618Lat^2 + 0.2289Lat + 24.4 \quad for\ T_{air} > 0 \quad Same\ as\ (5.7)$$

$$T_{low} = 0.859T_{air} + H(0.002 - 0.0007T_{air}) + 0.17 \quad for\ T_{air} \leq 0 \quad (5.9)$$

T_{high} = high asphalt pavement temperature at surface in ^{o}C.
T_{low} = low asphalt pavement temperature in ^{o}C.
T_{air} = Air temperature in ^{o}C.
Lat = latitude of site in degrees.

4.4.3.5. Alternative 5: LTPP Bind method

The Long-Term Pavement Performance (LTPP) is a Federal Highway Administration (FHWA) program established to monitor, collect and analyze data from test sites distributed across North America. Several pavement prediction methods are developed using the LTPP data such as the work done by Mohseni and Symons (1998), Diefenderfer et. al. (2002), Yavuzturk et. al. (2005), Chandrappa and Billigiri (2015), and Alavi et. al. (2014). The method developed by Mohseni and Symons (1998) is considered in the analysis, because it is used by FHWA in the LTPP-Bind model as shown in Eq.(5.10) and Eq.(5.11).

$$T_{high} = 54.32 + 0.78T_{air7} - 0.0025Lat^2 - 15.14\log(H + 25) + z\left(9 + 0.61S_{high}^2\right)^{0.5} \quad for\ T_{air} > 0 \quad (5.10)$$

$$T_{low} = -1.56 + 0.72T_{air} - 0.004Lat^2 - 6.26\log(H + 25) + z(4.4 + 0.52S_{low}^2)^{0.5} \quad for\ T_{air} \leq 0 \quad (5.11)$$

where,

T_{high} = high asphalt pavement temperature at surface in ^{o}C.

T_{low} = low asphalt pavement temperature in ^{o}C.

T_{air} = Air temperature in ^{o}C.

T_{air7} = High 7-day air temperature in ^{o}C.

S_{high} = Standard deviation of high 7-day mean air temperature.

S_{low} = Standard deviation of mean low air temperature.

z = Normal distribution deviate, z = 2.055 for 98% reliability.

4.5. Evaluation of Boundary conditions

Temperature data from December 2015 to October 2017 at the culvert test sites are evaluated in the analysis. The temperature data for site 3 was collected from December 2016 to November 2017, since it was constructed one year later, in November 2016. The evaluation process for the temperature data is based on a trend evaluation and statistical testing. The trend evaluations are to find the variation between the measured and the predicted soil temperatures from the five pavement temperature prediction methods. The statistical testing of the measured and predicted soil temperatures is evaluated through the F-test. A pavement temperature prediction method is considered successful, when it passes both the trends and F-test statistical evaluation. The successful method is used in the 2-D numerical model to determine the frost depth distribution below the pavement structure, and around the culvert barrels. Equations (5.1) throughout (5.11) provide the boundary conditions with time and the 2-D numerical model outputs. A sample of the boundary condition in the transient analysis (Figure *4.5*) and the 2-D numerical model outputs are presented (Figure *4.6*) are presented.

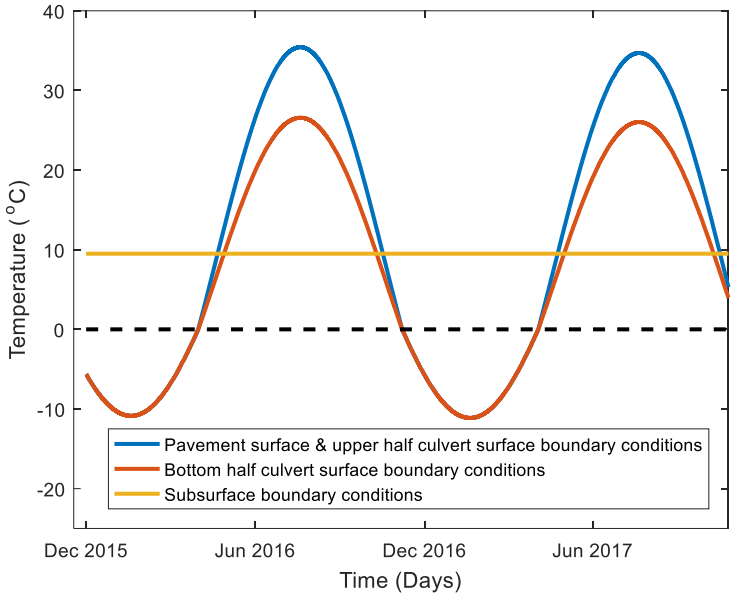

Figure 4.5: The boundary conditions in transient analysis

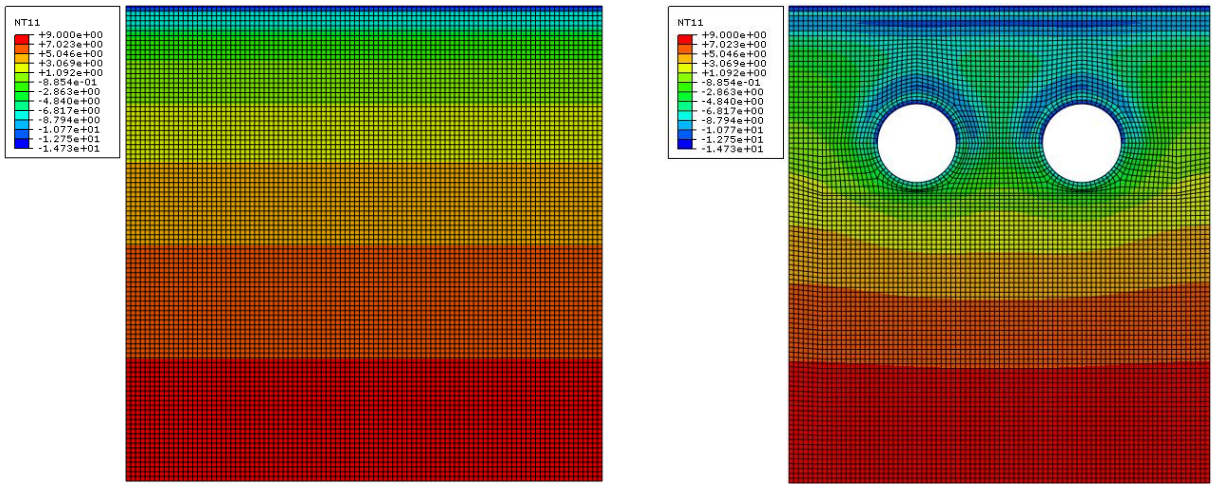

a) Undisturbed subgrade without culvert opening

b) Subgrade with culvert barrel opening

Figure 4.6: 2-D Numerical model thermal profile output

4.5.1. Trends Evaluation

The results of the trend analysis of the predicted soil temperatures from the five pavement temperature alternatives have good agreement with the measured soil temperatures, as shown in *Figure 4.7*) (at thermistor B), and summarized in *Table 4-2*) (for the second year). All the surface boundary conditions from the five methods accurately predicts the soil temperature during the winter, and the spring with an average temperature variation less than 4^{o}C. Two of the alternatives (LTPP and air) have lower accuracy in predicting soil temperature during the summer and the fall with variation up to 10^{o}C. All the methods over predict the soil temperature during the summer, except for the air temperature method, by a range from 1^{o}C to 10^{o}C. The n-factor alternative provides the highest accuracy in predicting the soil temperature below the pavement surface and near the culverts with maximum variation of ±3^{o}C. The SHRP and the C-SHRP alternatives have maximum variation between the measured and the predicted soil temperature of ±5^{o}C. The LTPP alternative over predicts the soil temperature by 10^{o}C in the summer, and 4^{o}C in the other seasons. This is possibly because the LTPP alternative considers the high 7-day air temperature in calculating the pavement temperature in warm seasons.

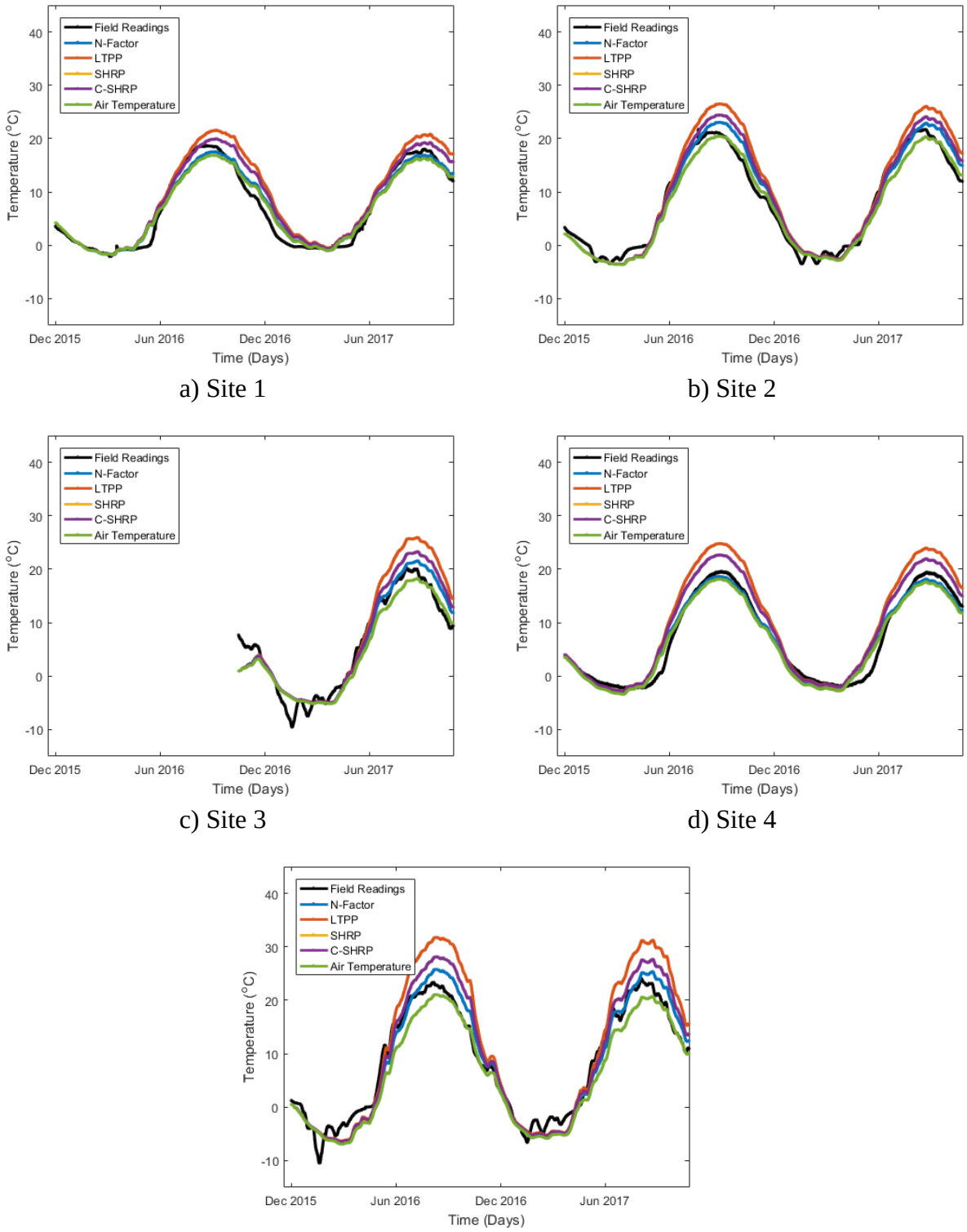

Figure 4.7: Temperature trends with time at thermistor B for all the sites (Between Culvert Barrels)

Table 4-2: Measured and predicted daily soil temperatures at thermistor B (Between Culvert Barrels)

Site location	Season	Date	Measured Soil Temp. (°C)	Predicted Soil Temp. (°C)				
				N-factor	LTPP	SHRP	C-SHRP	Air Temp
Site 1 (Clay Backfill)	Winter	Dec 15-2016	1	3	5	5	5	3
		Jan 15-2017	0	1	2	1	2	1
		Feb 15-2017	0	0	0	0	0	0
	Spring	Mar 15-2017	0	-1	0	0	0	-1
		Apr 15-2017	0	1	2	2	2	2
		May 15-2017	6	6	7	6	6	6
	Summer	Jun 15-2017	12	10	12	12	12	10
		Jul 15-2017	16	15	18	17	17	14
		Aug 15-2017	17	17	20	19	19	16
	Fall	Sep 15-2017	16	16	20	18	18	15
		Oct 15-2017	13	14	18	17	16	14
Site 2 (Granular Backfill)	Winter	Dec 15-2016	0	3	4	3	3	3
		Jan 15-2017	-2	0	1	1	1	0
		Feb 15-2017	-1	0	0	0	0	0
	Spring	Mar 15-2017	-1	0	0	0	0	-1
		Apr 15-2017	1	4	4	4	4	3
		May 15-2017	9	10	11	10	10	9
	Summer	Jun 15-2017	15	17	19	17	17	15
		Jul 15-2017	20	22	25	23	23	20
		Aug 15-2017	21	24	28	26	26	22
	Fall	Sep 15-2017	16	19	24	23	23	21
		Oct 15-2017	13	16	21	20	19	18
Site 3 (Granular Backfill)	Winter	Dec 15-2016	-8	-6	-6	-6	-6	-6
		Jan 15-2017	-7	-10	-10	-10	-10	-10
		Feb 15-2017	-5	-8	-8	-9	-8	-9
	Spring	Mar 15-2017	-3	-6	-6	-6	-6	-6
		Apr 15-2017	3	3	4	3	3	3
		May 15-2017	12	14	15	14	14	13
	Summer	Jun 15-2017	14	17	23	22	22	19
		Jul 15-2017	19	22	27	26	26	22
		Aug 15-2017	18	21	26	25	25	22
	Fall	Sep 15-2017	12	15	19	18	18	15
		Oct 15-2017	8	11	12	12	12	10
Site 4 (Clay Backfill)	Winter	Dec 15-2016	-1	-4	-7	-7	-7	-5
		Jan 15-2017	-1	-4	-4	-4	-4	-4
		Feb 15-2017	-2	-4	-8	-8	-8	-5
	Spring	Mar 15-2017	-2	-5	-7	-8	-7	-6
		Apr 15-2017	2	0	0	0	0	1
		May 15-2017	12	8	9	9	9	8
	Summer	Jun 15-2017	15	12	15	14	14	12
		Jul 15-2017	19	17	20	19	19	17
		Aug 15-2017	17	16	19	18	18	16
	Fall	Sep 15-2017	11	11	13	12	12	11
		Oct 15-2017	12	13	18	17	17	13
Site 5 (Clay Backfill)	Winter	Dec 15-2016	-3	-3	-3	-3	-3	-4
		Jan 15-2017	-2	-5	-5	-5	-5	-6
		Feb 15-2017	-2	-5	-5	-5	-5	-5
	Spring	Mar 15-2017	-1	-4	-4	-5	-4	-5

	Apr 15-2017	3	2	3	3	3	1
	May 15-2017	13	10	13	11	11	8
Summer	Jun 15-2017	16	18	23	20	20	14
	Jul 15-2017	22	23	30	26	26	19
	Aug 15-2017	21	24	30	26	26	20
Fall	Sep 15-2017	14	17	23	20	20	15
	Oct 15-2017	12	16	21	19	18	15

The predicted and the measured soil temperatures between the culvert barrels are plotted against depth. The data from winter, spring, summer, and fall are presented in Figure *4.8*) throughout Figure *4.11*) for all the sites. Thermistors E and F at the site 2 malfunction; therefore, they are excluded from the analysis. Figures from 4.8 to 4.10 show a reduction in the thermal variation between the measured and the predicted soil temperature between the culvert barrels with depth. The variations between measured and predicted soil temperatures from all the methods are less than 1 ^{o}C in the winter (Figure *4.8*). The variations are less than 3 ^{o}C in spring (Figure *4.9*), but they increase up to 10 ^{o}C in the summer for the LTPP methods (Figure *4.10*). The type of the backfill, and the depth of cover have minimal effect on the accuracy of the predictions for all the sites. However, a very shallow depth of cover, such as site 5 with 0.8m cover, affects the accuracy of all the models. For instance, the variation between the predicted and the measured soil temperatures increases by five times if the depth of cover is 0.8m (Figure *4.8*-e), while that is not the case with the depths of cover deeper than 0.8 m.

The predicted and the measured soil temperatures are plotted against depth for the undisturbed soil (Figure *4.11*). The coldest (Figure *4.9*-a & 4.9-b) and the warmest (Figure *4.9*-e & 4.9-f) soil temperatures in the winter and the summer respectively, and the soil temperatures during the spring (Figure *4.9*-c & 4.9-d) in the undisturbed soil are presented. The variations between the predicted and the measured soil temperatures are minimum during winter, and they reach their maximum during the summer, which matches the findings near the culvert barrels (Figure *4.8*, 4.9, & 4.10). The variations between predicted and measures soil temperatures reduce with depth.

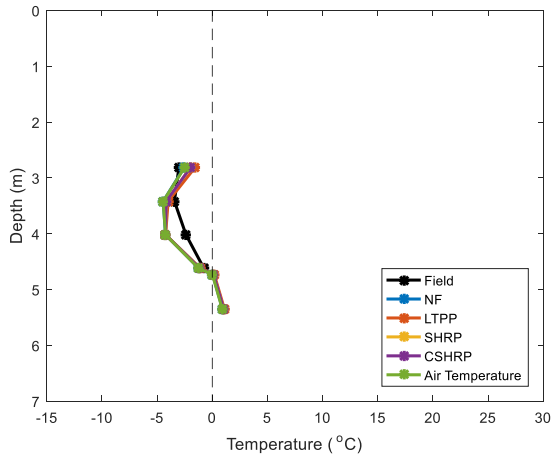

(a) Site 1 (Clay Backfill)

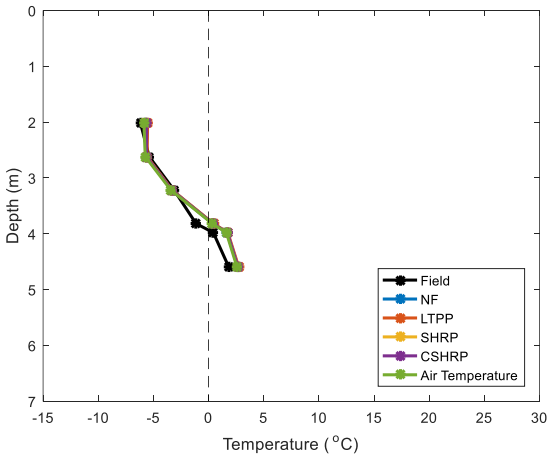

(b) Site 2 (Granular Backfill)

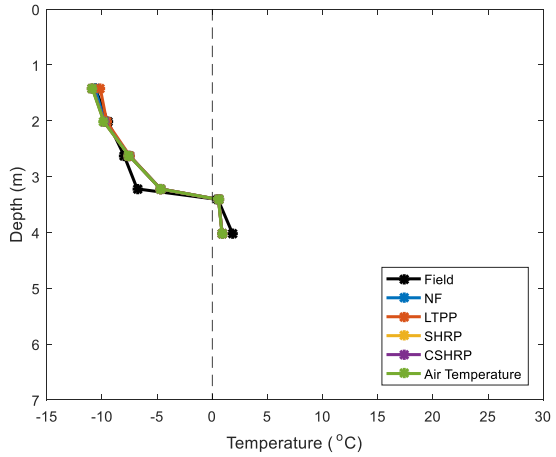

(c) Site 3 (Granular Backfill + Insulation)

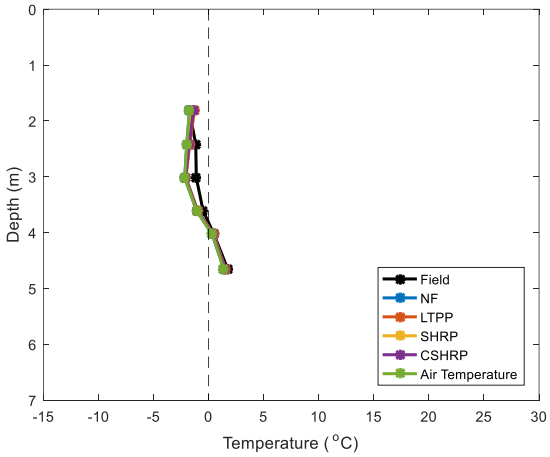

(d) Site 4 (Clay Backfill)

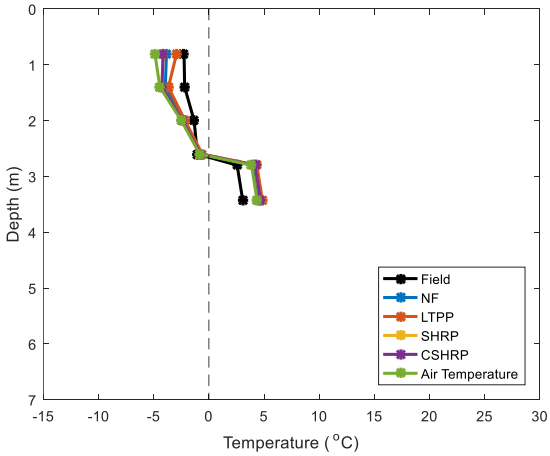

(e) Site 5 (Clay Backfill + Insulation)

Figure 4.8: Predicted and measured ground thermal profile between the culvert barrels in winter (23-February 2017).

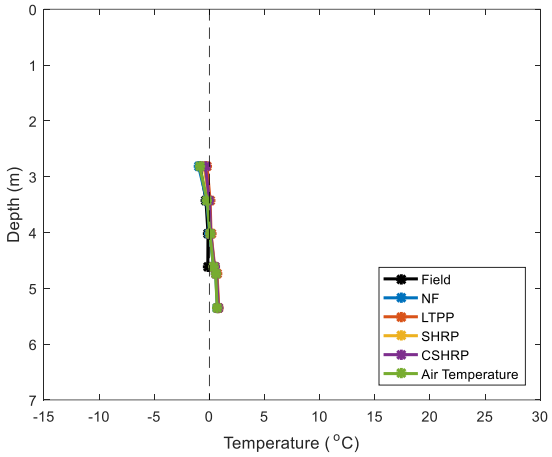

(a) Site 1 (Clay Backfill)

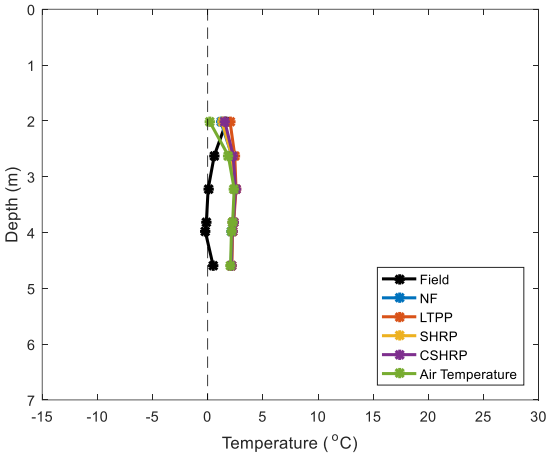

(b) Site 2 (Granular Backfill)

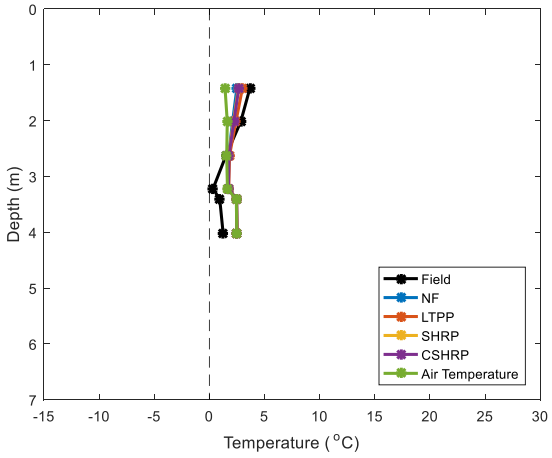

(c) Site 3 (Granular Backfill + Insulation)

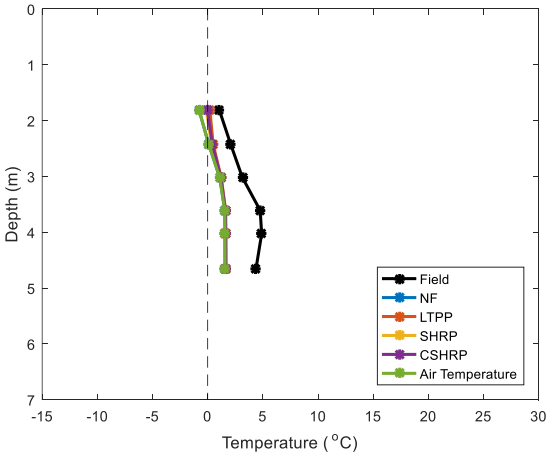

(d) Site 4 (Clay Backfill)

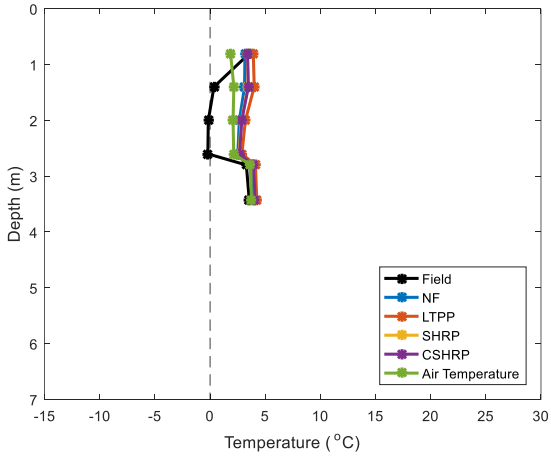

(e) Site 5 (Clay Backfill + Insulation)

Figure 4.9: Predicted and measured ground thermal profile between the culvert barrels in spring (23-April 2017).

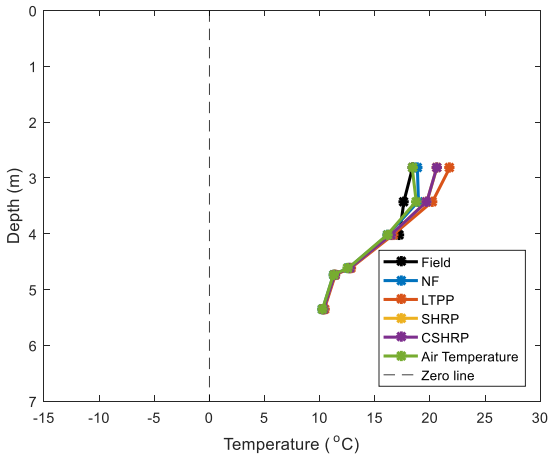

(a) Site 1 (Clay Backfill)

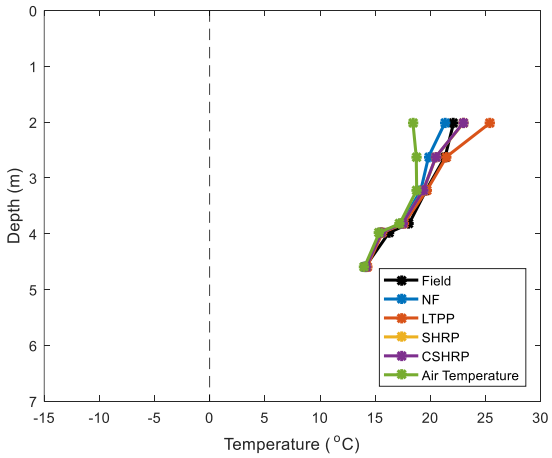

(b) Site2 (Granular Backfill)

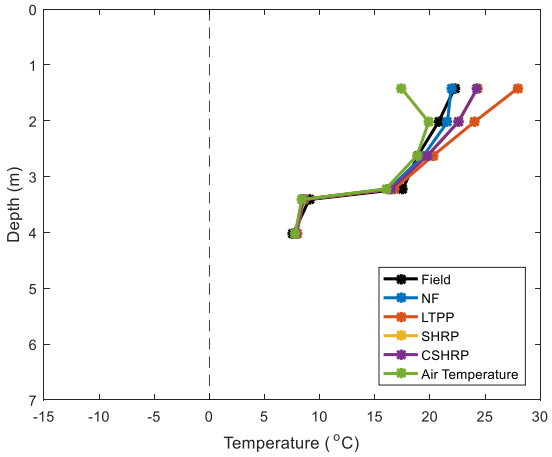

(c) Site3 (Granular Backfill + Insulation)

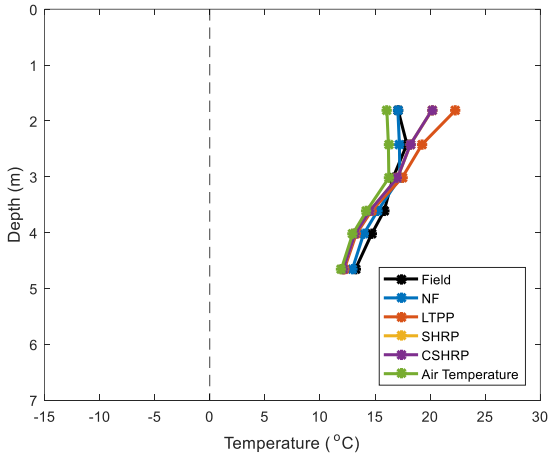

(d) Site4 (Clay Backfill)

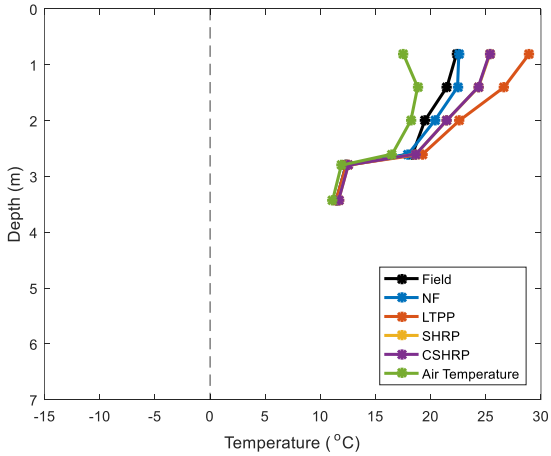

(e) Site 5 (Clay Backfill + Insulation)

Figure 4.10: Predicted and measured ground thermal profile between the culvert barrels in summer (23-July 2017).

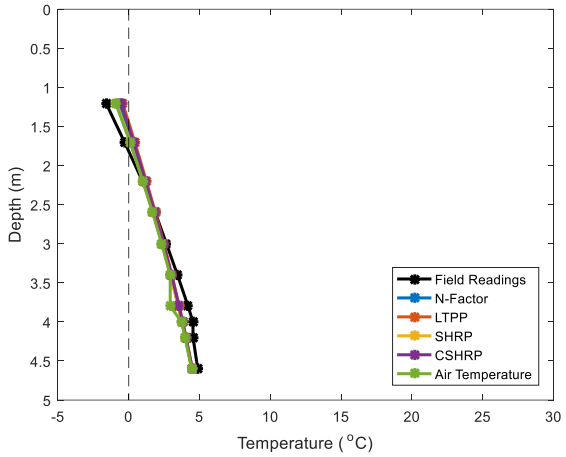

(a) Coldest temperatures (March-2016)

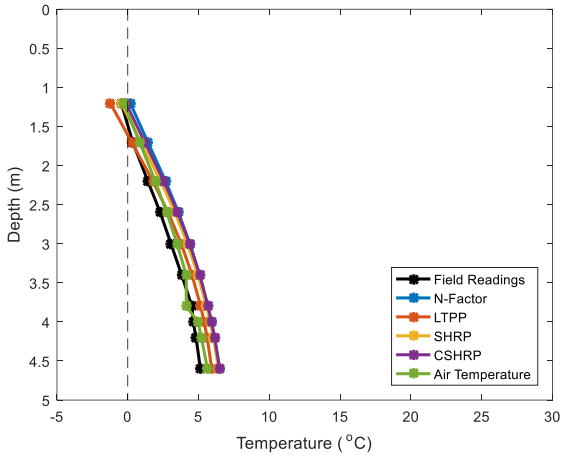

(b) Coldest temperatures (March-2017)

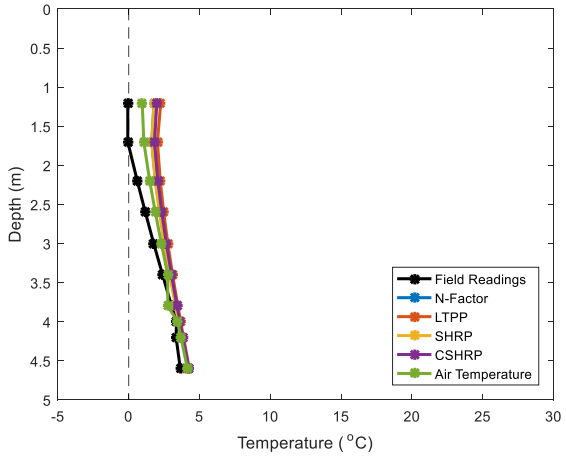

(c) During thaw (April-2016)

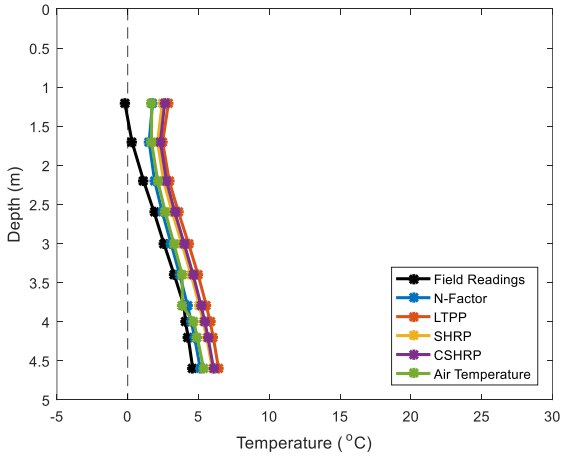

(d) During thaw (April-2017)

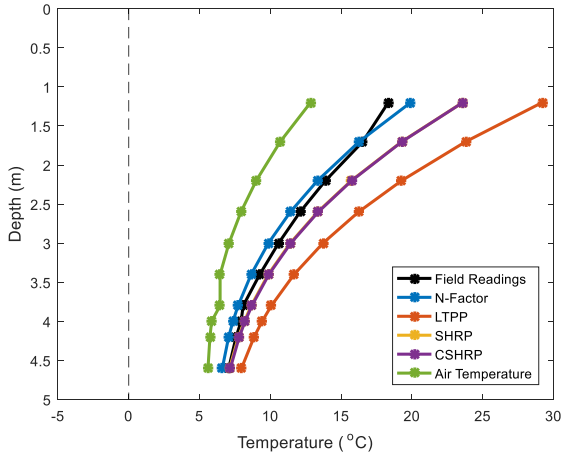

(e) Warmest soil temperatures (August-2016)

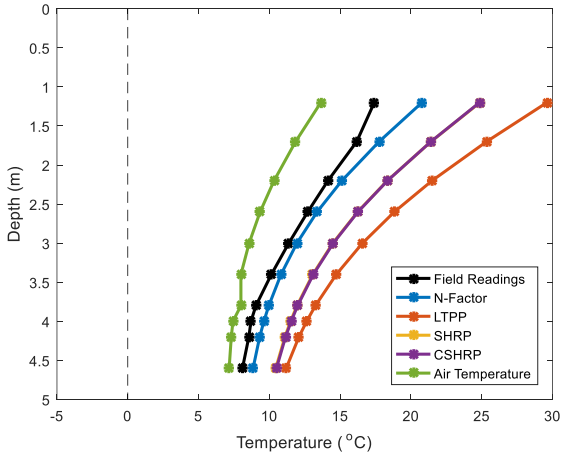

(f) Warmest soil temperatures (August-2017)

Figure 4.11: Predicted and measured ground thermal profile in the undisturbed soil (away from culvert barrels).

4.5.2. Statistical Testing

Statistical testing is considered in this study to determine which models have soil temperature predictions statistically identical to the measured soil temperatures. Statistical testing will provide accurate and detailed information about the performance of the models with time and depth.

The F-test is used in this study to evaluate whether the measured and the predicted soil temperatures from the five alternatives are statistically the same. The two tailed F-test evaluates the data sets under the null hypothesis (H=0) at a level of confidence 95% (two tailed α=0.025). The null hypothesis for the F-test assumes that the predicted and the measured temperatures have identical variances and standard deviations. For this study, the F-tests is applied over the 2-year study period with a total number of samples of 4165 (n = 4165), and degree of freedom of 4164 (df=n-1). The thermal prediction from the five methods is considered successful if the difference in the variances of the measured and the predicted soil temperatures have an F-value less than F-critical, and a probability greater than α=0.025 for all the seasons over two years.

The summary of the F-test analysis for each method by season is presented in Table *3-4*). The n-factor, the C-SHRP, and the SHRP alternatives pass the null hypothesis for the F-test with an F-value smaller than the F-critical, and a probability greater than α=0.025. The air temperature method failed the F-test for all the seasons and the LTPP method failed the test in the summer. Both alternatives have F-values greater than the F-critical, and probabilities less than α=0.025.

Table 4-3: Summary of the F-test results for each alternative per season

Season	Method	F-test				
		Probability ($F<F_{critical}$)	F-value	F-critical	Pass/Fail	DOF[1]
Winter	n-factor	0.785	0.697	1.02	Pass	1086
	LTPP	0.756	0.361	1.02	Pass	
	SHRP	0.744	0.518	1.02	Pass	
	C-SHRP	0.781	0.533	1.02	Pass	
	Air Temp	0.001	1.144	1.02	Fail	
Spring	n-factor	0.609	0.777	1.02	Pass	1098
	LTPP	0.507	0.401	1.02	Pass	
	SHRP	0.579	0.574	1.02	Pass	
	C-SHRP	0.562	0.599	1.02	Pass	
	Air Temp	0.010	1.124	1.02	Fail	
Summer	n-factor	0.774	0.416	1.02	Pass	1104
	LTPP	0.015	1.113	1.02	Fail	
	SHRP	0.469	0.703	1.02	Pass	
	C-SHRP	0.478	0.711	1.02	Pass	
	Air Temp	0.012	3.820	1.02	Fail	
Fall	n-factor	0.386	0.686	1.02	Pass	876
	LTPP	0.149	0.230	1.02	Pass	
	SHRP	0.239	0.407	1.02	Pass	
	C-SHRP	0.243	0.412	1.02	Pass	
	Air Temp	0.024	2.904	1.02	Fail	

[1]DOF = Degree of freedom

A summary of the standard deviations, means, and variances of the predicted temperatures is compared to the measured thermal data (Figure *4.12*). The figure explains the results of the statistical testing. As discussed earlier, the F-test evaluates the standard deviations and variances of two sets of data. The standard deviation and the variance of the predictions using the LTPP method as the pavement surface boundary conditions in warm seasons ($T_{soil}>0$) (Figure *4.12*-b) are higher than the standard deviations and the variances of the measured field soil temperatures. While the standard deviation and the variance of the predictions from the air temperature method in the warm season are smaller than the those of the measured soil temperatures.

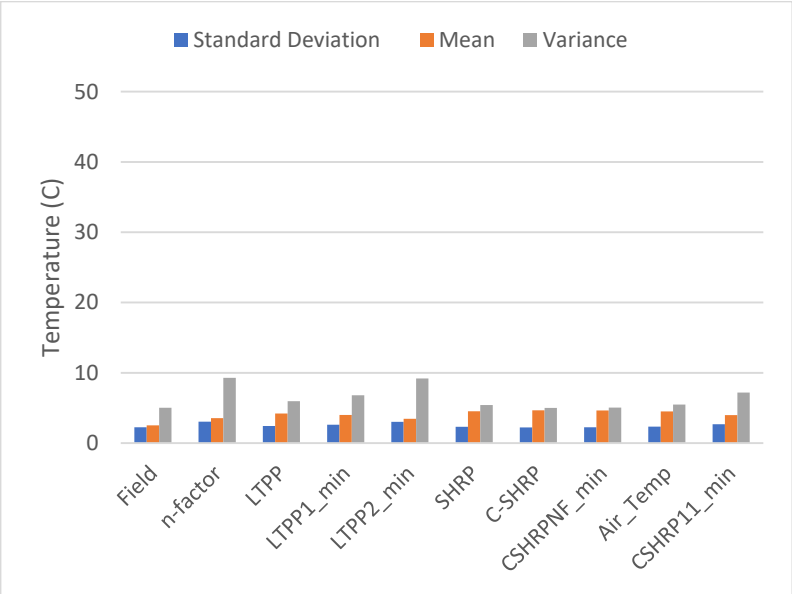

(a) Soil Temperatures smaller than 0°C

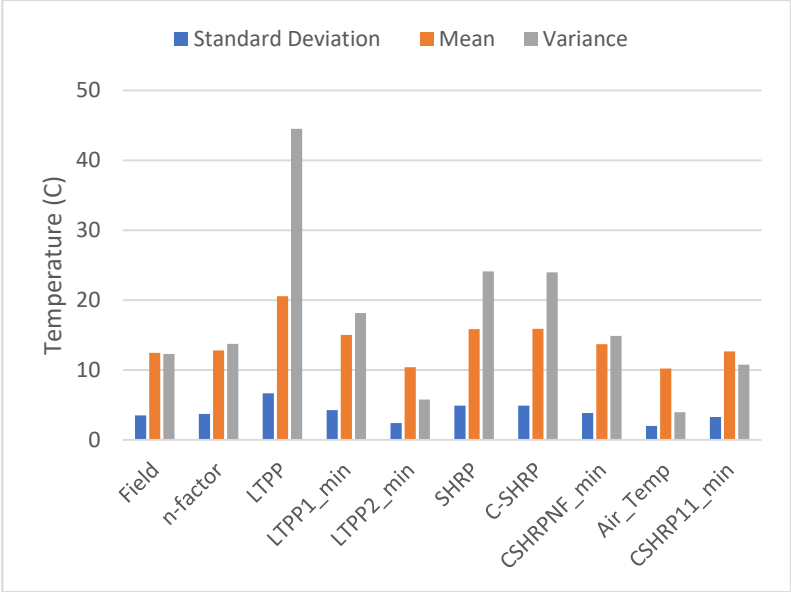

(b) Soil Temperatures greater than 0°C

Figure 4.12: The standard deviations, the means and the variances for the soil temperatures

4.6. Numerical model calibration and validation

The n-factor, C-SHRP, and SHRP are the successful methods, and are expected to provide higher accuracy when used as the pavement surface boundary condition in the 2-D numerical model. The successful methods are calibrated using the soil temperature from the natural undisturbed soil with coefficient of determinations (R^2), and the root mean square errors (RMSE) for the n-factor, C-SHRP, and SHRP methods presented in Figure *4.13*). The R^2 values for the n-factor, the SHRP, and the C-SHRP are 0.942, 0.938, and 0.939, respectively. The n-factor, the SHRP, and the C-SHRP have close R^2 values indicating that the three alternatives provide close predictions for the soil temperatures in Manitoba. However, validation is needed for the n-factor, the SHRP, and the C-SHRP for sites at different location outside Manitoba. The n-factor has the highest R^2 and the lowest RMSE; therefore, for this study, the n-factor method is applied on the pavement surface boundary condition to predict the ground thermal profile under the pavement surface.

The predictions from the thermal numerical model with the n-factor as the pavement surface boundary condition is validated with the measured soil temperatures near the culvert barrels with coefficient of determination from 0.89 to 0.96 (Figure *4.14*).

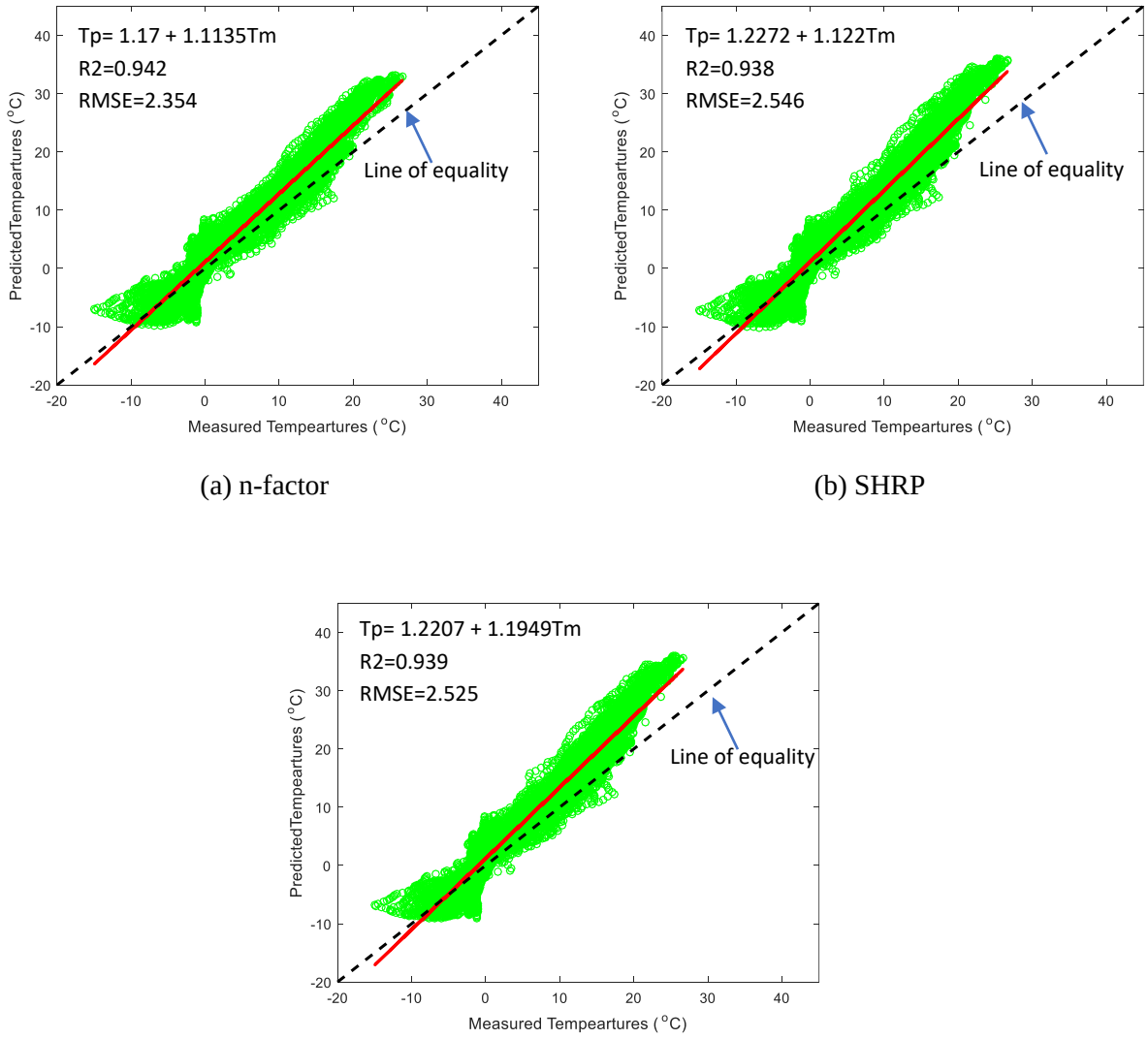

(a) n-factor

(b) SHRP

(c) C-SHRP

Figure 4.13: Calibration of the 2-D numerical model with the undisturbed natural soil

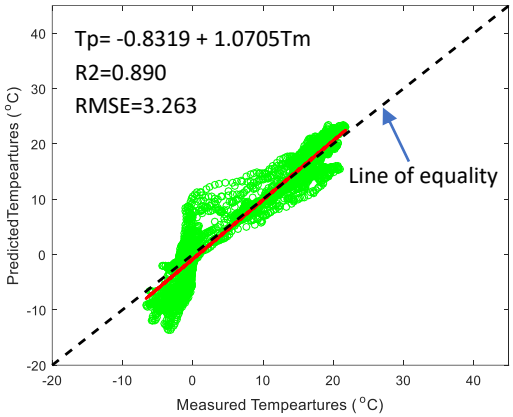

(a) Site 1(Clay backfill)

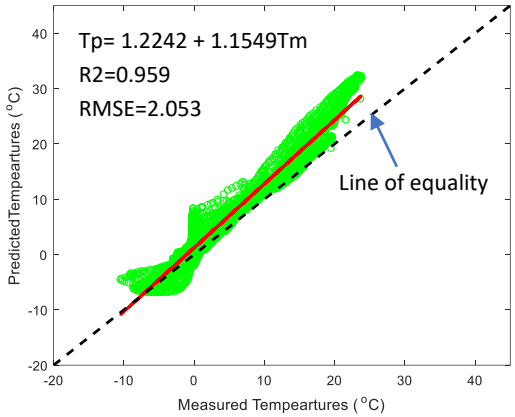

(b) Site 2 (Granular Backfill)

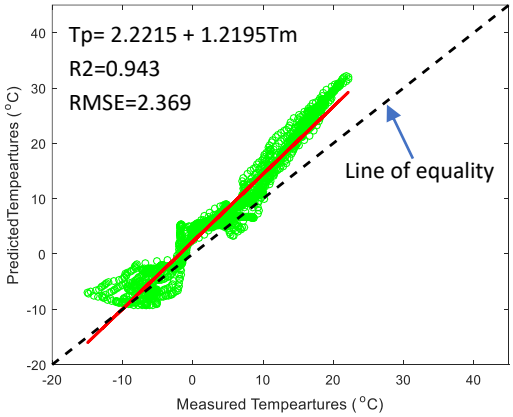

(c) Site 3(Granular backfill +Insulation)

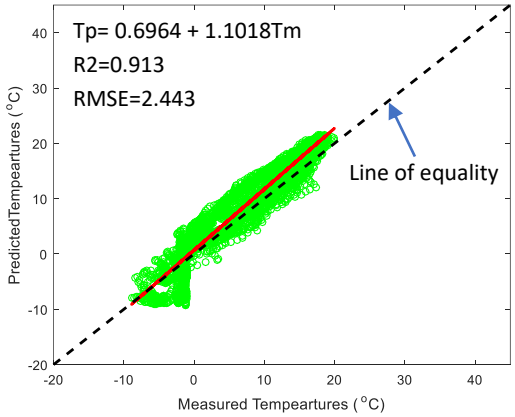

(d) Site 4 (Clay backfill + Geosynthetics)

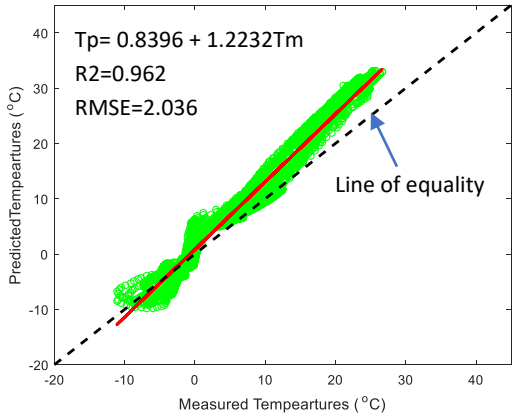

(e) Site 5 (Clay backfill + Insulation)

Figure 4.14: Validation of the 2-D numerical model with the five culvert sites

Chapter 5: Geotechnical applications of the numerical model in cold regions[2]

5.1. Ground thermal profile and frost depth in the vicinity of through-grade culverts

5.1.1. Thermal distribution around culverts

The validated numerical model is used to predict the thermal profile around the culvert openings for all the sites during several times of the year. Snapshots of the predicted thermal profile at all the sites are shown in Figure *5.1*) throughout Figure *5.4*). The predicted thermal profiles around the culverts, (Figure *5.1*) throughout (Figure *5.4*), shows that the disturbance in the soil thermal profile at the culvert area is caused by the culvert openings. This is because the culverts acted as buried heat source during the spring and the summer, and as cooling source during the Fall and the Winter. The thickness of the thermally disturbed region around the culvert openings increased as the depth of cover increased. The ground thermal disturbance below the rigid insulation is reduced due to the high thermal resistivity of the insulation (Figure *5.3* and Figure *5.4*), which keeps the ground below the insulation from freezing during the winter time.

The freeze and thaw process started from the pavement surface and from the culvert barrels. The thermal profile of the ground at sites 2 and 3 are different because of the difference in the backfill materials, thermal properties, and the depth of over. The culvert openings increase the depth of the active layer, which matched the findings of Nixon (1978). The active layer around the culvert openings is relatively deeper than the depth of the active layer away from the culvert openings (*Figure 5.1*-b & *Figure 5.2*-b).

[2] Part of the manuscript in this in chapter can be found in the proceeding of the Geohazards 7 conference, and submitted to the ASCE cold regions engineering for publication as an article.

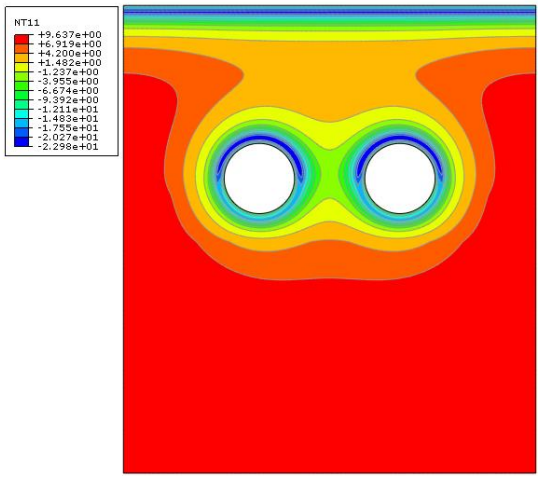

a) Beginning of Winter
(15-Dec-2016)

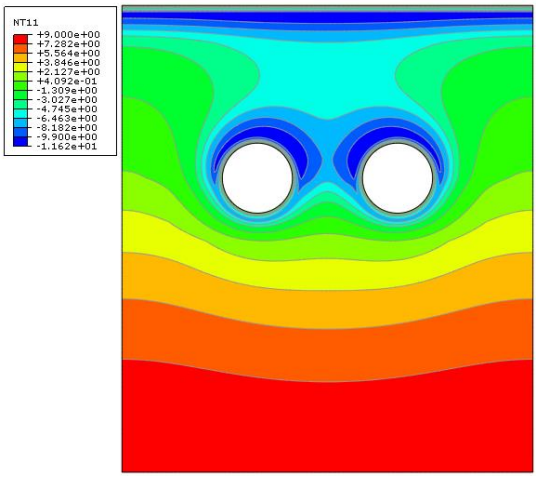

b) Beginning of Spring
(15-Mar-2017)

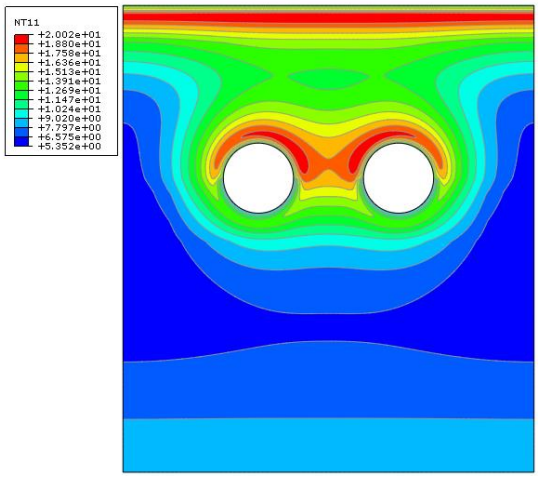

c) Beginning of Summer
(15-June-2017)

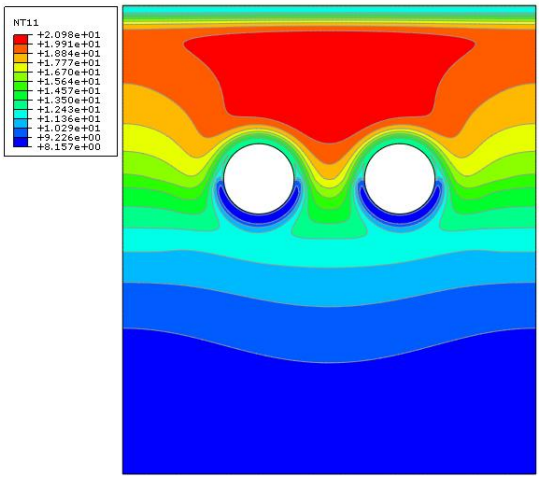

d) Beginning of Fall
(15-Sept-2017)

Figure 5.1: Thermal distribution at site 1 (Clay backfill).

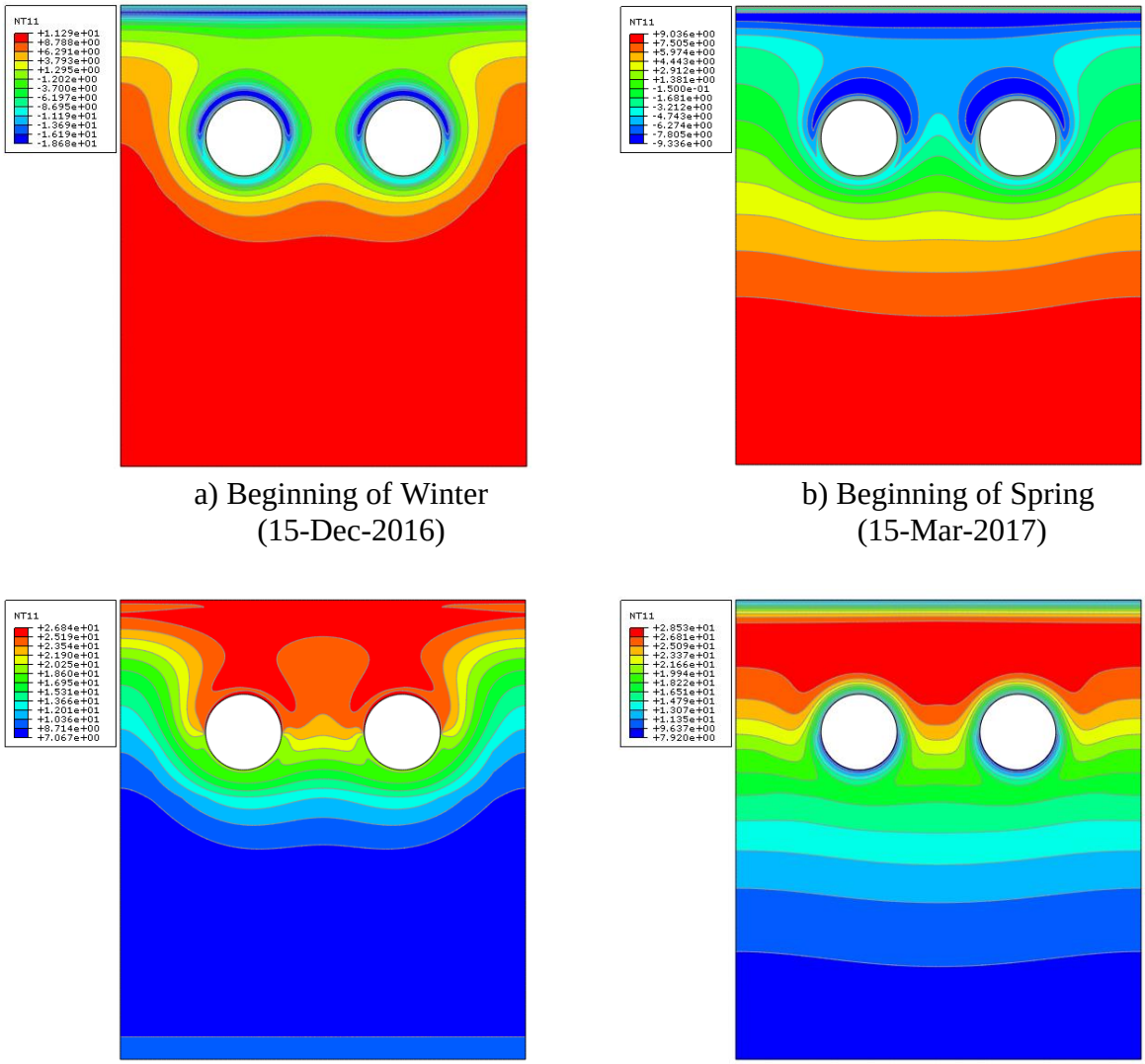

a) Beginning of Winter (15-Dec-2016)

b) Beginning of Spring (15-Mar-2017)

c) Beginning of Summer (15-June-2017)

d) Beginning of Fall (15-Sept-2017)

Figure 5.2: Thermal distribution at site 2 (Granular backfill).

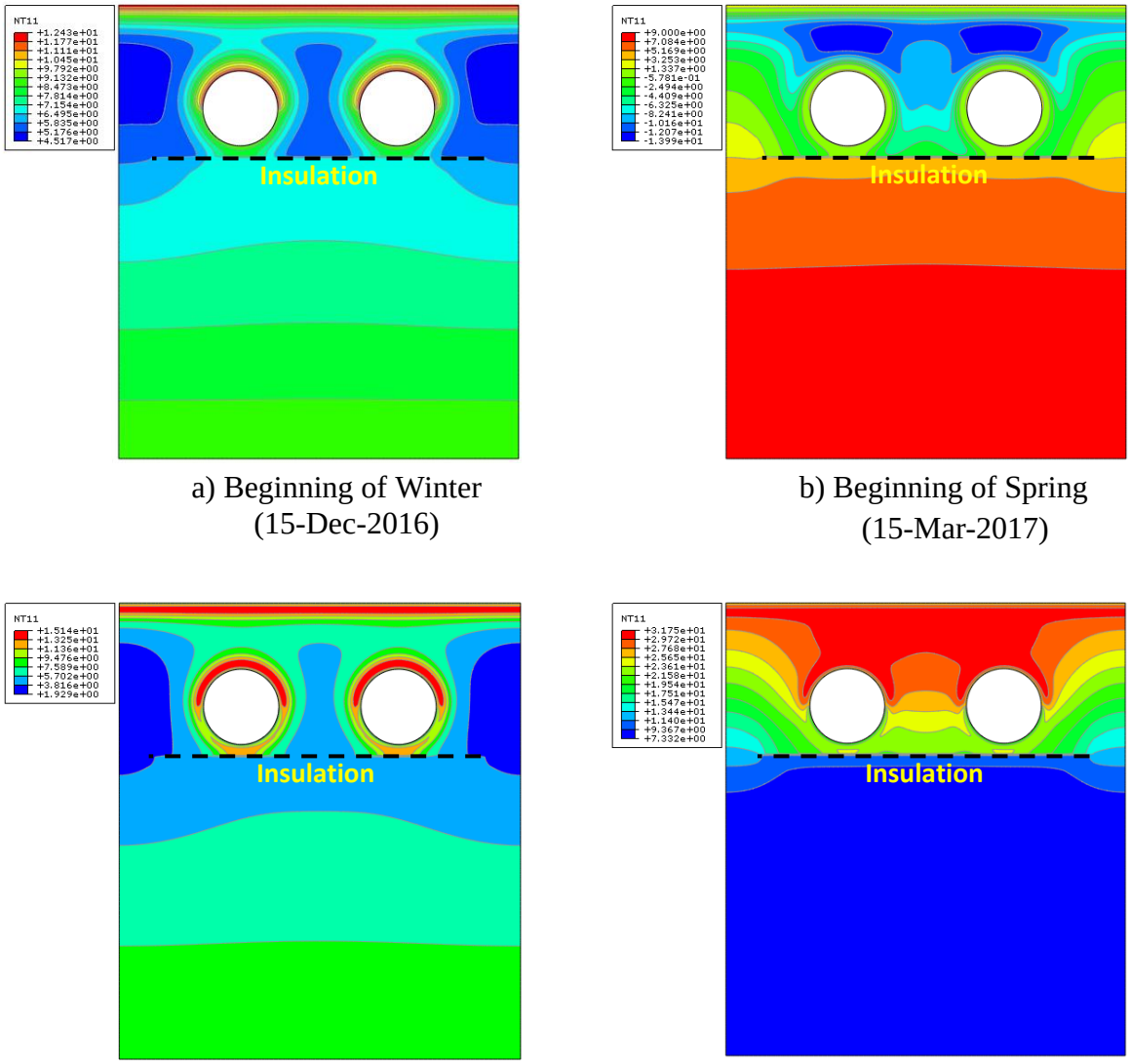

a) Beginning of Winter (15-Dec-2016)

b) Beginning of Spring (15-Mar-2017)

c) Beginning of Summer (15-June-2017)

d) Beginning of Fall (15-Sept-2017)

Figure 5.3: Thermal distribution at site 3 (Granular backfill + Insulation).

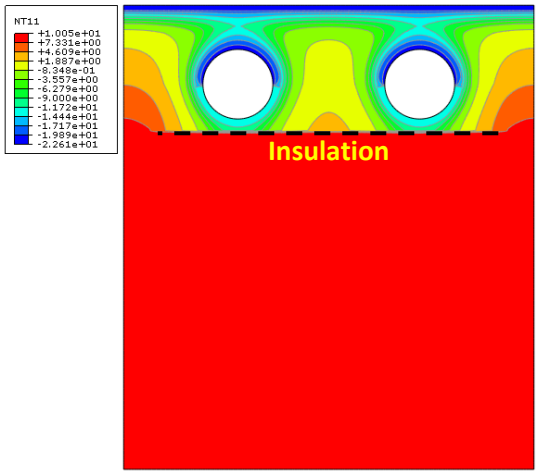

a) Beginning of Winter
(15-Dec-2016)

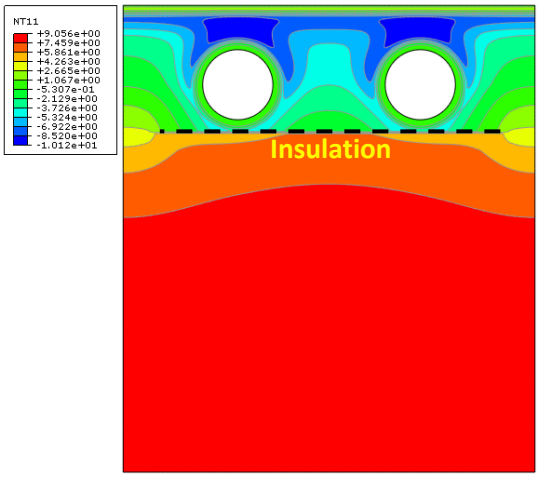

b) Beginning of Spring
(15-Mar-2017)

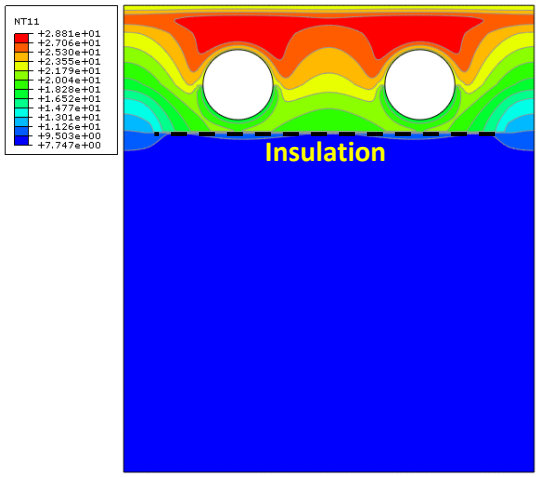

c) Beginning of Summer
(15-June-2017)

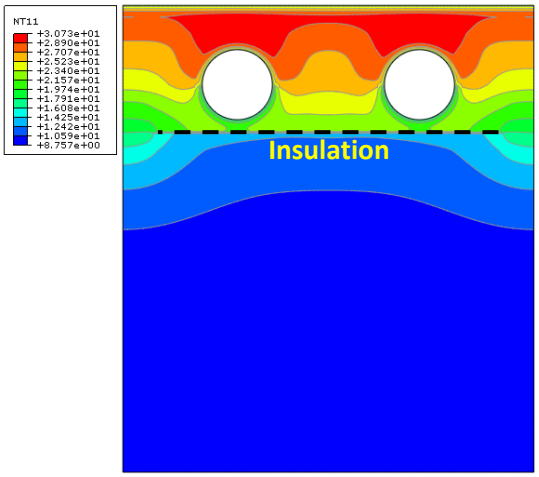

d) Beginning of Fall
(15-Sept-2017)

Figure 5.4: Thermal distribution at site 4 (Clay backfill + Insulation).

5.1.2. Frost depth around culverts and the effect of thermal insulation

The maximum frost penetration depths and their time of occurrence at each site are shown in Figure 5.5). The site 1 has the deepest frost penetration, because it has the deepest thermally disturbed soil (Figure 5.5-a). The frost penetration did not penetrate through the thermal insulation at sites 3 and 5 as shown in Figure 5.5-c) and (5.5-d). This is because the rigid insulation has high thermal resistivity, which prevented disruption in the thermal regime below insulation level.

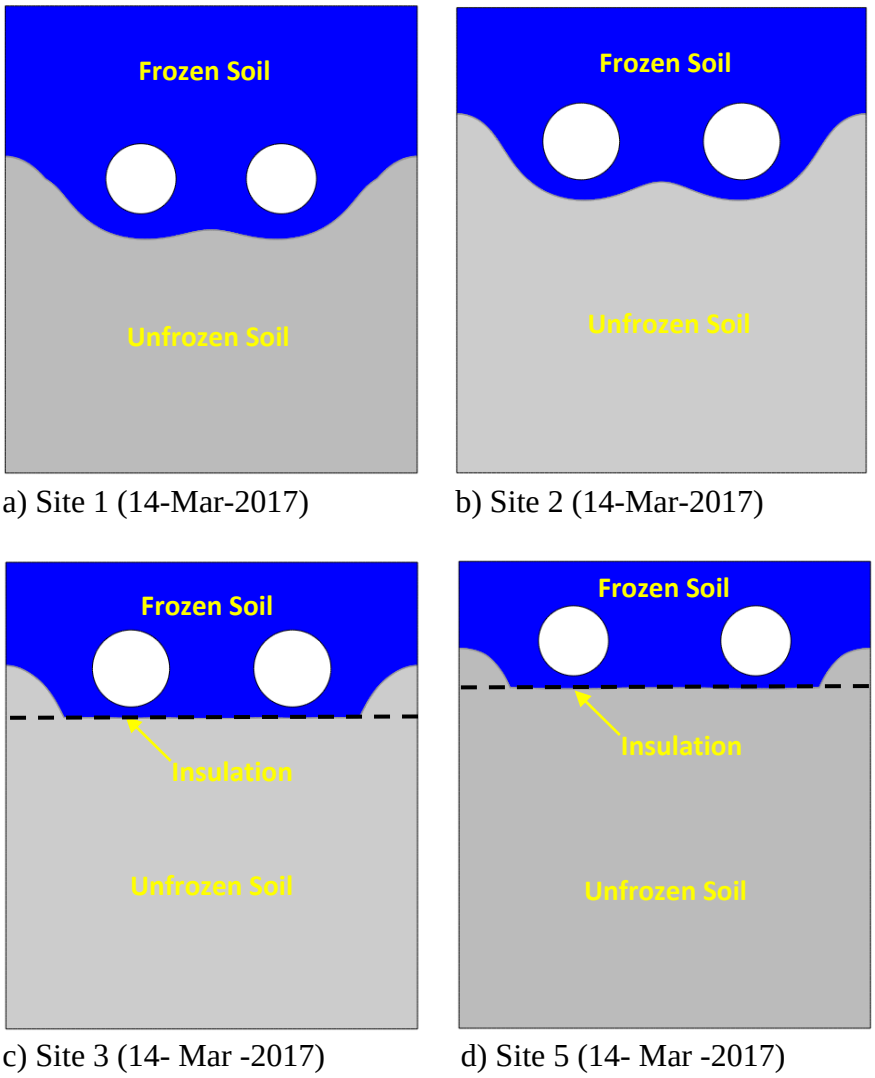

a) Site 1 (14-Mar-2017) b) Site 2 (14-Mar-2017)

c) Site 3 (14- Mar -2017) d) Site 5 (14- Mar -2017)

Figure 5.5: The maximum frost depth with and without the effect of thermal insulation below the culvert barrels

5.1.3. Conclusions from modeling the thermal profile at the vicinity of culverts

Based on the results, the conclusions from modeling the culvert sites are the following:

- The culverts cause disturbance in the ground thermal profile, because they acted as heating source during Spring and Summer, and as cooling source during fall and Winter.
- The thermal disturbance cause by the culvert barrels is the reason behind the increase in the thickness of the active layer around the culvert area.
- The deeper the culvert openings the thicker the active layer.
- The thick layer of frozen soil over culverts are created because of the cooling coming from the culvert barrels, which would produce thicker layer of weak thawed soil during spring. This would increase potential roughness at pavement surface.
- The rigid insulation successfully reduces the disturbance in the ground thermal profile, which kept the ground temperature below the insulation above the freezing point.

5.2. Parametric study on the effective use of rigid geofoam thermal insulation near culverts

To the best of authors' knowledge, the effective distribution of geofoam thermal insulations near culverts to reduce the differential frost actions is poorly documented in the scientific literature. Therefore, more comprehensive research and field studies are needed to evaluate the performance of the thermal insulation in the vicinity of culverts.

Hua et. al. (2014) studied, through a case study, the impact of using anti-frost berm and a 100mm geofoam thermal insulation placed at the top of a box culvert passing through a railroad embankment in the cold regions in China. The objective of this study was to mitigate the deformation in the railway embankment over box culverts due to nonuniform frost actions using thermal insulation. Hua et. al. (2014) concluded that having insulation at the inner or the outer surface of the culvert is expected to create more uniform frost and thawing actions. However, insulating the inner surface is expected to affect the hydrological design and the water flow through the culvert.

A numerical study of insulated circular concrete culvert was performed by Duquennoi and Sterling (1991) in Minnesota, USA. The culvert was a single barrel with 600mm diameter placed under 250mm asphalt pavement with a 600mm depth of cover, which is the distance from the road surface to the top of the culvert. The study considered evaluating 1 inch (25mm), 2 inches (50mm), and 3 inches (75mm) thick rigid geofoam insulations along the outer surface of the circular concrete culvert. The study showed that the insulation reduces the thermal disturbance near the culvert in the winter by 18% for 1 inch (25mm) thick insulation, and by 27% for the 2 inches (50mm) and the 3 inches (75mm) thick insulation. Duquennoi and Sterling (1991) concluded that

insulation along the outer surface of the culverts reduces thermal disturbance caused by the culvert barrel.

Luo et. al. (2017) studied, through a case study in Japan, the effect of placing an inverted U-shaped geofoam thermal insulation attached to a box culvert located at 5.7m below the pavement surface along with a 150mm thick thermal insulation placed on top of the backfill materials. This study concluded that the differential frost heave at the top of the box culvert was relatively low when the geofoam insulation was placed on top of the subgrade.

Another case study and a numerical analysis was conducted by Kavanagh and Shalaby (2017) and Moussa et. al. (2018) on double barrel concrete culvert sites in Manitoba, Canada. A total of four instrumented culvert sites were considered in this study, two of which were backfilled with clay and the other two sites were backfilled with granular soil. Rigid geofoam thermal insulation was placed 100mm below the culvert barrels, at one of the granular backfilled culverts and one of the clay backfilled culverts. The two studies concluded that the frost could not penetrate through the insulation level. The geofoam thermal insulation maintained temperatures above $0^{o}C$ below the insulation level at the sites with granular and clay backfill. This prevented differential settlement below the culverts.

Table *5-1*) presents a summary of the suggested placements of the thermal insulation near culverts to reduce the thermal disturbance in the soil and the corresponding differential frost heave and differential thaw settlement.

Table 5-1: Suggested placement of the geofoam thermal insulation near culverts to reduce the road roughness

Alternative	Geofoam location relative to the culvert barrels	Reference	Location
1	At the top of the clay backfill	Luo et. al. (2017)	Japan (Case Study)
2	150mm at the top of the culvert	Hua et. al. (2014)	China (Case study)
3	100mm below the culvert	Kavanagh and Shalaby (2017); and Moussa et. al. (2018)	Manitoba (Case study)
4	On the outer surface of the culvert	Duquennoi and Sterling (1991)	Minnesota (Numerical study)
5	No Insulation	Control alternative	

5.2.1. Parametric study

This section studies the effect of the different arrangements of geofoam insulations close to culverts to reduce the road roughness resulting from the thermal disturbance. Four alternatives for the location of the geofoam insulation near culverts are considered based on the findings from literature (*Table 5-1*). The first alternative (Alternative 1) is to place the geofoam thermal insulation at the top of the clay backfill (*Figure 5.6*-a). The second alternative (Alternaive 2) is to place the geofoam at 150mm above the culvert barrels within the clay backfill (*Figure 5.6*-b). The recommended distance between the culvert and the insulation on the top should not be less than 150 mm according to Andersland and Ladanyi (2004). The third alternative (Alternative 3) is placing the geofoam insulations at 100mm below the culvert barrels within the granular backfill (*Figure 5.6*-c), which is currently used by the Manitoba department of Infrastructure (MI). The fourth alternative (Alternative 4) is to insulate the outer surface of the concrete culvert barrels with

the geofoams (*Figure 5.6*-d) as recommended by Duquennoi and Sterling (1991) and used by the Minnesota Department of Transportation (MnDOT). Finally, no-insulation alternative (Alternative 5) is also considered in this study. The five alternatives are modeled near culverts with three different depths of cover 0.8m, 1.8m, and 2.8m, respectively. A 50mm thick insulation is applied for alternatives 1,2, and 3, while three thicknesses, 25mm, 50mm, and 75mm, are considered for alternative 4 (*Figure 5.6*-d).

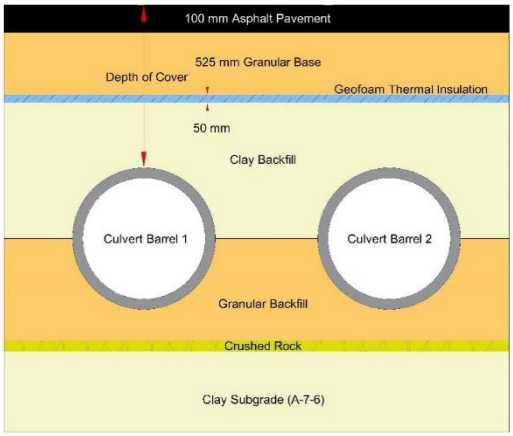

(a) Alternative 1: Thermal insulation at the top of the subgrade

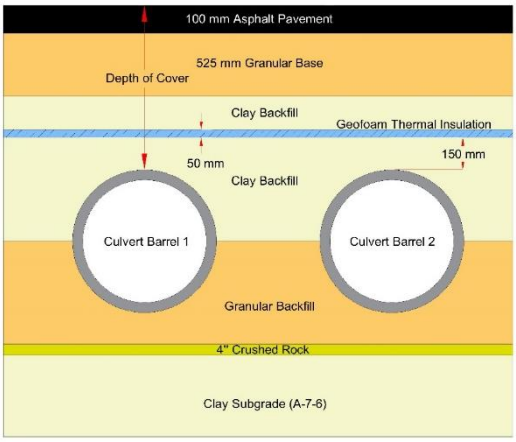

(b) Alternative 2: Thermal insulation 150mm at the top of the culvert barrels

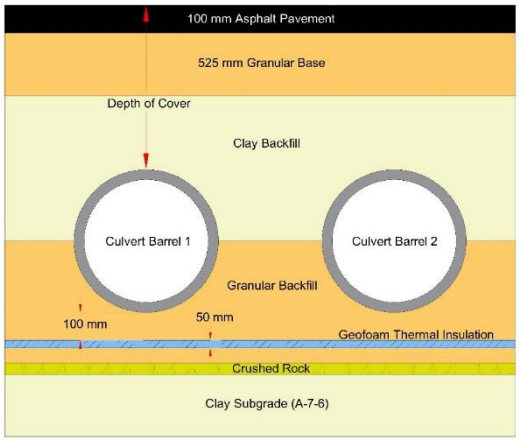

(c) Alternative 3: Thermal insulation below the culvert barrels

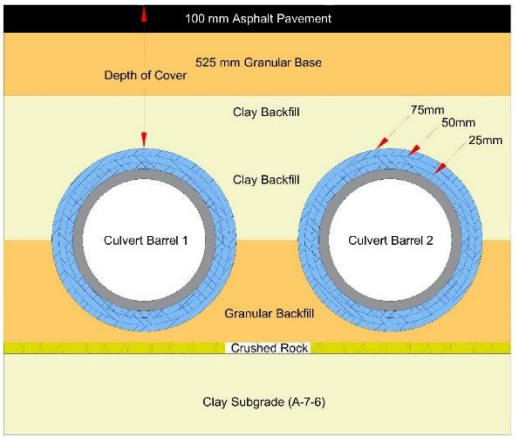

(d) Alternative 4: Thermal insulation on the outer surface of the culvert barrels

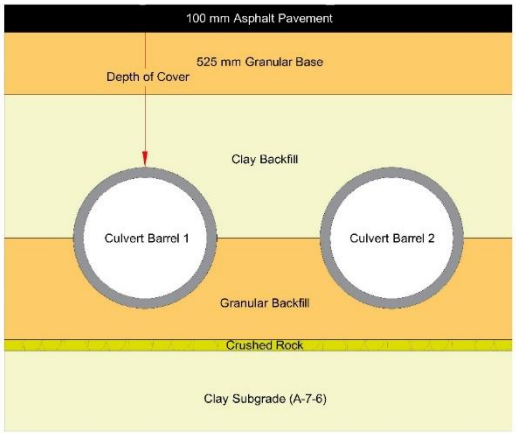

(e) Alternative 5: no insulation

Figure 5.6: Alternative placements of geofoam thermal insulation near culverts (Not to Scale)

5.2.2. Effect of the position of geofoam insulation on the freezing and thawing rates

The location of the thermal insulation for the same type of soil can affect the duration of the frost and thawing actions periods, which are evaluated by the freezing (FI) and the thawing (TI) indices of the soil. These indices are calculated by using the cumulative soil temperature (^{o}C.day) predicted from the 2-D model at the centerline between the culvert barrels. The cumulative temperature is the algebraic sum of the soil temperatures during the 2-year study period. The freezing and the thawing indices are the algebraic difference between the consecutive minimum and maximum cumulative soil temperature. High freezing and thawing indices indicate high rate of freezing and thawing in the soil. The higher the freezing or the thawing rates the less efficient the design of thermal insulation.

Table 4 shows that Alternative 4 with 75mm thick insulation has the lowest freezing and thawing indices at various depths of cover (*Table 5-2* and *Figure 5.7*). This indicates that alternative 4 with 75mm thick insulation has the most efficient performance regarding reducing the thermal disturbance in the soil. Conversely, alternative 2 has the highest freezing and thawing (*Table 5-2* and *Figure 5.7*).

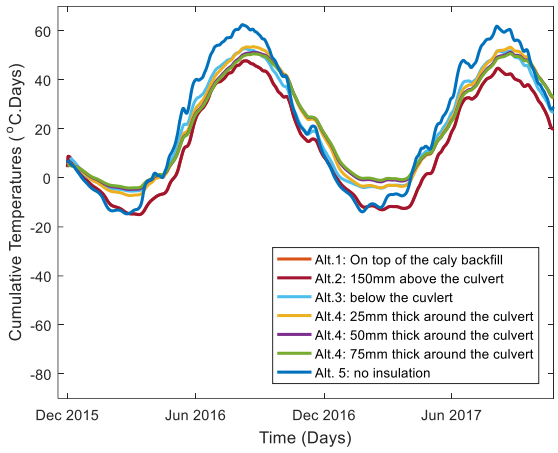

(a)

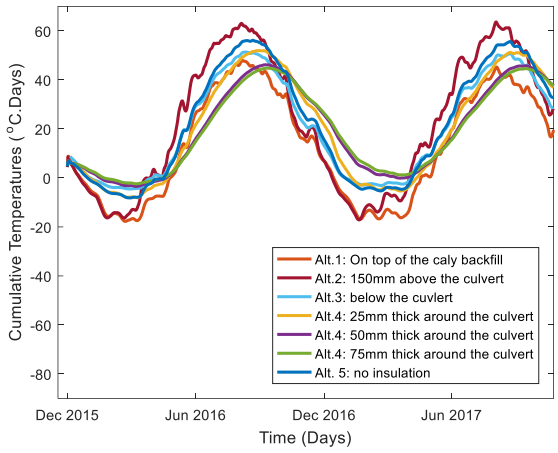

(b)

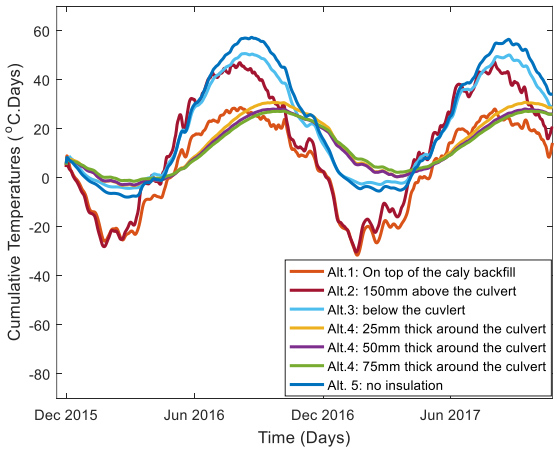

(c)

Figure 5.7: Cumulative soil temperature at the vicinity of culvert with depths of cover (a) 0.8m , (b) 1.8m, & (c)2.8m

Table 5-2: the freezing and thawing indices of all the alternatives at various depths of cover

Alternative #	Location of the thermal insulation	Depth of cover					
		0.8 m		1.8 m		2.8 m	
		FI	TI	FI	TI	FI	TI
1	on top of the clay backfill	-64	63	-64	63	-61	55
2	150mm above the culvert	-80	78	-80	78	-77	75
3	100mm below the culvert	-56	55	-56	55	-53	55
4 (25mm)	attached to the culverts' walls	-56	60	-56	60	-31	34
4 (50mm)	attached to the culverts' walls	-46	48	-46	48	-28	31
4 (75mm)	attached to the culverts' walls	-42	44	-42	46	-28	27
5	No insulation	60	64	60	64	62	65

5.2.3. Effect of the position of geofoam insulation on the frost depth

Frost depth can be estimated by determining the temperature of the freezing isotherm. Andersland and Ladanyi (2004) defines the freezing isotherm as "the interface location between frozen and unfrozen soil". The temperature of the freezing isotherm is -1 ^{o}C (Adamson et. al., 1973; and Trogersen, 1976). While according to Andersland and Ladanyi (2004) the temperature of the freezing isotherm ranges between -1 ^{o}C to 0 ^{o}C. For highway applications, the Long Term Pavement Performance (LTPP) and the Enhanced Integrated Climatic Models (EICM) used by departments of transportation in North America assumes a 0 ^{o}C for freezing isotherm for determining the frost depth below pavement surface (Selezneva et. al., 2008). This assumption increases the factor of safety in determining the frost penetration depth (Andersland and Ladanyi, 2004). For this study, a freezing isotherm with a 0 ^{o}C is assumed to determine the frost penetration depth.

Table *5-3*) presents the predicted frost depth from the 2-D numerical model for the five alternative locations for the geofoam insulation at various depths of cover, over the 2-year study. The results show that placing the thermal insulation at the top of the subgrade (Alternative 1) produces the maximum frost depth under different depths of cover (Table *5-3*). Also, Alternative 1 produces frost depth greater than the frost depth produced by alternative 5 (Table *5-3*). This is because the thermal insulation placed at the top of the subgrade stores the cold temperatures coming from the culvert walls producing the coldest soil temperatures between the culvert barrels (*Figure 5.8*). Alternative 4 with 75mm thick insulation has the least frost depth (Table *5-3* and *Figure 5.8*). There is no noticeable difference in reducing the frost depth between alternative 4 with 25mm thick insulation and alternative 5 with no insulation for all the depths of cover; therefore, alternative 4 with 25mm thick insulation is not recommended for insulating culverts.

Table 5-3: Estimated Maximum depth of frost based on the position of the geofoam

Depth of cover (m)	**Alternative #**						
	Alt. 1	Alt. 2	Alt. 3	Alt. 4			Alt. 5
				25mm	50mm	75mm	
0.8 m	2.7	2.7	2.6	2.5	2.2	2.1	2.7
1.8 m	4.2	3.9	3.7	3.5	3.0	2.8	3.8
2.8 m	5.2	5.0	4.6	4.6	4.0	3.6	4.7

The uniform distribution of frozen soil around the culvert barrels is achieved with alternative 3 under 0.8m and 1.8m depths of cover (*Figure 5.9*-c and *Figure 5.10*-c). While a uniform distribution of frozen soil is produced with alternative 4 using 75mm thick insulation under a 2.8m depth of cover (*Figure* 5.11-f).

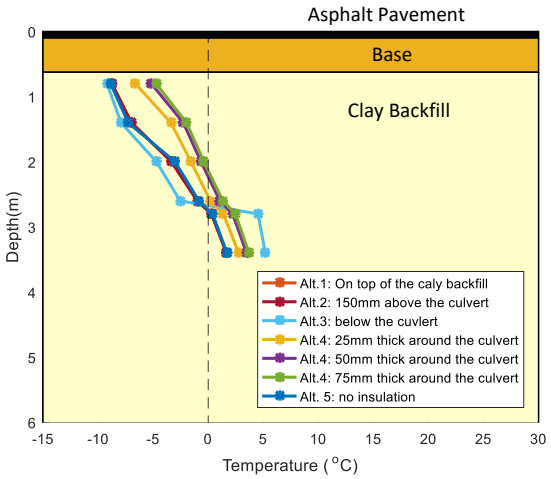

(a) 0.8m depth of cover in year 1

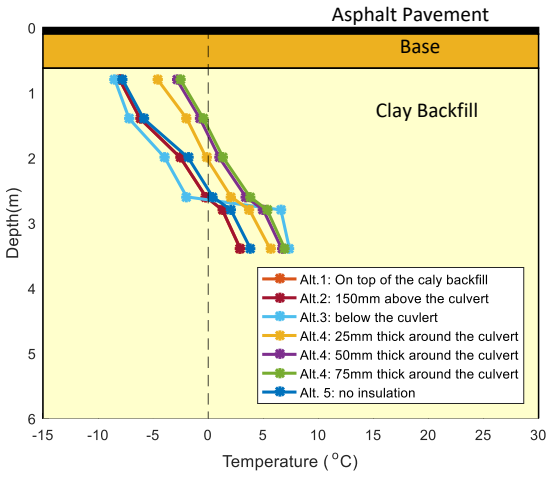

(b) 0.8m depth of cover in year 2

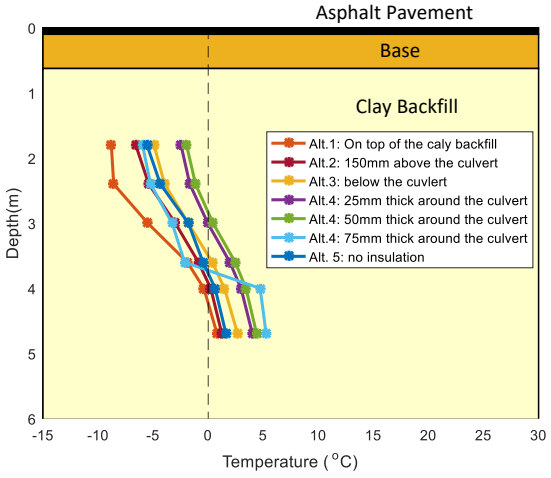

(c) 1.8m depth of cover in year 1

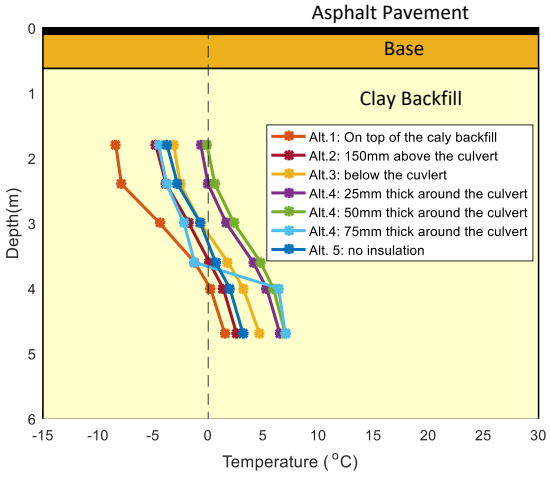

(d) 1.8m depth of cover in year 2

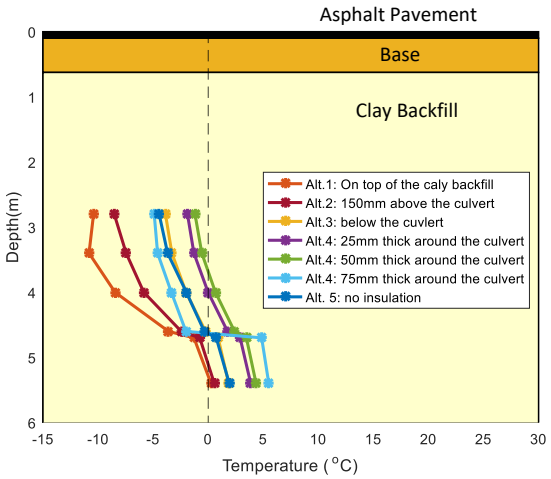

(e) 2.8m depth of cover in year 1

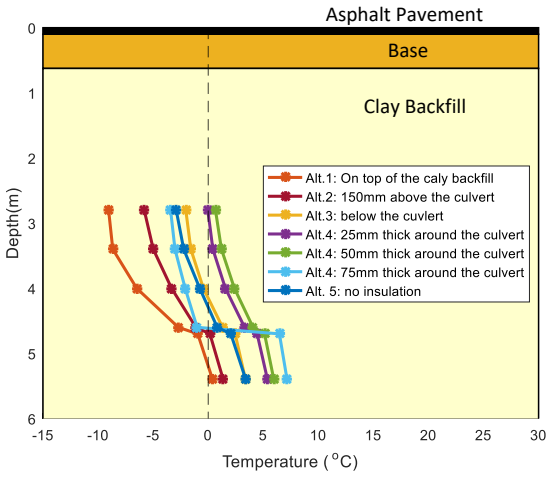

(f) 2.8m depth of cover in year 2

Figure 5.8: Coldest soil temperatures predicted between the culvert barrels from the 2-D numerical model at various depths of cover.

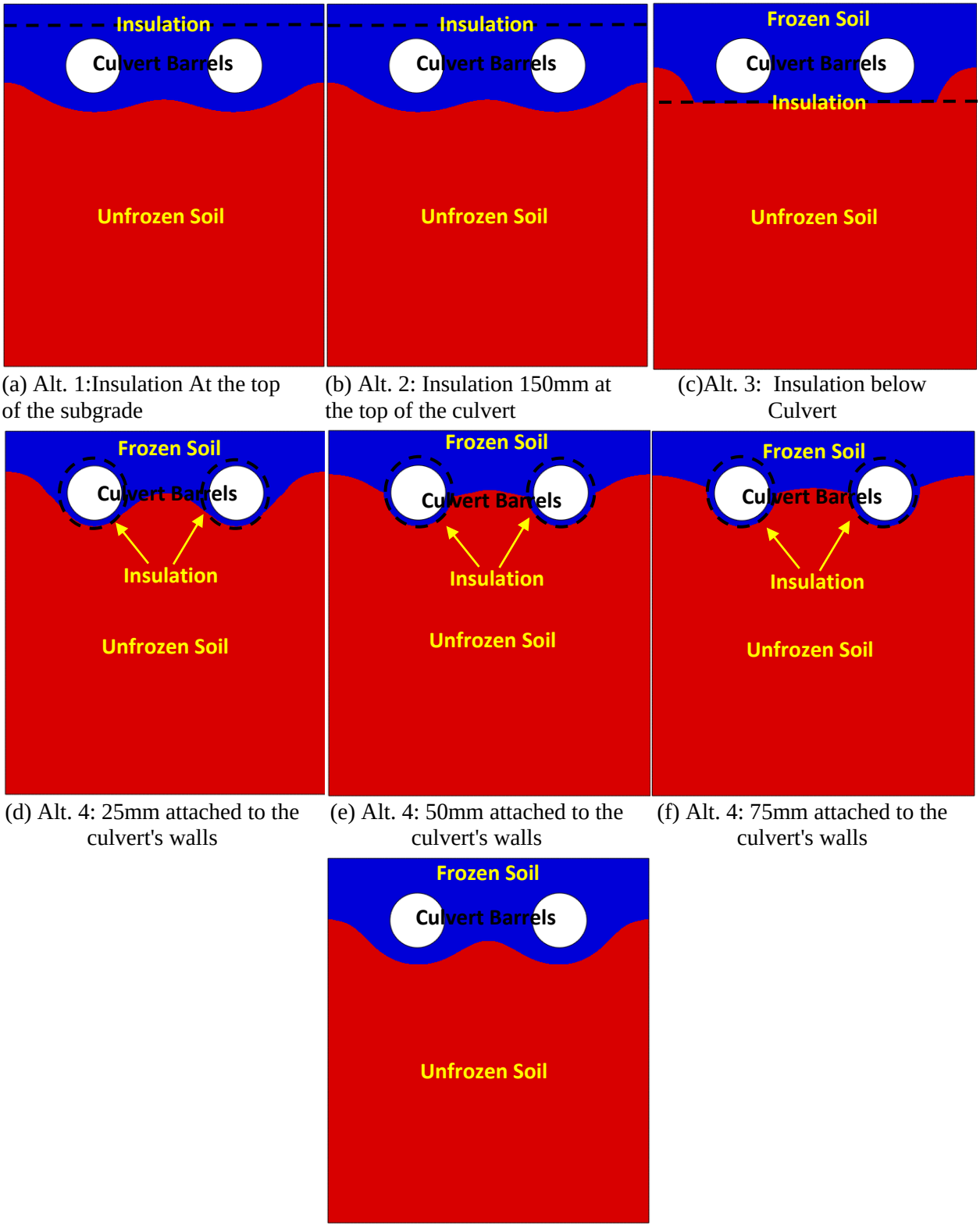

(a) Alt. 1:Insulation At the top of the subgrade

(b) Alt. 2: Insulation 150mm at the top of the culvert

(c)Alt. 3: Insulation below Culvert

(d) Alt. 4: 25mm attached to the culvert's walls

(e) Alt. 4: 50mm attached to the culvert's walls

(f) Alt. 4: 75mm attached to the culvert's walls

(g) Alt. 5: No Insulation

Figure 5.9: Frozen soil distribution with different arrangement of insulation at 0.8m depth of cover.

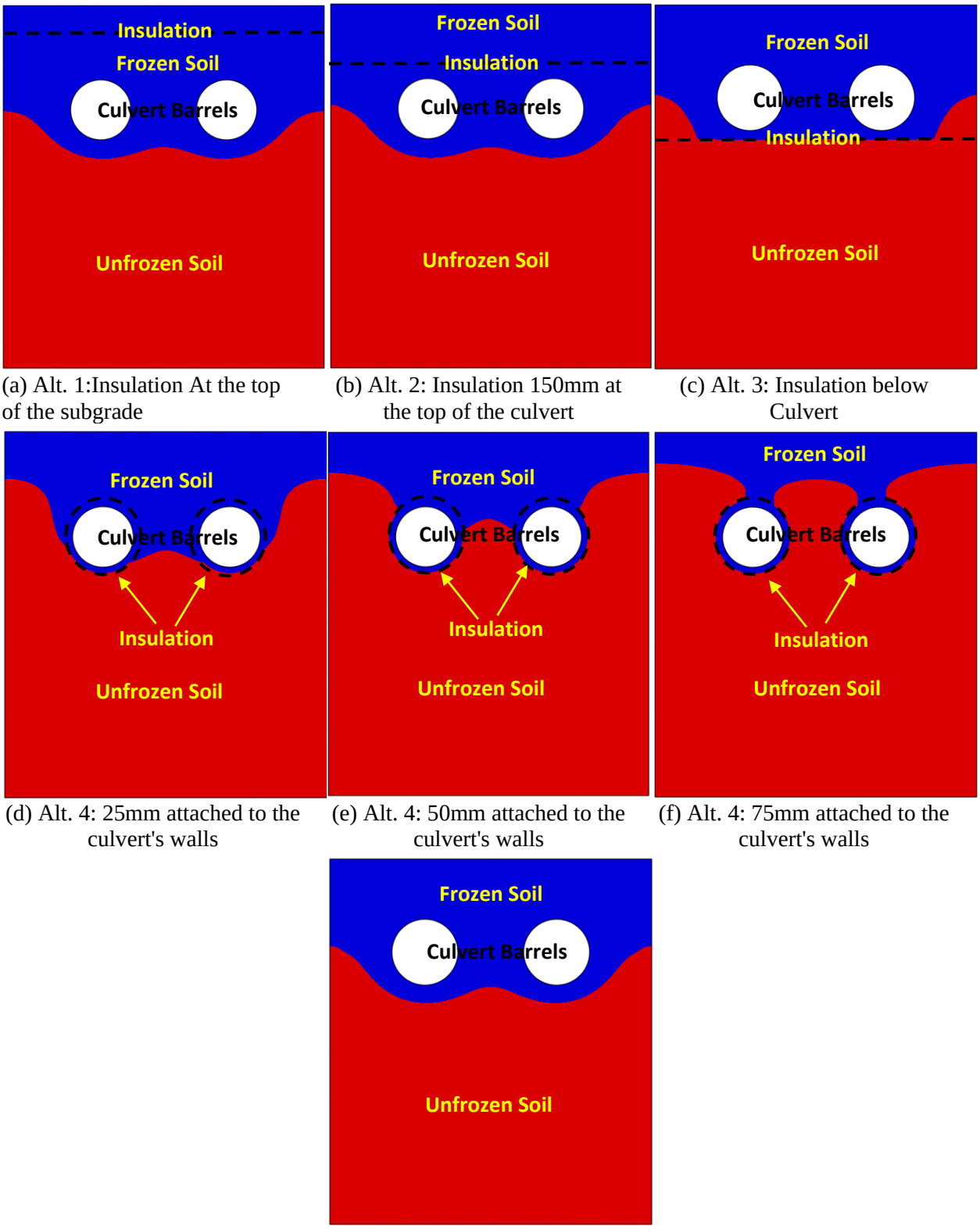

(a) Alt. 1:Insulation At the top of the subgrade

(b) Alt. 2: Insulation 150mm at the top of the culvert

(c) Alt. 3: Insulation below Culvert

(d) Alt. 4: 25mm attached to the culvert's walls

(e) Alt. 4: 50mm attached to the culvert's walls

(f) Alt. 4: 75mm attached to the culvert's walls

(g) Alt. 5: No Insulation

Figure 5.10: Frozen soil distribution with different arrangement of insulation at 1.8m depth of cover.

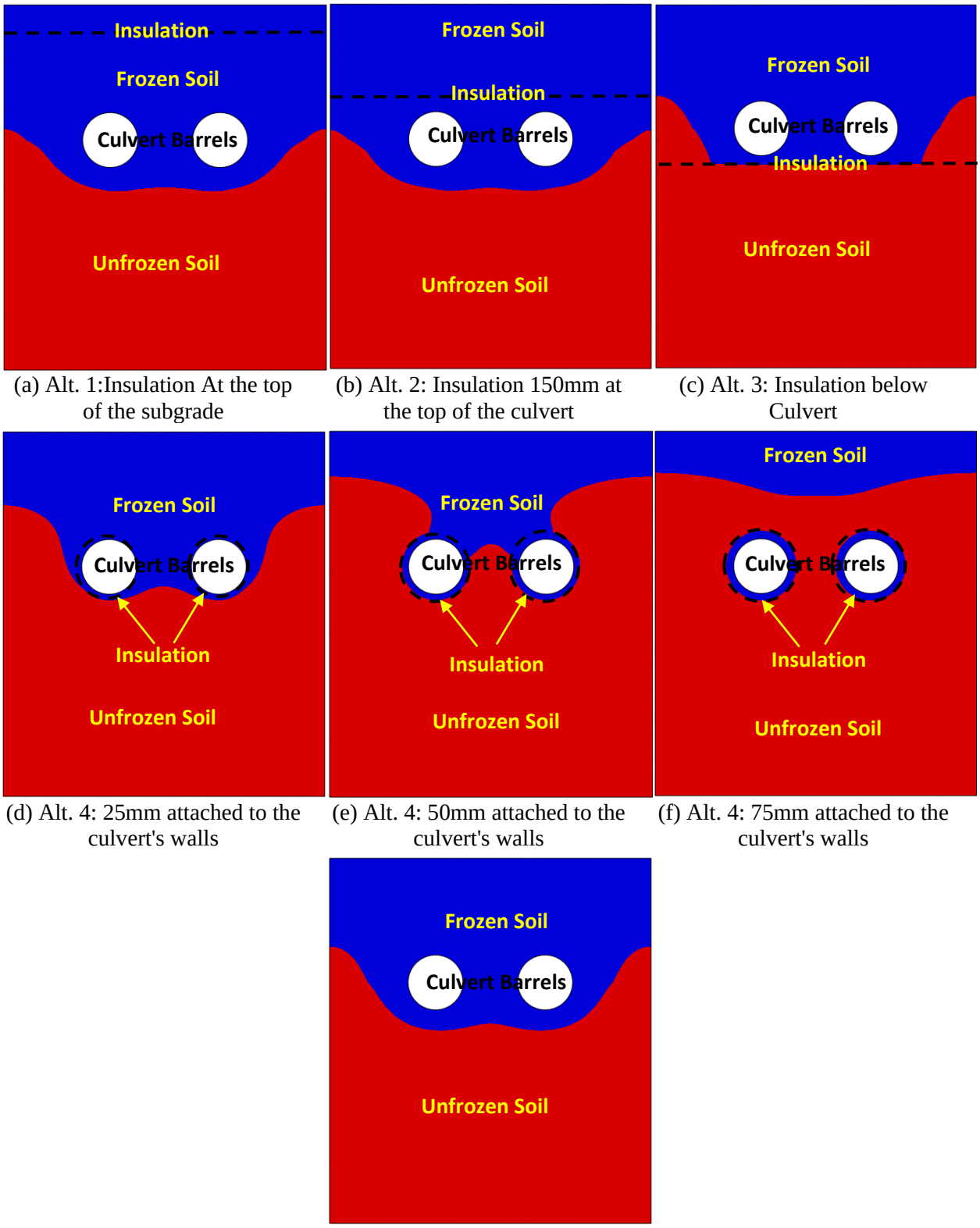

(a) Alt. 1:Insulation At the top of the subgrade

(b) Alt. 2: Insulation 150mm at the top of the culvert

(c) Alt. 3: Insulation below Culvert

(d) Alt. 4: 25mm attached to the culvert's walls

(e) Alt. 4: 50mm attached to the culvert's walls

(f) Alt. 4: 75mm attached to the culvert's walls

(g) No Insulation

Figure 5.11: Frozen soil distribution with different arrangement of insulation at 2.8m depth of cover.

5.2.4. Effect of the position of geofoam insulation on the soil thawing

In spring, placing the thermal insulation on top of the clay backfill (Alternative 1) delays the thawing process of the soil near the culverts. In contrast, during simulation of the insulation placed 150mm above the culverts (Alternative 2), the thawing is found to propagate in the horizontal direction below the geofoam insulation level, which advances the thawing process in the soil (*Figure 5.12*). The distance between thermal insulation at alternative 1 and the culvert barrels varies with the depth of cover, while the distance between the insulation and the culvert barrels for alternative 2 is the same for the different depths of cover; therefore, alternative 1 and 2 behave differently.

Figures (5.12, 5.13, and 5.14) show snapshots of the thawing process under the influence of the different geofoam positions. All the culverts insulated using alternative 4 with the 50 and 75 mm thaws earlier than the rest of the alternatives, as they produce the shallowest frost depth (*Figure 5.12*, 5.13, and 5.14). The culverts insulated with geofoam at the top of the culvert (alternative 2) thaws faster than the ones insulated at the road base (alternative 1). This confirms the findings in Table 5 where alternative 2 has the highest freezing and thawing indices. Geofoam placed at the top of the subgrade (alternative 1) delays the thawing process (*Figure 5.12*-a, 5.13-a, and 5.14-a). This is expected to be useful in insulating culverts in the permafrost zones, as it preserves the cold temperature of the permafrost. This is expected to reduce the degradation of the permafrost.

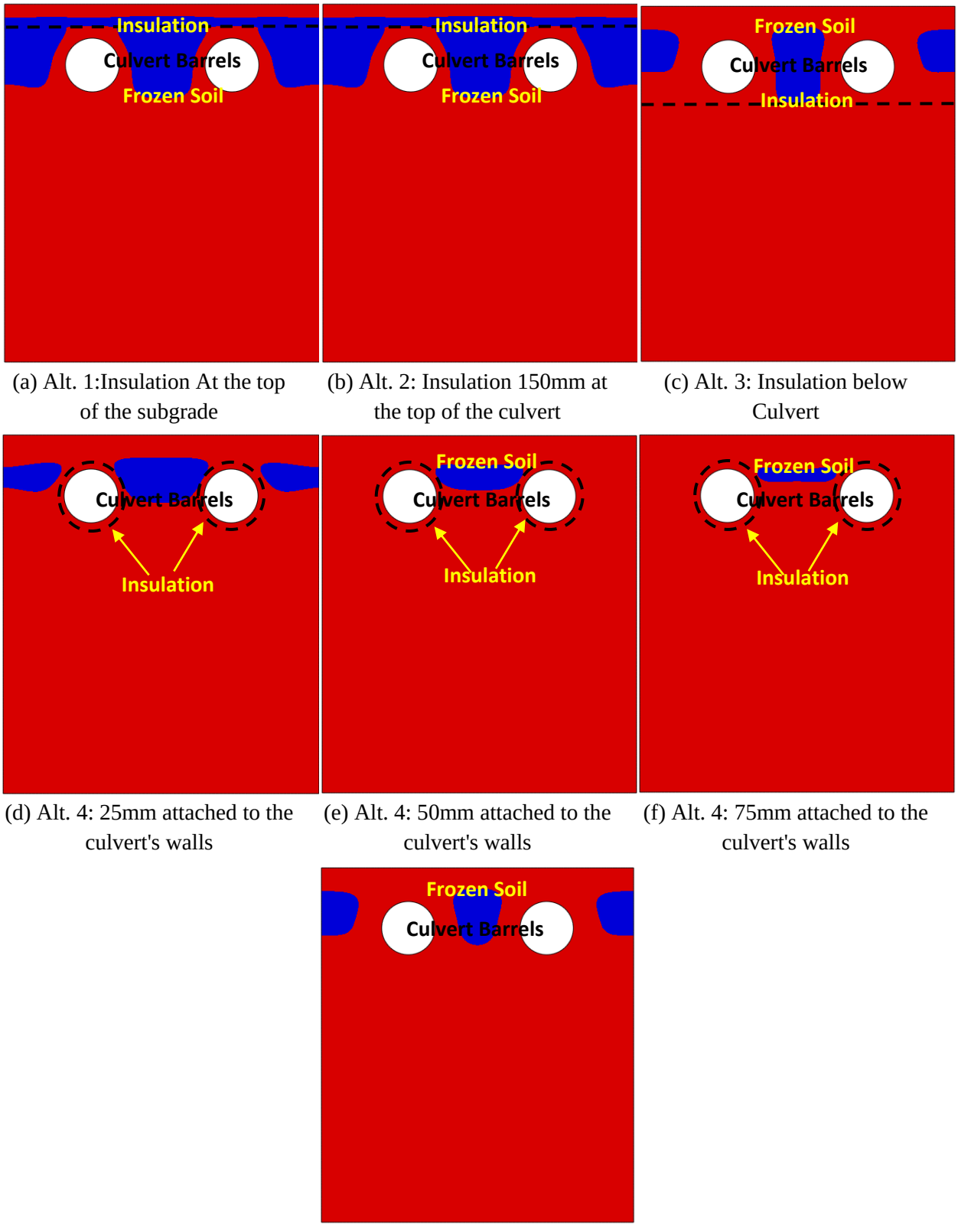

(a) Alt. 1:Insulation At the top of the subgrade

(b) Alt. 2: Insulation 150mm at the top of the culvert

(c) Alt. 3: Insulation below Culvert

(d) Alt. 4: 25mm attached to the culvert's walls

(e) Alt. 4: 50mm attached to the culvert's walls

(f) Alt. 4: 75mm attached to the culvert's walls

(g) No Insulation

Figure 5.12: Thawing process under different arrangements of insulation at 0.8m depth of cover.

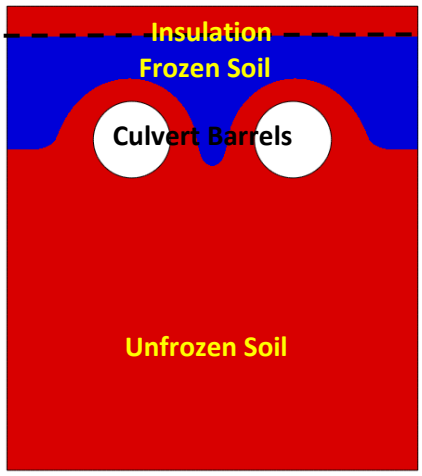

(a) Alt. 1:Insulation At the top of the subgrade

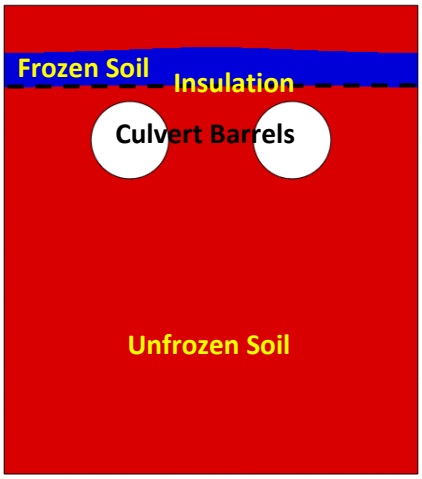

(b) Alt. 2: Insulation 150mm at the top of the culvert

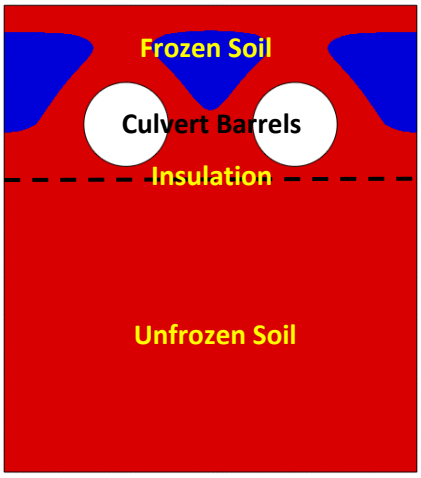

(c) Alt. 3: Insulation below Culvert

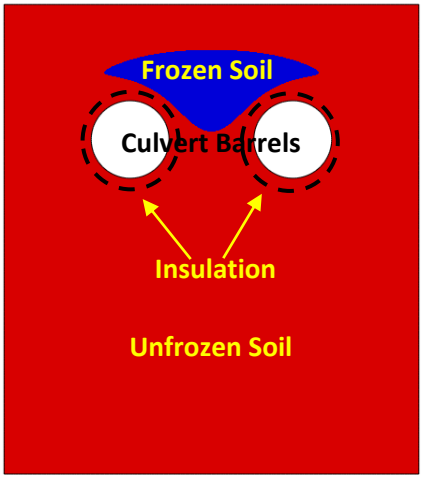

(d) Alt. 4: 25mm attached to the culvert's walls

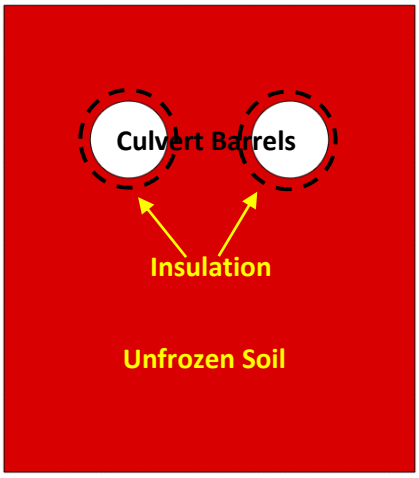

(e) Alt. 4: 50mm attached to the culvert's walls

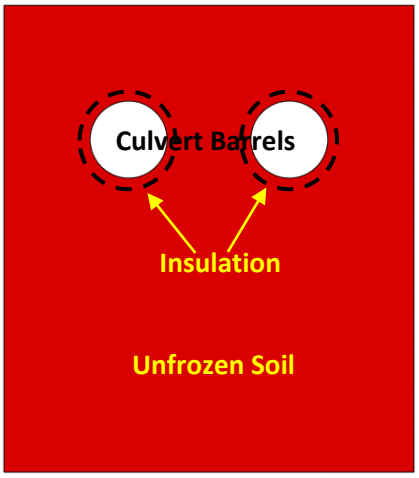

(f) Alt. 4: 75mm attached to the culvert's walls

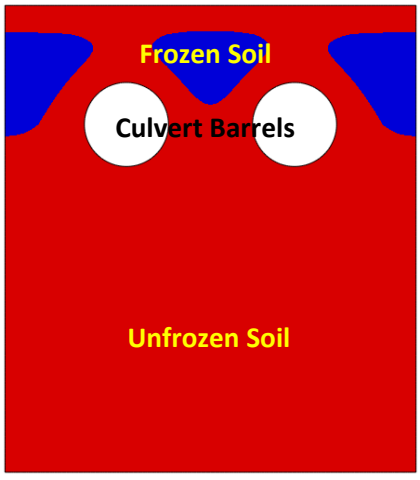

(g) No Insulation

Figure 5.13: Thawing process under different arrangements of insulation at 1.8m depth of cover.

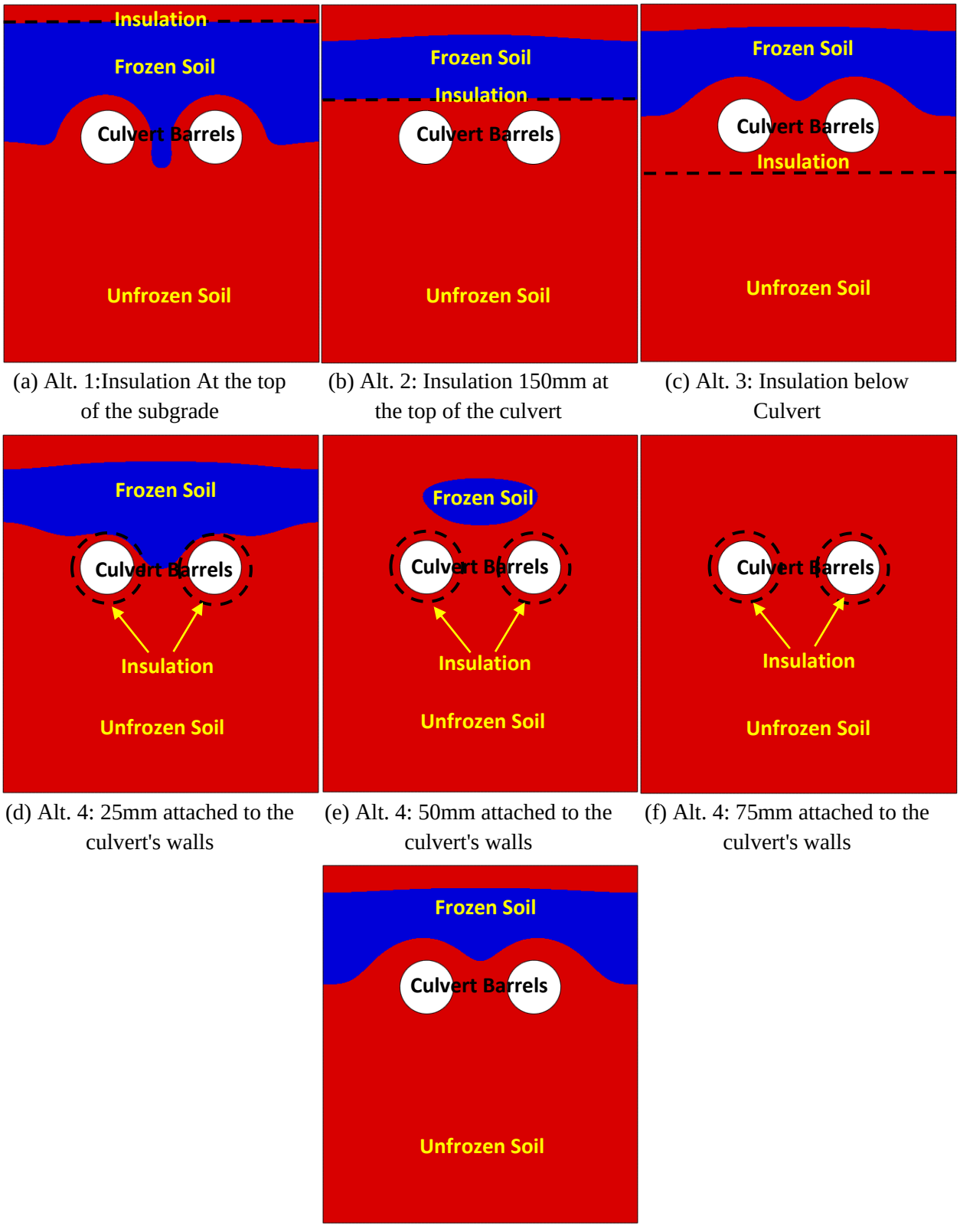

(a) Alt. 1:Insulation At the top of the subgrade

(b) Alt. 2: Insulation 150mm at the top of the culvert

(c) Alt. 3: Insulation below Culvert

(d) Alt. 4: 25mm attached to the culvert's walls

(e) Alt. 4: 50mm attached to the culvert's walls

(f) Alt. 4: 75mm attached to the culvert's walls

(g) No Insulation

Figure 5.14: Thawing process under different arrangements of insulation at 2.8m depth of cover.

5.2.5. Conclusions and recommendations on the placement of thermal insulation

A 2-D thermal numerical model of culvert is validated using the thermal data of three instrumented culvert sites. The culverts are different in the diameters of the barrels, and the depth of cover. The coefficient of determination (R^2) of the model are 0.96, 0.91, and 0.89 for 0.8m, 1.8m and 2.8m depths of cover, respectively. The numerical model is used to evaluate effect of the different placements of the geofoam thermal insulation around the culvert on reducing the thermal disturbance in clay soil.

Geofoams are placed on top of the clay backfill (Alternative 1), 150mm above the culvert (Alternative 2), 100mm below the culvert openings (Alternative 3), on the outer surface of the culvert barrels with three thicknesses (Alternative 4), and a site with no insulation is used as a control site (alternative 5). The findings from each alternative are summarized in *Table 5-4*). The pros and cons of each alternatives and suggested applications are summarized in *Table 5-5*).

In conclusion, placing the thermal insulation on top of the clay backfill (Alternative 1) is found to produce the maximum frost depth (*Table 5-4* and *5-5*), which is expected to increase the differential frost heave. Rapid change in the soil temperatures due to the high freezing and thawing indices is observed on the sites with thermal insulation placed 150 mm above the culvert barrels (Alternative 2) (*Table 5-4* and *5-5*). This is expected to produce differential frost heave and thaw settlements. Placing the thermal insulation 100mm below the culvert barrels (Alternative 3) produced uniform distribution of the thermal insulation around the culverts, which is expected to reduce the differential frost heave. Conversely, a minimum frost depth is produced when 75mm thermal insulation is attached to the culverts' walls (Alternative 4) (*Table 5-4* and *5-5*).

Table 5-4: Summary of the findings

Alternative (Thickness of Insulation)	1 (50mm)	2 (50mm)	3 (50mm)	4			5
				(25mm)	(50mm)	(75mm)	
Max frost depth	√						
Minimum frost depth						√	
Uniform distribution of frost			√	√	√		
Uniform distribution of thaw		√					
Rapid change in soil temperature		√					√
Slow change in soil temperature	√						

Table 5-5: The pros, cons, and suggested applications

Alternative	Thickness (mm)	Pros	Cons	Suggested application
1	50mm	• The delay in the thaw preserve the cold temperature. • Easy to build	• Extend the thawing period	• Insulate culverts in permafrost zones.
2	50mm	• The uniform and fast thawing of soil is expected to reduce the differential settlement in spring. • Easy to build.	• Rapid change in soil temperature. • Differential thaw settlement	• Not recommended
3	50mm	• Maintain soil temperature above freezing point. • No differential frost heave. • Easy to build.	-	• Insulate culverts in seasonally frozen soils and permafrost zones.
4	25mm	• No frost below culvert barrels. • Insulation can be attached to the culvert wall during manufacturing or on-site.	• Has performance similar to alternative 3 • Difficult to handle in the site.	• Not recommended
	50mm	• Uniform frost depth at 0.8m shallow culvert or shallower. • Insulation can be attached to the culvert wall during manufacturing or on-site.	• Nonuniform frost action at culverts deeper than 0.8m. • Difficult to handle in the site.	• Insulate culverts with 0.8m depth of cover or less.
	75mm	• Reduces the frost depth. • No frost below culvert barrels. • Insulation can be attached to the culvert wall during manufacturing or on-site.	• Nonuniform frost action at culverts with depth of cover less than 2.8m. • Difficult to handle in the site.	• Insulating culverts with 2.8m depth of cover or greater.
5		• Low initial cost	• High maintenance cost	-

Chapter 6: Summary, conclusions, and recommendations

6.1. Summary

Five culvert sites are built with different designs to reduce the road deformation over the culvert sections. The designs include using clay and granular backfill materials, and geosynthetics in the soil (e.g. geotextile, geogrids, and geofoams). The geofoam rigid insulations are placed below the culvert openings to prevent frost action below culverts (Figure *A.4*). Two layers of geogrids and on layer of geotextile are placed at the top of the culvert barrels to reduce the road roughness due to soil deformations (Figure *A.5*). Field instrumentations are installed in the culvert sites to monitor the thermal changes at the vicinity of culverts measured by the thermistors, and the deformations in the geosynthetics measured by strain gauges. Also, the deformations over the culverts are measured using GPR scans. The field data are used to calibrate and validate the 2-D numerical model to provide more data on the sites, predict frost depth, and to model other scenarios to be applied in the future.

6.2. Conclusions

6.2.1. Field experiment and GPR scans

1. The rigid insulation successfully maintained warm soil temperatures greater than zero degrees below the culverts, because of its high thermal resistivity.
2. The geosynthetics reduced the road roughness over the culvert relative to other sites with no soil reinforcement, because the geosynthetics increase the overall stiffness of the unfrozen soil, and redistribute the soil deformations (e.g. frost heave and thawing depression) over larger area.

6.2.2. Numerical model

1. The culvert barrels create thermal disturbance in the ground thermal regime, because culvert barrels acted as source of heat during spring and summer, and as a source of cold during fall and winter.
2. The depth of the active layer at the vicinity of culverts is greater than the depth of the active layer in the natural soil away from the culvert barrels.
3. The deeper the culvert barrels in the soil the deeper the thickness of the active layer.
4. The thick layer of frozen soil over culverts are created because of the cooling coming from the culvert openings, which would produce deep layer of weak thawed soil during the spring. This would increase potential deformations in the soil and the corresponding roughness at pavement surface.
5. The rigid insulation successfully reduces the disturbance in the ground thermal profile, which keeps the ground temperature below the insulation above the freezing point.

6.2.3. Placement of geofoam thermal insulation near culverts

1. Placing the thermal insulation at the interface between the road base and the backfill preserves the cold temperature of the ground by delaying the thaw, which is expected to reduce the degradation of the permafrost under the road embankments.
2. Placing the thermal insulation 150 mm from the top of the culverts creates uniform frost and thawing action, which is expected to reduce the differential frost heave and thaw settlements.
3. Placing the thermal insulation below the culvert barrels prevents the occurrence of frost action below the insulation level.

4. The 25mm thermal insulation attached to the culvert walls has no impact on reducing the thermal disturbance coming from the culvert barrels.
5. The 50mm insulation attached to the culvert walls reduces the nonuniformity in the frost action at shallow culverts. Conversely, the performance of the 50mm insulation improves at deep culverts.
6. The 75mm insulation attached to the culvert walls eliminates the thermal disturbance effect of the culverts deeper than 2.5m.

6.3. Recommended future work

The following future researches are proposed

1. Local calibration of pavement temperature prediction models (e.g. SHRP, C-SHRP, and LTPP) for geotechnical thermal application.
2. Studying the culvert soil interaction with different types of backfill.
3. The effectiveness of using culverts with low thermal conductive concrete.
4. Coupled thermo-hydro-mechanical analysis of the culvert.

References

AASHTO (Americal Association of State Highway and Transportation Officials), (1993) “Guide of Design of Pvement Structures”, Washington D.C.

Adamson, B., Claesson, J., and Eftring, B. (1973). Floor slabs on ground–thermal insulation and floor temperatures. *Swedish Council for Building Research, Report, 40*. (In Norwegian)

Alavi, M., Pouranian, M., & Hajj, E. (2014). Prediction of asphalt pavement temperature profile with finite control volume method. *Transportation Research Record: Journal of the Transportation Research Board*, (2456), 96-106.

Andersland, O. B., & Ladanyi, B. (2004). *Frozen ground engineering*. John Wiley & Sons, pp. 4-7, 32-35, 44-52, 56-61.

Argue, G. H., & Denyes, B. B. (1974). Estimating the depth of pavement frost and thaw penetrations. *Transportation Research Record*, (497).

Bentz, D. P. (2000). *A computer model to predict the surface temperature and time-of-wetness of concrete pavements and bridge decks* (No. NIST Interagency/Internal Report (NISTIR)-6551).

Bergman, T. L., Incropera, F. P., DeWitt, D. P., & Lavine, A. S. (2011). *Fundamentals of heat and mass transfer*. John Wiley & Sons. pp. 136-138.

Black, P. B., & Hardenberg, M. J. (1991). *Historical perspectives in frost heave research: The early works of S. Taber and G. Beskow* (No. CRREL-SR-91-23). Cold Regions Research and Engineering Lab Hanover NH.

Chandrappa, A. K., & Biligiri, K. P. (2015). Development of pavement-surface temperature predictive models: Parametric approach. *Journal of Materials in Civil Engineering*, *28*(3), 04015143.

Côté, J., & Konrad, J. M. (2005). Thermal conductivity of base-course materials. *Canadian Geotechnical Journal*, *42*(1), 61-78.

Diefenderfer, B. K., Al-Qadi, I. L., & Diefenderfer, S. D. (2006). Model to predict pavement temperature profile: development and validation. *Journal of Transportation Engineering*, *132*(2), 162-167.

Doré, G., & Zubeck, H. K. (2009). *Cold regions pavement engineering*.

Duquennoi, C., Sterling, R., Center, U. S., and Maplewood, M. N. (1991). *Frost Heave Patterns and Optimal Design of Insulated Culverts* (MN/RC-91-08 Final Report). Office of Materials and Research, Minnesota Department of Transportation.

Farouki, O. (1992). *European foundation designs for seasonally frozen ground* (No. CRREL-MONO-92-1). Cold Regions Research and Engineering Lab Hanover Nh.

Farouki, O. (1982). *Thermal properties of soils*. US Army Corps of Engineers, Cold Regions Research and Engineering Laboratory.

Gedafa, D. S., Hossain, M., & Romanoschi, S. A. (2013). Prediction of Asphalt Pavement Temperature. In *Airfield and Highway Pavement 2013.* pp. 373-382.

Green, A. E., & Naghdi, P. M. (1965). A general theory of an elastic-plastic continuum. *Archive for rational mechanics and analysis*, *18*(4), 251-281.

Soliman, H., Kass, S., & Fleury, N. (2008). A simplified model to predict frost penetration for Manitoba soils. In *2008 Annual Conference of the Transportation Association of Canada. Transportation Association of Canada, Toronto, Ontario*.

Harlan, R.L., and Nixon, J.F. (1978). Ground thermal regime. Chapter 3 in *Geotechnical Engineering for Cold Regions*. O.B. Andersland and D.M. Anderson. New York: McGraw-Hill, pp. 103-63.

Hinkel, K. M., Nelson, F. E., Parker, W., Romanovsky, V. E., Smith, O., Tucker, W., ... & Brigham, L. W. (2003). Climate change, permafrost, and impacts on civil infrastructure. US Arctic Research Commission, Permafrost Task Force Report.

Hua, L., Fujun, N., Yonghong, N., and Xifeng, Y. (2014). Study on thermal regime of roadbed–culvert transition section along a high-speed railway in seasonally frozen regions. *Cold Regions Science and Technology*, *106*, 216-231.

Ishikawa, T., Kijiya, I., Tokoro, T., & Sato, M. (2016). Application of coupled thermo-hydro-mechanical analysis to frost-heave behavior of earth structures. *Japanese Geotechnical Society Special Publication*, *2*(13), 531-536, pp. 533.

Johansen, O. (1975). Thermal conductivity of soils. PhD Thesis, University of Trondheim, Norway: CRREL Draft English Translation 637. US Army Corps of Engineers, Cold Regions Research and Engineering Laboratory, Hanover, NH, pp. 230-253.

Kavanagh, L., Moussa, A., Shalaby, A. (2018). *Recommendations for Innovative Options for Culvert Installation to Mitigate Bumps and Depressions at Through-Grade Culverts in Manitoba: Demonstration Project PTH 68. Submitted to Manitoba Department of Infrastructure.* Technical Report.

Kavanagh, L., Shalaby, A., Moussa, A., Sparrow, S. (2017). Analysis of Measured Strains in Geogrid and Geotextile Reinforcement Clay Backfill Over Through-grade Culverts in Cold Climate, *Transportation Research Board 96th Annual Meeting*, Washington DC, USA.

Kavanagh, L., and Shalaby, A. (2017). Case study of innovative culvert installation techniques to mitigate pavement roughness at through-grade culverts in cold climate. *World Conference on Pavement and Asset Management, WCPAM 2017, Milan, Italy.*

Kersten, M.S. (1949). Laboratory research for the determination of the thermal properties of soils. Arctic Construction and Frost Effects Laboratory (ACFEL), Technical Report 23, AD71256.

Kim, K., Zhou, W., & Huang, S. L. (2008). Frost heave predictions of buried chilled gas pipelines with the effect of permafrost. *Cold Regions Science and Technology*, *53*(3), 382-396.

Konrad, J. M., & Lemieux, N. (2005). Influence of fines on frost heave characteristics of a well-graded base-course material. *Canadian geotechnical journal*, *42*(2), 515-527.

Konrad, J. M., & Shen, M. (1996). 2-D frost action modeling using the segregation potential of soils. *Cold regions science and technology*, *24*(3), 263-278.

Ladanyi, B. (1996). La conception et la rehabilitation des infrastructures de transport en regions Nordiques (Design and rehabilitation of transportation facilities in northern regions). Ministere des Trasnports de Quebec, Canada, RTQ-94-07. (In French)

Liu, Z., & Yu, X. (2011). Coupled thermo-hydro-mechanical model for porous materials under frost action: theory and implementation. *Acta Geotechnica*, *6*(2), 51-65, pp. 52.

Luca, J., & Mrawira, D. (2005). New measurement of thermal properties of superpave asphalt concrete. *Journal of Materials in Civil Engineering*, *17*(1), 72-79.

Lukanen, E. O., Stubstad, R., & Briggs, R. (2000). *Temperature predictions and adjustment factors for asphalt pavement* (No. FHWA-RD-98-085).

Lunardini, V. (1978, July). Theory of n-factors and correlation of data. In *Proceedings of the Third International Conference on Permafrost* (Vol. 1, pp. 40-46). Ottawa: National Research Council of Canada.

Luo, B., Ishikawa, T., Tokoro, T., and Lai, H. (2017). Coupled Thermo-Hydro-Mechanical Analysis of Freeze–Thaw Behavior of Pavement Structure over a Box Culvert. *Transportation Research Record: Journal of the Transportation Research Board*, (2656), 12-22.

Manitoba Ministry of Infrastructure (MI) (2017). *Manitoba ministry of infrastructure annual report (2016-2017).* Winnipeg, Manitoba.

McGaw, R. (1969). Heat conduction in saturated granular materials. *Highway Research Board Special Report*, (103).

Michalowski, R. L., & Zhu, M. (2007). Freezing and Ice Growth in Frost-Susceptible Soils. In *Soil Stress-Strain Behavior: Measurement, Modeling and Analysis* (pp. 429-441). Springer, Dordrecht.

Ministry of Highways and Infrastructure of Saskatchewan (MHIS) (2016) *Ministry of Highways and Infrastructure of Saskatchewan Annual report (2015-2016).* Regina, Saskatchewan.

Mohseni, A., & Symons, M. (1998). Improved AC pavement temperature models from LTPP seasonal data. In *transportation research board 77th annual meeting, Washington, DC.*

Moussa, A., Kavanagh, L., and Shalaby, A. (2018a). *Ground thermal profile and frost depth in the vicinity of through-grade culverts*. *Geohazards 7 Conference. The Canadian Geotechnical Society.*

Nishimura, S., Gens, A., Olivella, S., & Jardine, R. J. (2008). THM-coupled finite element analysis of frozen soil: formulation and application.

New York State Depatment of Transportation (NYSDOT) (2006). *Culvert inventory and inspection manual.*

Nixon, J. F. (1978). First Canadian Geotechnical Colloquium: Foundation design approaches in permafrost areas. *Canadian Geotechnical Journal*, *15*(1), 96-112.

Ohio Department of Transportation (ODOT) (2003). *Culvert management manual.* Columbus, Ohio.

Ryynänen, T. (2000). *Instrumentoidun tierakenteen mittaukset: ympäristötekijät 1998-99*. Tielaitos.

Selezneva, O. I., Jiang, Y. J., Larson, G., & Puzin, T. (2008). *Long term pavement performance computed parameter: Frost penetration* (No. FHWA-HRT-08-057). Turner-Fairbank Highway Research Center (Technical report).

Shoop, S., Affleck, R., Haehnel, R., & Janoo, V. (2008). Mechanical behavior modeling of thaw-weakened soil. *Cold Regions Science and Technology*, *52*(2), 191-206.

Torgersen, S. E. (1976). Frost protection of floor on groundwall. *Frost I Jord*, *17*(10), 287-314. (In Norwegian)

Tice, A. R., Anderson, D. M., & Banin, A. (1976). The prediction of unfrozen water contents in frozen soils from liquid limit determinations. Cold Regions Research & Engineering Laboratory. *US Army Corps of Engineers*.

Wang, D. (2015). Simplified analytical approach to predicting asphalt pavement temperature. *Journal of Materials in Civil Engineering*, *27*(12), 04015043.

Yavuzturk, C., Ksaibati, K., & Chiasson, A. D. (2005). Assessment of temperature fluctuations in asphalt pavements due to thermal environmental conditions using a two-dimensional, transient finite-difference approach. *Journal of Materials in Civil Engineering*, *17*(4), 465-475.

Zhang, Y., & Michalowski, R. L. (2015). Thermal-hydro-mechanical analysis of frost heave and thaw settlement. *Journal of Geotechnical and Geoenvironmental Engineering*, *141*(7), 04015027, pp. 7.

Zhu, M., & Michalowski, R. L. (2005). Simulation of heat transfer in Freezing soils using Abaqus. In *Abaqus Users' Conference* (pp. 1-7).

Appendices

Appendix A – Detailed cross sections of the five culvert sites (As-built cross sections)

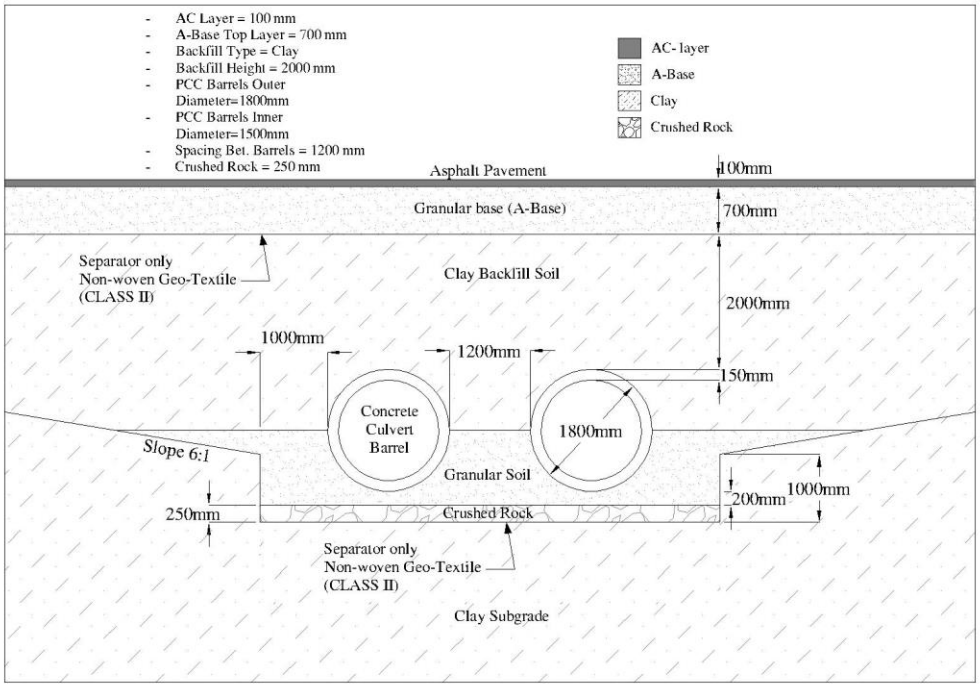

Figure A.1: Detailed cross section of culvert site 1

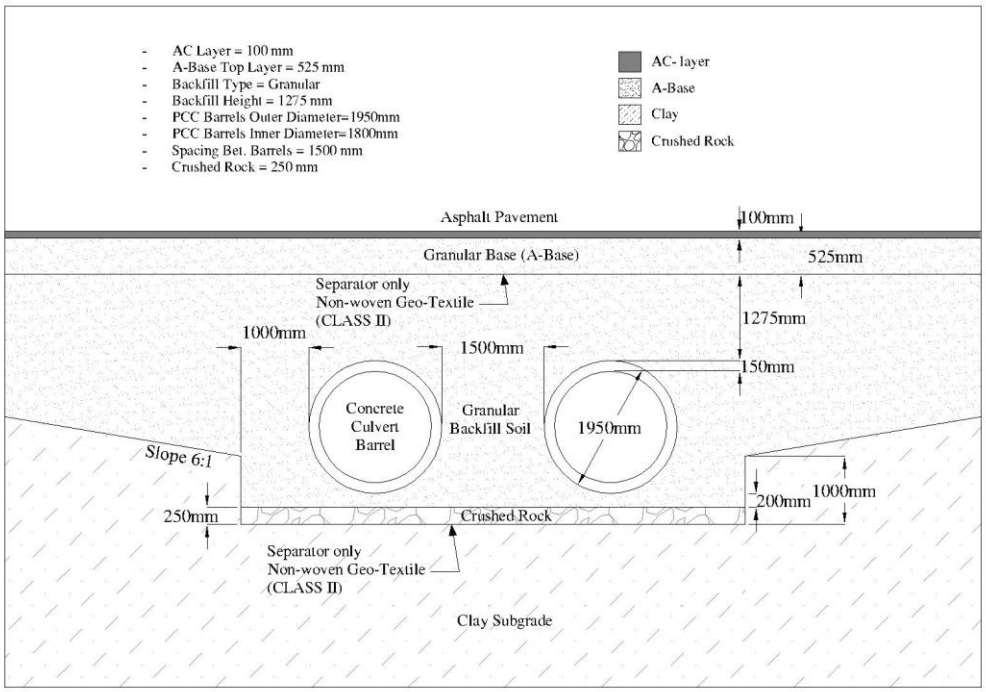

Figure A.2: Detailed cross section of culvert site 2

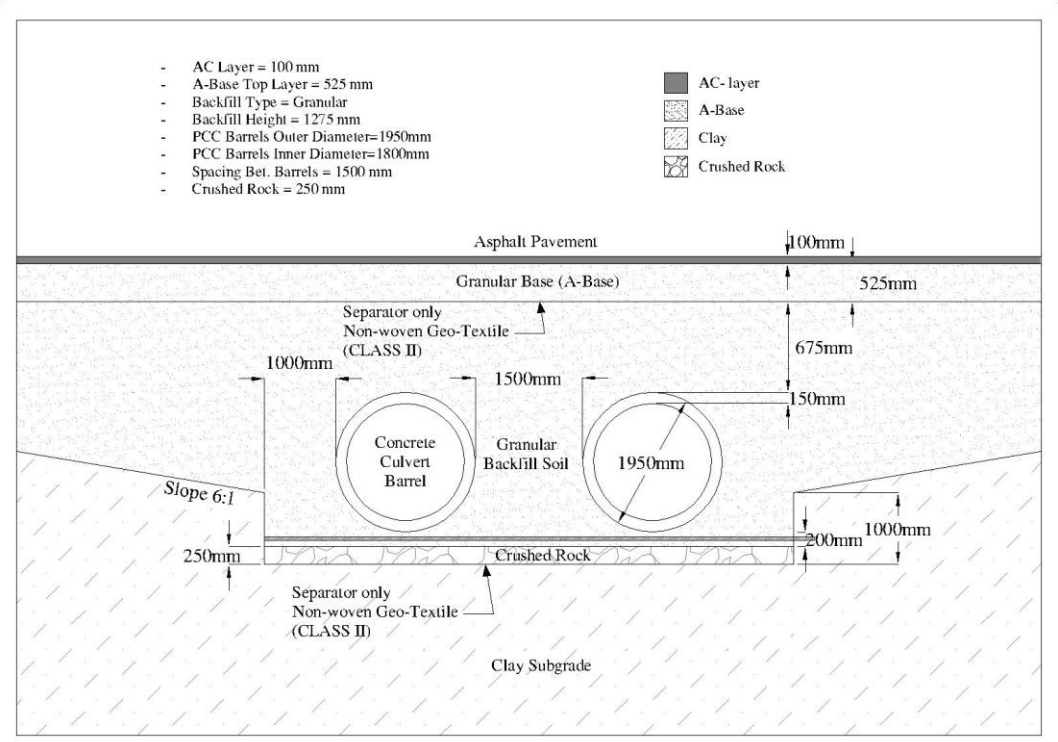

Figure A.3: Detailed cross section of culvert site 3

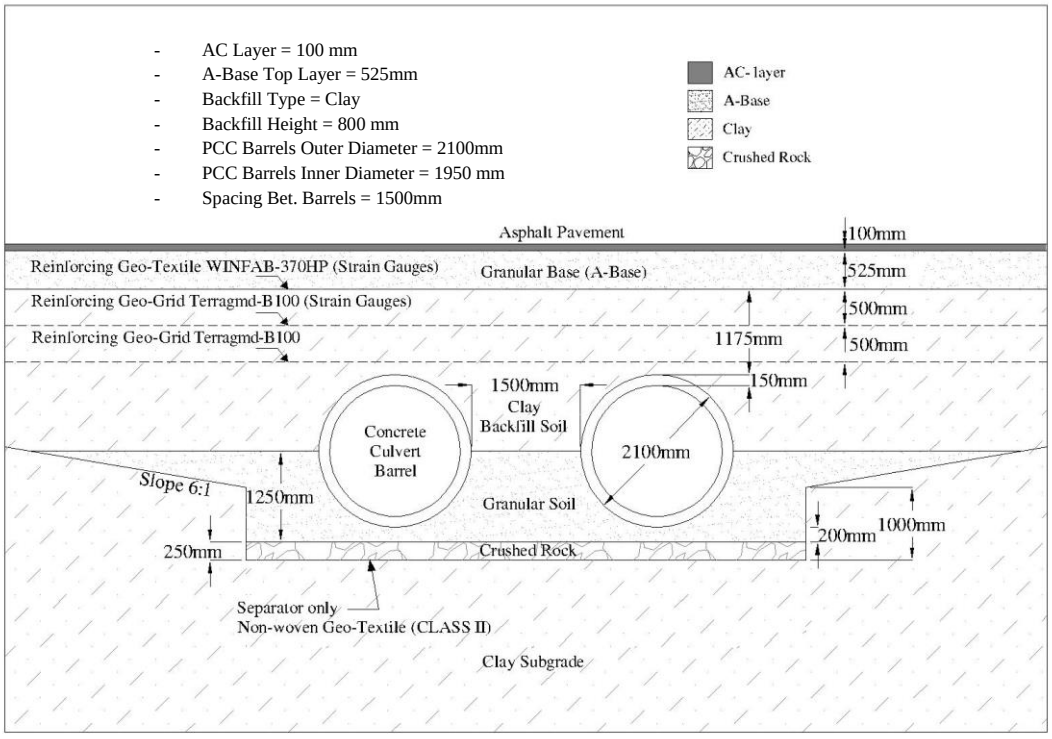

Figure A.4: Detailed cross section of culvert site 4

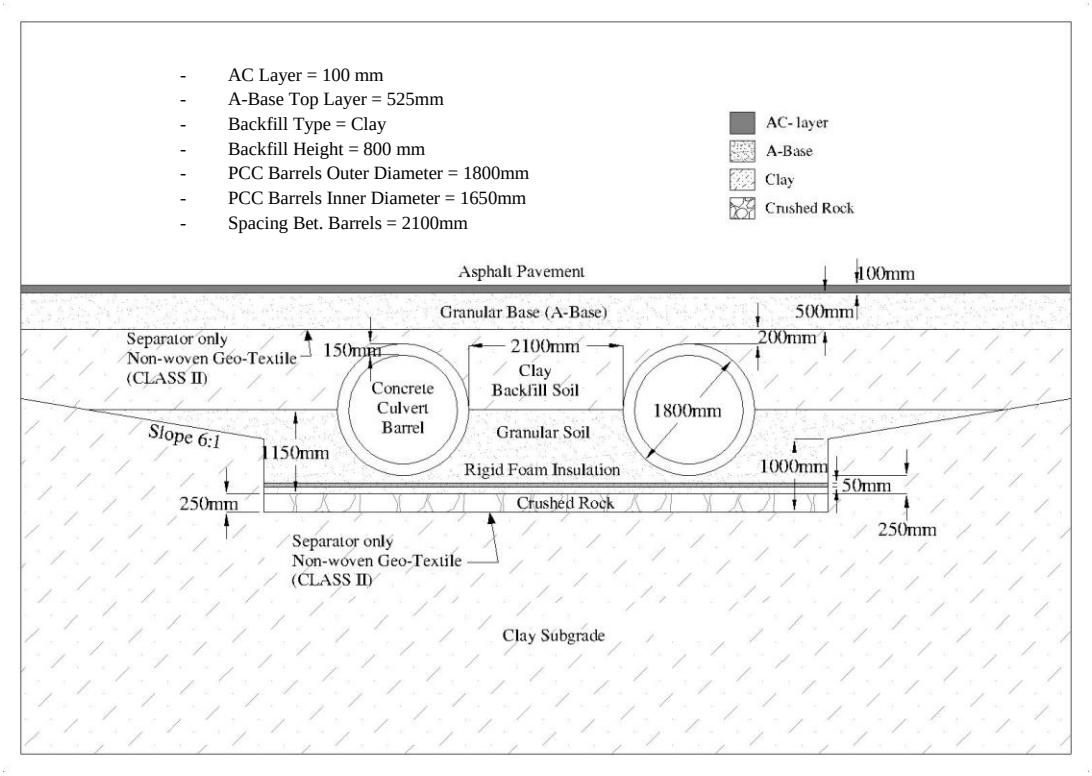

Figure A.5: Detailed cross section of culvert site 5

Appendix B – Original size of the numerical model

The original size of the numerical model was 22m by 10m. The dimensions of the model were reduced to 8m by 7m to reduce the analysis time. The outputs for the models with the reduced dimensions (8m by 7m) were exactly the same with the 22m by 15m models. The figures below show a sample of the full-size (22m by 10m) models for the sites 2,4, and 5. The culvert site 2 is backfilled with granular soil. The culvert site 4 is backfilled with clay. The culvert site 5 is backfilled with clay and thermal insulation is placed 100mm below the culvert barrels.

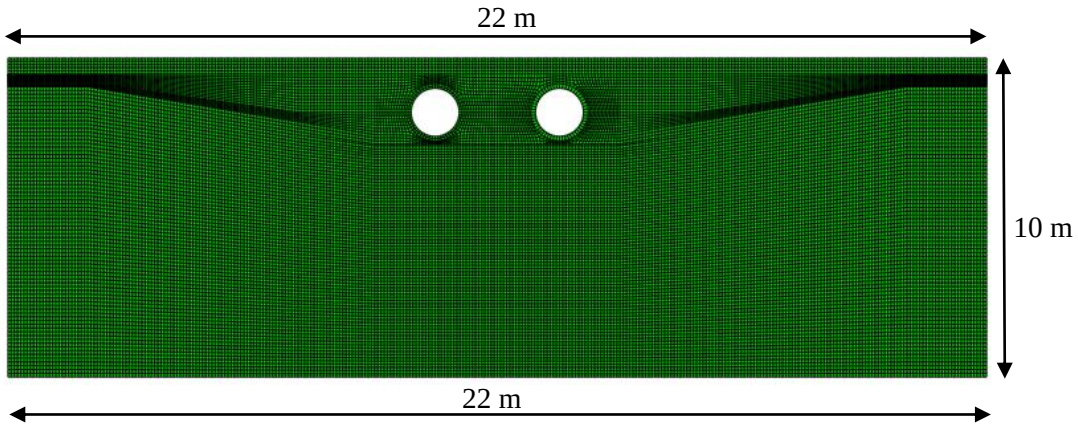

Figure B.1: The numerical model geometry with 25 m width and 10m depth for the culvert sites

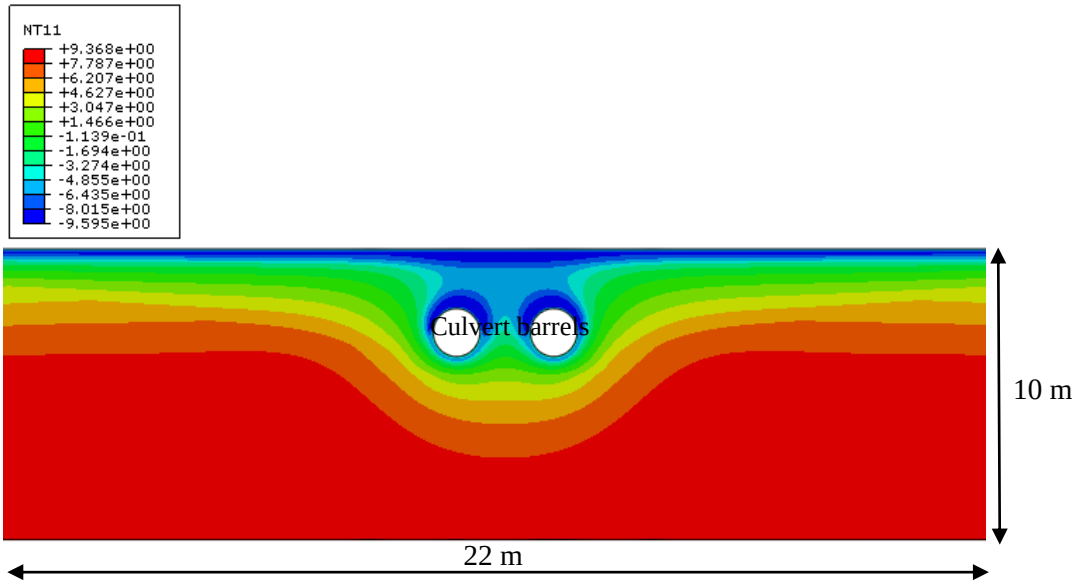

Figure B.2: Ground thermal profile in the winter at site 2

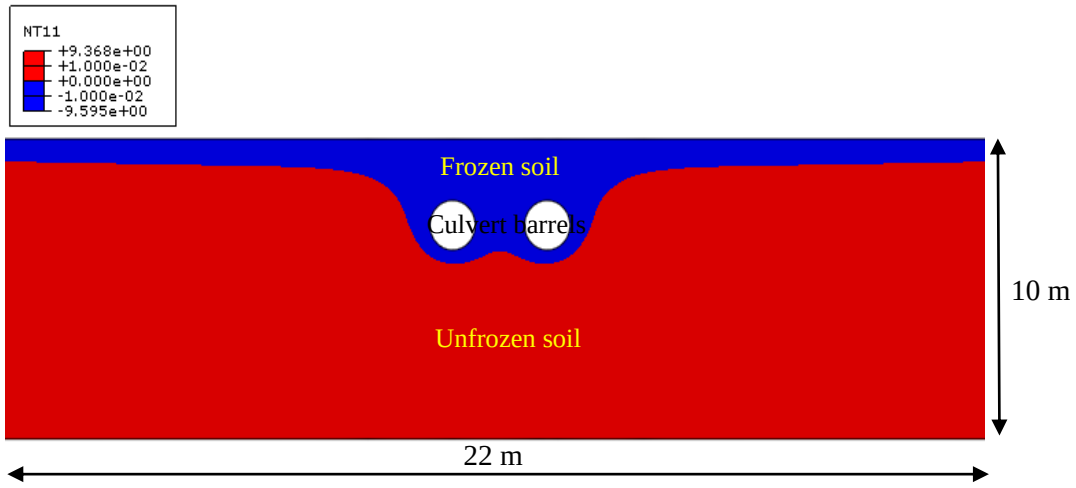

Figure B.3: Frost penetration distribution in the winter at site 2

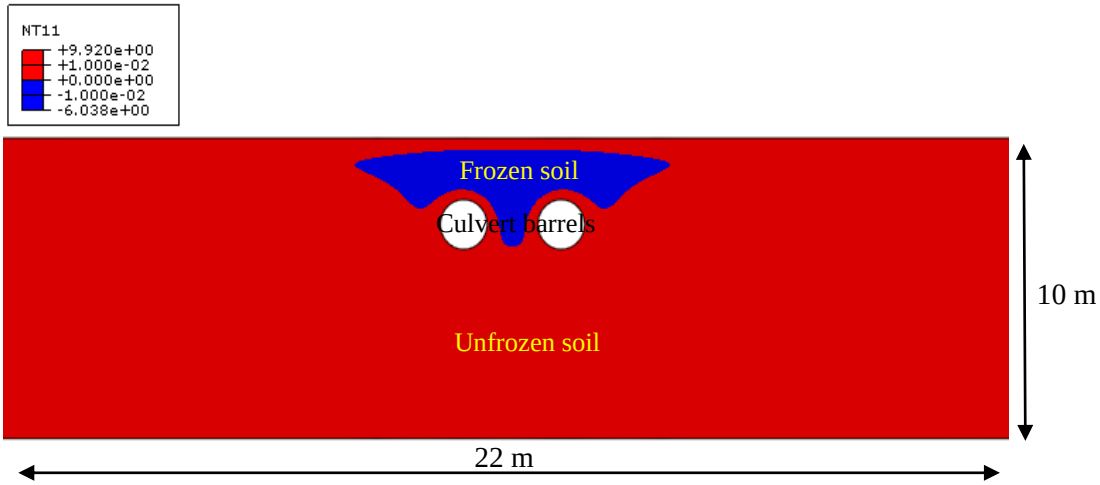

Figure B.4: Frost penetration distribution in the spring at site 2

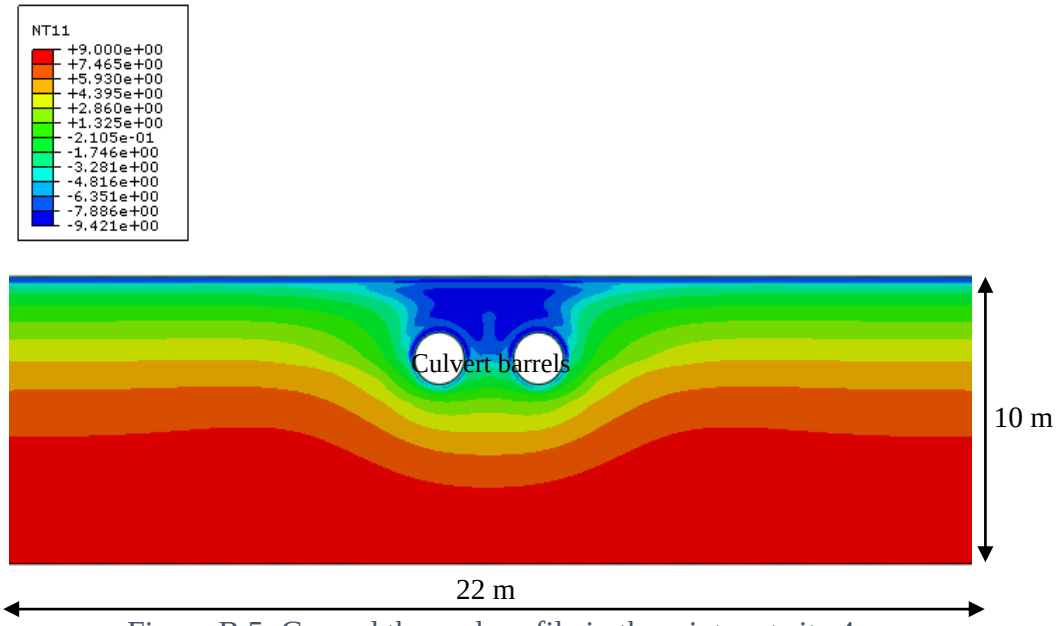

Figure B.5: Ground thermal profile in the winter at site 4

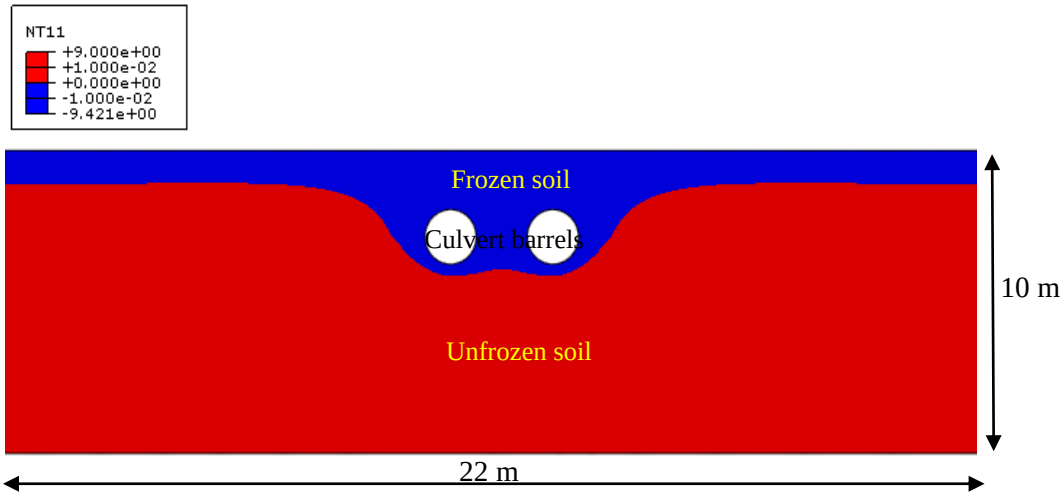

Figure B.6: Frost penetration distribution in the winter at site 4

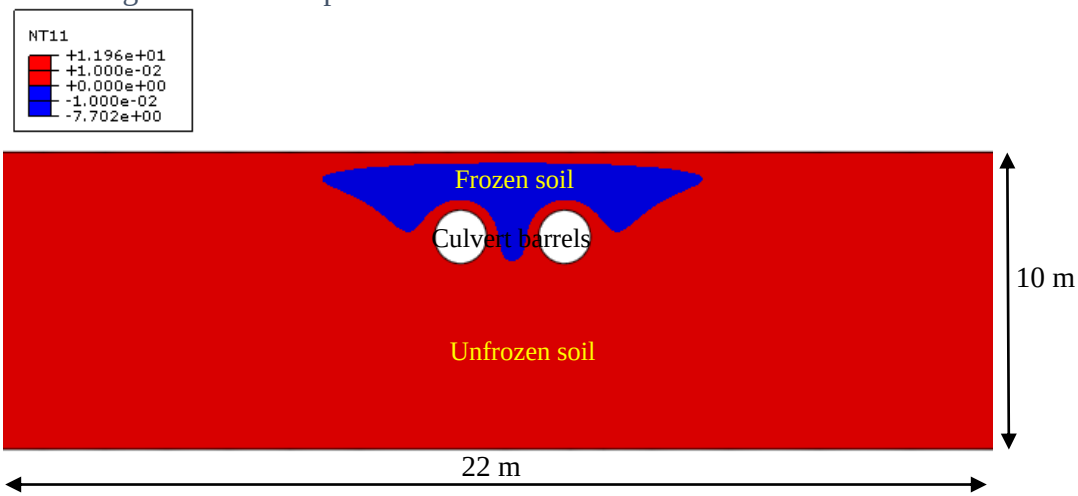

Figure B.7: Frost penetration distribution in the spring at site 4

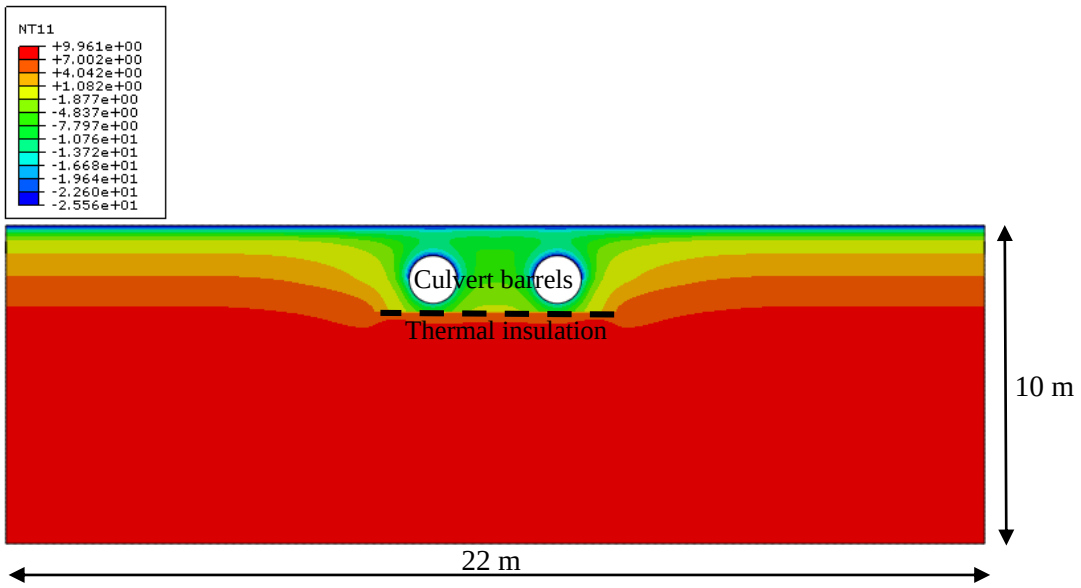

Figure B.8: Ground thermal profile in the winter at site 5

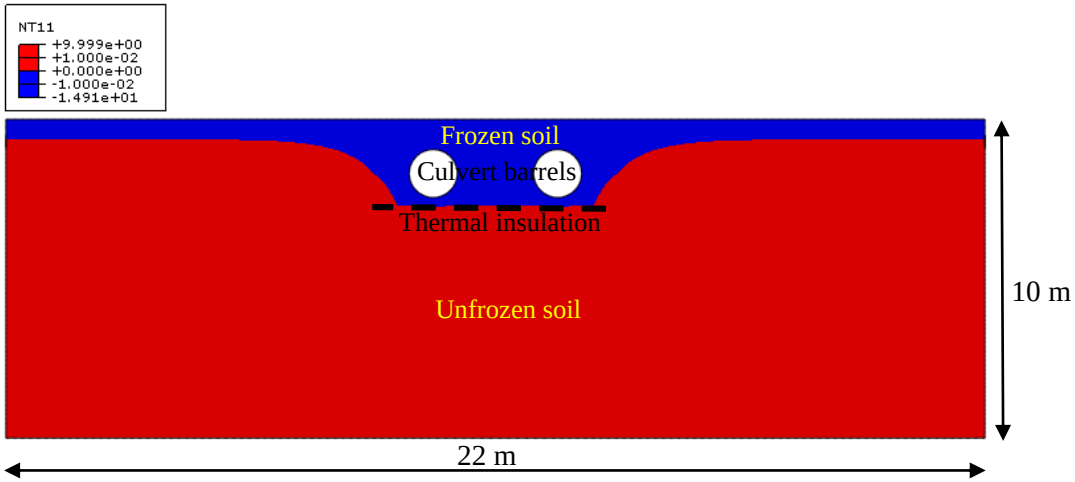

Figure B.9: Frost penetration distribution in the winter at site 5

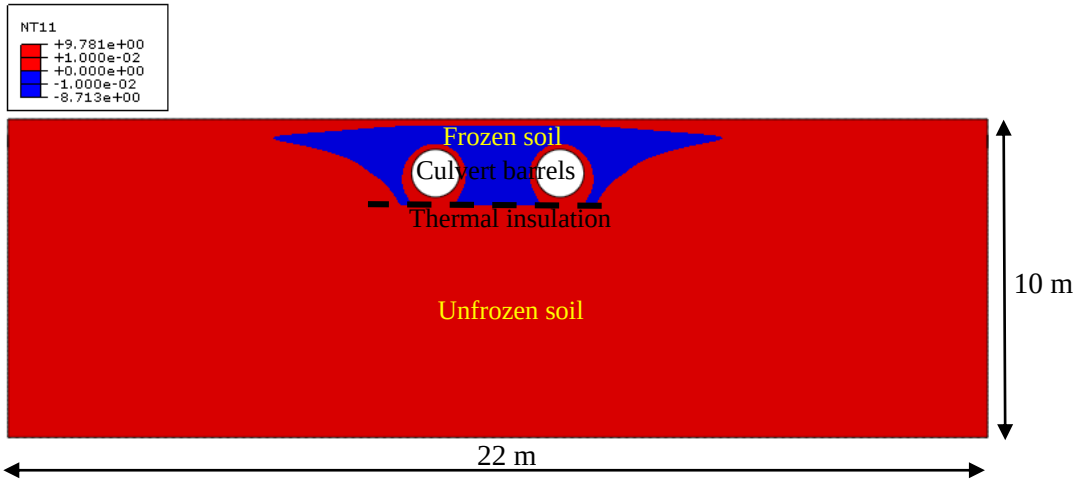

Figure B.10: Frost penetration distribution in the spring at site 5